Analysis and Planning of Manipulation Using the Theory of Polyhedral Convex Cones

Shinichi Hirai

March 1991

Abstract

A new approach to the analysis and planning of manipulation using the theory of polyhedral convex cones is presented. The majority of manipulative tasks, including assembly and grasps, are performed through mechanical contacts. The constraints due to the mechanical contacts are non-holonomic, because they are unidirectional constraints described by a set of inequalities. One of the fundamental difficulties in the analysis of manipulative tasks is to deal with a number of inequalities resulting from the unidirectional nature of mechanical constraints. In this paper, we develop a methodology based on the theory of polyhedral convex cones that allows us to deal with complex inequalities in an efficient and systematic manner.

First, the kinematic and static analysis of rigid bodies constrained by contacts is presented. We derive a general form of linear simultaneous inequalities that result from the formulation of task models. The inequalities are then represented and solved by using polyhedral convex cones. Algorithms for fundamental operations on these cones are developed and implemented on a computer. Second, the analysis of gross motion of rigid bodies constrained by mechanical contacts is presented. The process of an assembly operation is analyzed with regard to how workpieces contact each other. The assembly operation is then described with a contact state graph, where individual nodes of the graph represent the contact states between workpieces and the possible transition between two contact states is denoted by an arc connecting the corresponding nodes. We develop an efficient algorithm for automatically generating the graph from the geometric data of workpieces. Third, A model-based approach to the recognition of assembly process states is presented. Sensory information acquired in the process is interpreted using state classifiers in order to estimate the current state of the assembly process. The classifiers of the assembly process state are formulated by using the theory of polyhedral convex cones. We develop a systematic method for generating the classifiers automatically based on geometric models of assembly parts.

Contents

List of Figures

List of Tables

Nomenclature

$A(\boldsymbol{q})$	admissible displacement set at configuration $\boldsymbol{q}$
$D(S_i, S_j)$	minimum set of vectors to differentiate two PCC's
$DS(S_i, S_j)$	minimum set of vectors to differentiate two states
$DT(N_i, N_j)$	minimum set of vectors to differentiate one state among multiple states
$F(\boldsymbol{q})$	admissible force set at configuration $\boldsymbol{q}$
$g_j(\boldsymbol{x})$	signed distance between facet j and coordinates $\boldsymbol{x}$
$h_j(\boldsymbol{x})$	distance between facet j and coordinates $\boldsymbol{x}$
$H_{ij}(\boldsymbol{q})$	distance between apex i and facet j at configuration $\boldsymbol{q}$
N_i	i-th contact state
$N_i \rightarrow N_j$	direct state transition from N_i to N_j
$\boldsymbol{p}$	force and moment
$\boldsymbol{q}$	configuration of object (position and orientation)
$\Delta\boldsymbol{q}$	infinitesimal displacement
R	set of admissible configurations
R_i	set of configurations involved in state N_i
∂R_i	boundary set of region R_i
S_i	set of possible measurements at state N_i
$\boldsymbol{s}_m$	vector consisting of measured sensor signals
$S(\boldsymbol{q})$	set of possible measurements at configuration $\boldsymbol{q}$
$face\{\boldsymbol{a}_1, \boldsymbol{a}_2, \cdots, \boldsymbol{a}_m\}$	face-form of polyhedral convex cone
$span\{\boldsymbol{u}_1, \boldsymbol{u}_2, \cdots, \boldsymbol{u}_k\}$	span-form of polyhedral convex cone
X^{int}	interior set of X
X^*	polar of set X
$X \cap Y$	intersection of sets X and Y
$X \cup Y$	union of sets X and Y
$X + Y$	convex sum of sets X and Y

Chapter 1
Introduction

A new approach to the analysis and planning of manipulation using the theory of polyhedral convex cones is presented. Robots must perform tasks successfully in the presence of uncertainties, including workpiece tolerances, positioning errors, frictions and so on. In manipulative tasks such as assembly and grasps, robots contact with the environment. Robots must adapt themselves to unpredicatable change of the environment and perform dextrous operations in order to cope with uncertainties. Force feedback control is a key to the advanced manipulation, where robots interact with the environment.

In the past decades, a number of theories and techniques have been developed, including bi-lateral servo [Inoue, 71], generalized spring and damper [Whitney, 77], hybrid position/force control [Mason, 82] [Raibert and Craig, 81], impedance control [Hogan, 85] and so on. These provides efficient means to construct force feedback control systems, where force information is needed to modify the robot motion in accordance with predetermined control laws and control schemes. The majority of manipulative tasks, however, are still out of the range of today's robotics technologies. These are often so complex and intricate that efficient strategies cannot be generated by single control laws and schemes. Real control laws are highly nonlinear and varying depending on the state of the process. A selection matrix in hybrid control, for example, must be switched if the geometric constraints vary in the process. A particular stiffness matrix, which is valid for a certain range of tasks, will be inadequate when the task condition varies significantly. The direct feedback of force signals is thus limited in validity, unless the control law is modified in accordance with the change in the process state. A higher-level control is therefore necessary to extend the task range and deal with varying task conditions, which are often uncertain. The objective of this paper is to provide a fundamental technique to construct the higher-level force controller that allows the robot to recognize the process state and modify the task strategy depending on the process state.

Figure 1 shows a schematic of the argumented control system that comprises both the direct feedback of force signals and the higher-level feedback which causes the change of control strategies. While the former is primarily a signal-level feedback, the latter is a symbol-level feedback, where the original sensory information is mapped into a process state described at a symbolic-level or signed-level [Rasmussen, 83]. Note that the latter requires the interpretation of sensory information to recognize the process state and the modification of task strategies

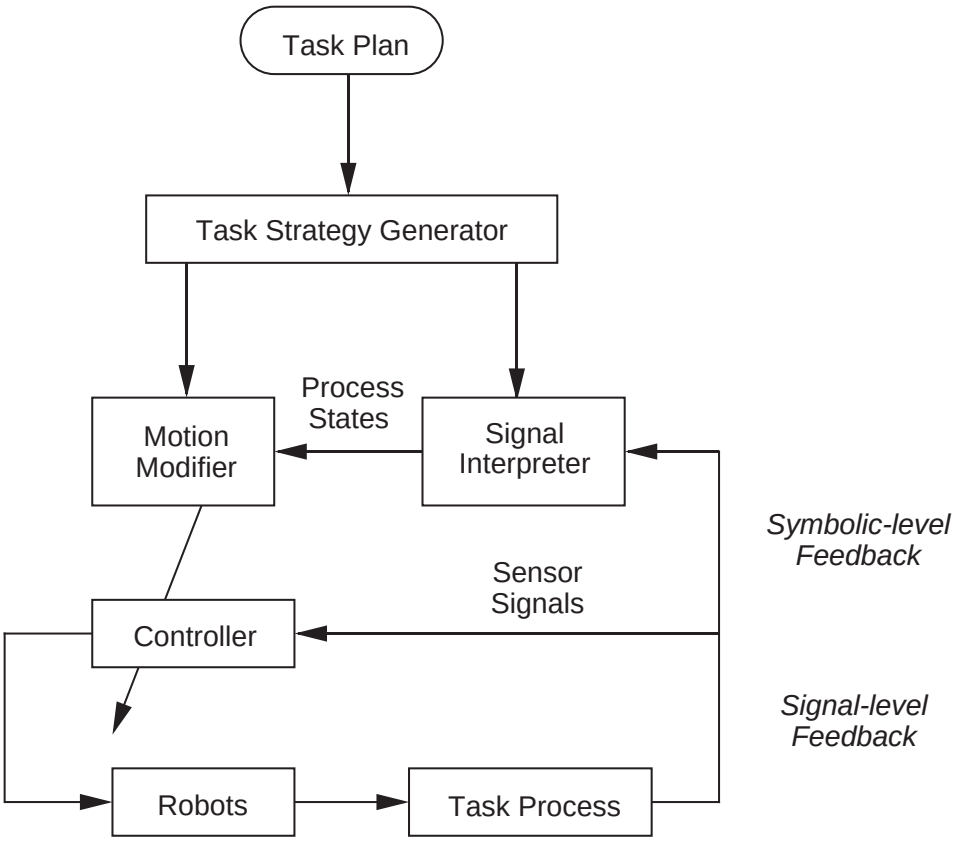

Figure 1: Symbolic-level feedback

to cope with unpredicatable change of the process state [Lozano-Pérez et al., 84] [Donald, 88] [Desai and Volz, 89]. Understanding the mechanism of manipulation is necessary to construct a higher-level control system. This research provides a fundamental methodology for analysis and planning of manipulative tasks based on the theory of polyhedral convex cones.

In chapter 2, the kinematic and static analysis of rigid bodies constrained by contacts is presented. The majority of manipulative tasks are performed through mechanical contacts with the environment. The mechanical contacts are unidirectional constraints described by a set of inequalities. We develop a mathematical tool based on the theory of *Polyhedral Convex Cones* in order to deal with complex inequalities in an efficient and systematic manner. In chapter 3, we analyze the process of the assembly operation with regard to how the workpieces contact each other and represent the process by a *Contact State Graph*. The gross motion of workpieces can be described by the graph. An algorithm for generating a contact state graph is derived. In chapter 4, we develop a technique for recognizing the current process state from the sensory information. *State Classifiers* that discriminate contact states are formulated by using the polyhedral convex cones, which directly provide a set of discriminant functions. The classifiers are simplified to a minimum set of discriminant functions by using reduction rules of polyhedral convex cones. Using this technique, it is expected that the robot can identify the process state in order to perform a higher-level control including the switching of control strategies and schemes.

1.1 Example

Let us present an overview of this research by taking a simple example shown in Figure 2. This figure shows a moving object contacting with a fixed environment. The moving object is in contact with two facet of the environment, F_1 and F_2. Assume that the moving and the fixed objects are rigid bodies. First, let us analyze the kinematic and static behavior of objects. Let $\Delta \boldsymbol{x} = [\Delta x, \Delta y]^T$ be an infinitesimal displacement of the moving object. Let $\boldsymbol{n}_i$ be the inward normal vector of the i-th facet F_i. The motion of the moving object is constrained by contacts with the environment. The condition that a translational displacement $\Delta \boldsymbol{x}$ is geometrically admissible is then given by an inequality, $\boldsymbol{n}_i^T \Delta \boldsymbol{x} \leq 0$. Note that constraints are unidirectional since the objects may separate in one direction. The inequality results from the unidirectional constraints. An arbitrary admissible displacement of the moving object must satisfy all of the conditions due to individual contact points.

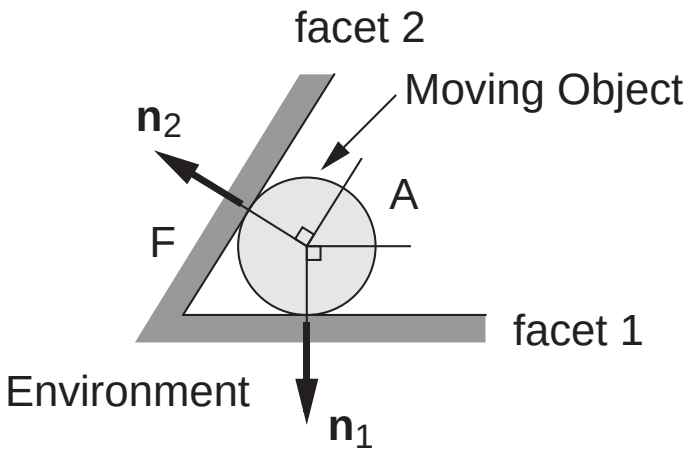

Figure 2: Simple example of planar object and environment

Therefore, a set of geometrically admissible displacements is derived as:

$$A = \{\Delta \boldsymbol{x} \mid \boldsymbol{n}_i^T \Delta \boldsymbol{x} \leq 0, \;\; i = 1, 2\}.$$

Let us derive the range of forces that satisfy static equilibrium condition. A normal reaction force acting at the contacting point between the moving object and the i-th facet F_i is described by $\boldsymbol{R}_i = -R_i \boldsymbol{n}_i$, where R_i denotes the magnitude of the reaction force. Let $\boldsymbol{f} = [f_x, f_y]^T$ be a collective force acting on the moving object. If all the contacting points are frictionless, the equilibrium equation is given by

$$\boldsymbol{f} + \sum_{i=1}^{2} (-R_i \boldsymbol{n}_i) = \mathbf{o}.$$

Note that all the coefficients R_i are non-negative since the contacts are unidirectional. The range of forces that satisfy the static equilibrium condition is thus described by

$$F = \{\sum_{i=1}^{2} R_i \boldsymbol{n}_i \mid R_i \geq 0, \;\; i = 1, 2\}.$$

As illustrated in the figure, both A and F are mathematically described by cones, since all the contacts are unidirectional. In chapter 2, we will provide a more generalized approach which allows us to treat translational and rotational motion of three- dimensional objects using the theory of polyhedral convex cones.

Let us analyze a global motion of objects. Assembly is a process of locating and fixing workpieces together in a desired configuration. During the operation,

the workpieces contact each other at different surfaces as shown in Figure 3. The contacting pair of surfaces may change as the operation proceeds and the geometric constraints change during the assembly process. Thus, the assembly process can be modeled by a successive change of the geometric constraints and can be described by a contact state graph as illustrated in the figure. Individual nodes of the graph represent the assembly process states, that is, how objects contact each other. Depending upon whether the moving object is in contact with the i-th facet F_i, there exist four process states N_1 through N_4 in this example. Let $\boldsymbol{x}_0 = [x_0, y_0]^T$ be the position of the moving object and $h_i(\boldsymbol{x}_0)$ be the distance between the moving object and the i-th facet F_i. Note that function $h_i(\boldsymbol{x}_0)$ is dependent on the position $\boldsymbol{x}_0$. Individual nodes are then formulated whether each distance function $h_i(\boldsymbol{x}_0)$ is positive or equal to zero. For example, an arbitrary position $\boldsymbol{x}_0$ involved in state N_3 must satisfy the following condition:

$$h_1(\boldsymbol{x}_0) > 0 \quad \text{and} \quad h_2(\boldsymbol{x}_0) = 0.$$

This shows that a contact state graph describes the global motion of an object under unidirectional constraints. The possible direct transition between two constraints is denoted by an arc connecting the corresponding nodes. In this example, a direct transition from N_2 to N_3 is not admissible since it is impossible to change the geometric constraints directly from N_2 to N_3 without transiting N_1 or N_4. In chapter 3, we will provide an approach to the analysis of assembly processes using contact state graphs, which allows us to treat translational and rotational motion of three-dimensional objects. We will also develop a method for generating a contact state graph from the geometric model of workpieces.

The robot needs to change its control law or task strategy according to the process state so that the robot can perform the task successfully. A selection matrix in hybrid control must be switched if the geometric constraints change significantly. For example, control mode along y-axis must be switched from position-control mode to force-control mode when the geometric constraints vary from N_1 to N_3 as shown in Figure 3. Therefore, robots need to recognize the process state and modify the task strategy depending on the process state. In chapter 4, we will develop a new technique for mapping sensory information into the process state described at a symbolic-level. State classifiers are derived automatically from the geometric model of workpieces using the theory of polyhedral convex cones, which formulates the kinematics and the statics of manipulation. Then, robots can identify the geometric constraints from force and displacement information using the state classifiers.

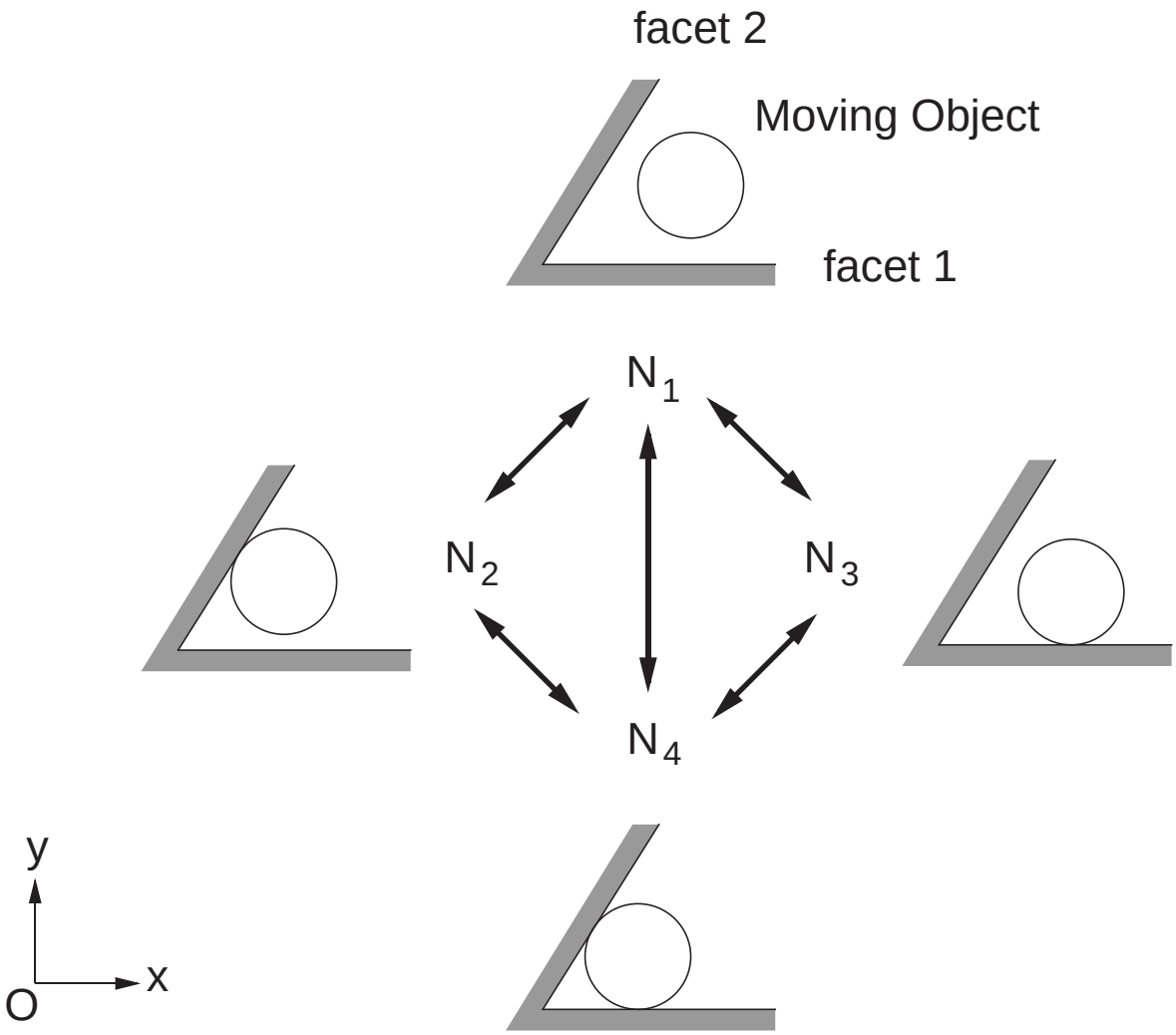

Figure 3: Simple example of contact state graph

1.2 Previous Work

Mechanical contacts between objects have been studied in screw theory, grasp analysis, assembly analysis and so on. In screw theory, mechanical contacts between objects have been characterized by repelling and reciprocal screws [Ohwovoriole and Roth, 81]. In grasp analysis, constraints by fingers have been addressed in the analysis of form closure [Lakshminarayana, 78] and force closure [Ohwovoriole and Roth, 81] [Nguyen, 86] [Nguyen, 87]. Contacts between fingers and objects are analyzed extensively [Salisbury and Craig, 82] [Kerr and Roth, 86]. Rolling contacts between fingers and objects have been analyzed [Cole et al., 88]. Enveloping grasps using the surface of a hand have been addressed [Trinkle et al., 87]. Squeezing operations have been studied [Brost, 88]. Contacts with soft fingers have been modeled [Akella and Cutkosky, 89]. In fixture analysis, the accessibility and detachability conditions have been derived [Asada and By, 85]. Assembly tasks such as peg-into-hole mating have been also analyzed extensively. Static behavior of objects in peg-into-hole insertions has been analyzed [Nevins et al., 80] [Whitney, 82] and a hand for fine insertion tasks has been developed [Whitney and Rourke, 86]. Conditions where jamming or wedging can occur for peg-into-hole insertions have been derived [Whitney, 82]. Object motion under frictional contacts has been analyzed [Rajan et al., 87]. Pushing operation with frictions has been studied [Mason, 86]. Object motion in contact has been formulated using instantaneous centers of motion [Suehiro and Takase, 89]. In collision avoidance, the motion of rigid objects is analyzed to obtain collision-free paths [Lozano-Pérez and Wesley, 79] [Schwartz and Sharir, 83] [Schwartz and Sharir, 89] and configuration space approaches have been developed [Arnold, 78] [Lozano-Pérez, 81] [Lozano-Pérez, 83].

Robots must execute tasks in the presence of uncertainties. Compliant motion is an effective technique to cope with the uncertainties. In compliant motion, robots utilize the task constraints which may not be known precisely in order to guide objects along the constraints and eliminate relative uncertainties. Force feedback control has been developed for the compliant motion. In a force feedback control system, force information is needed to modify the robot motion in accordance with a predetermined control law. Uncertainties can be reduced through sensing and modifying operations. A number of control schemes have been proposed, including bi-lateral servo [Inoue, 71], generalized spring and damper [Whitney, 77], generalized stiffness control [Salisbury, 80], hybrid position/force control [Mason, 81] [Raibert and Craig, 81], impedance control [Hogan, 85] and so on [Mason, 82] [Whitney, 87]. For a certain range of tasks, uncertainties can be reduced without sensing operations. Sensorless manipulation has been explored [Mason, 85]. Pushing oper-

ations without sensing have been studied [Mason, 86] [Brost, 88]. Guarded motion strategies are alternative techniques to cope with uncertainties. In guarded motion, robots combine some sensor signals in order to eliminate ambiguities of the individual signals. Assembly operations using position and force sensing have been studied [Will and Grossman, 75]. Representation of uncertainties has been studied. Symbolic constraints among uncertainties have been addressed [Brooks, 82]. Uncertainties in motion commands have been represented using uncertainty cones [Erdmann, 86]. Uncertainties have been represented using probabilistic relations [Kamel and Kaufmann, 88].

A number of approaches to the automatic synthesis of robot programs have been proposed. The motivation of these researches is to reduce human intervention in robot programming tasks by utilizing workpiece models generated by computer aided design systems. A fine-motion planning method using preimages has been addressed [Lozano-Pérez et al., 84]. Starting a task from a point involved in the preimage of a goal, robots can preform the task successfully and can recognize the success of the task. Based on the preimage approach, backprojection techniques have been developed [Erdmann, 86] [Juan and Paul, 86]. An automatic programming system based on inductive learning has been addressed [Dufay and Latombe, 84]. This system consists of a training phase that produces traces of execution and an inductive phase that transforms these traces into a robot program. Planning of assembly sequences have been studied [Yamada et al., 87]. An approach to the planning and teaching of compliant motion strategies have been addressed [Buckley, 87]. Teaching for the hybrid position/force control has been developed [Asada and Izumi, 87]. Many manipulative tasks are preformed with multiple step execution, which can be described by a sequence of process states. Stages in a peg-into-hole insertion have been considered [Whitney, 82]. Contact formulations have been proposed to describe and classify mechanical contacts between objects [Desai and Volz, 89]. The process states of an assembly operation have been addressed [Lozano-Pérez et al., 84] [Donald, 88] [Xiao and Volz, 89].

Chapter 2
Kinematics and Statics of Manipulation Using the Theory of Polyhedral Convex Cones

2.1 Introduction

Kinematics and statics of arm linkages have been studied extensively in past decades. An arm linkage is a holonomic system consisting of multiple bodies, for which standard analytic methods have been established. In contrast, process models of manipulative tasks such as assembly are generally non-holonomic. Objects are in contact with each other and thereby constrained mechanically, but constraints are unidirectional since the objects may separate in one direction. The difference between the bidirectional and the unidirectional constraints is critical, since the latter refers to non-holonomic constraints, to which standard techniques do not apply.

In screw theory, unidirectional constraints have been characterized by repelling and reciprocal screws [Ohwovoriole and Roth, 81]. In grasp analysis, the unidirectional nature of constraints by fingers has been addressed in the analysis of form closure [Lakshminarayana, 78] and force closure [Ohwovoriole and Roth, 81] [Nguyen, 86] [Nguyen, 87]. Contacts between fingers and objects are also analyzed extensively [Salisbury and Craig, 82] [Kerr and Roth, 86] [Akella and Cutkosky, 89]. In fixture analysis, the accessibility and detachability conditions have been derived from a non-holonomic model of workpiece positioning [Asada and By, 85]. Assembly tasks such as peg-into-hole mating are non-holonomic processes with unidirectional constraints. These assembly processes have been analyzed based on unidirectional constraint models [Rajan et al., 87] [Suehiro and Takase, 89].

In these papers, the unidirectional constraints are described by a set of inequalities or in some equivalent formulae. In these analyses, the intractable nature of inequalities creates difficulties; simultaneous inequalities are much harder to solve explicitly than equalities. Solutions are complex to represent and difficult to interpret. Unlike the solutions to simultaneous equations, the solutions to simultaneous inequalities are not given in an explicit, comprehensive, and understandable form, even if the inequalities are linear. This is a bottleneck in the analysis of manipulative tasks where objects are subject to unidirectional constraints.

In this paper, we will develop a mathematical tool for dealing with linear simultaneous inequalities in an efficient and systematic manner. First, a general form of inequalities representing unidirectional constraints is derived. Applying the inequality representation to various problems including grasp planning, fixture design, and the synthesis of hybrid position/force control systems, we will find general problems to solve. The general form of problems is then formulated with use of polyhedral convex cones, which provide an efficient approach to dealing with a large number of inequalities.

2.2 Formulation of Unidirectional Constraints

2.2.1 The Admissible Displacement Set

In this paper, we deal with a rigid body consisting of a finite number of smooth surfaces, called facet j. Let $g_j(\boldsymbol{x})$ be the distance between facet j and an arbitrary point in space whose coordinates are $\boldsymbol{x} \in R^3$, as shown in Figure 4. The distance function $g_j(\boldsymbol{x})$ is defined to be a signed distance so that it is negative inside the rigid body. We assume that all of the contacts are formulated by a finite number of point contacts. In this section, we formulate unidirectional constraints in order to derive the range of geometrically admissible displacements.

Let $\boldsymbol{x}_i$ be the coordinates of the i-th apex of the moving object. When the i-th apex of the moving object is on the j-th facet of the fixed object, the following equation is satisfied.

$$g_j(\boldsymbol{x}_i) = 0 \tag{2-1}$$

Let $\Delta\boldsymbol{q}$ be an infinitesimal displacement of the moving object:

$$\Delta\boldsymbol{q} = \begin{bmatrix} \Delta\boldsymbol{x}_0 \\ \Delta\boldsymbol{\theta}_0 \end{bmatrix} \tag{2-2}$$

where $\Delta\boldsymbol{x}_0$ is an infinitesimal displacement of the object position and $\Delta\boldsymbol{\theta}_0$ is that of the object orientation. When the moving object changes its location slightly, the signed distance between the i-th apex and j-th facet changes to:

$$d = g_j(\boldsymbol{x}_i + \Delta\boldsymbol{x}_0 + \Delta\boldsymbol{\theta}_0 \times \boldsymbol{x}_i), \tag{2-3}$$

where $\times$ represents the outer product of vectors. We assume that the function g_j is differentiable. Let $\boldsymbol{n}_{ij}$ be the inward normal vector of the j-th facet at coordinates

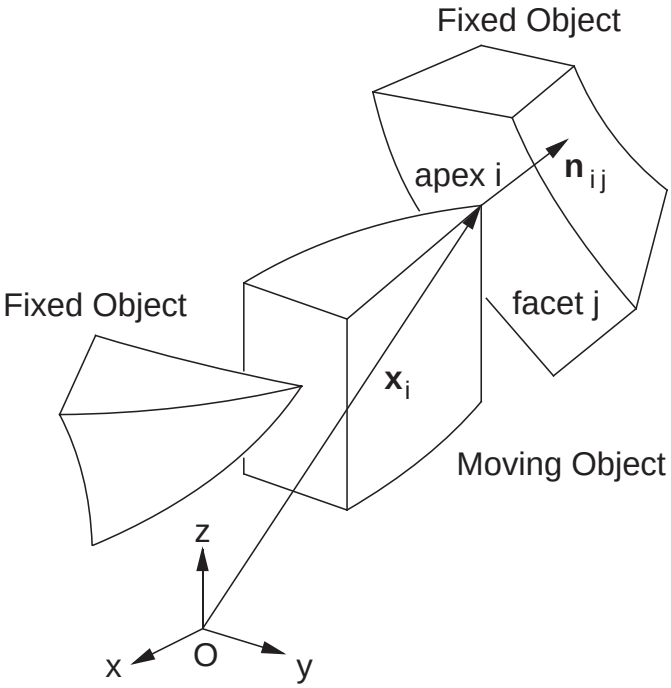

Figure 4: Model of constraints

$\boldsymbol{x}_i$. Expanding eq.(2-3) and substituting eq.(2-1) into the expanded function, we have

$$\begin{aligned} d &= \left.\frac{\partial g_j}{\partial \boldsymbol{x}}\right|_{\boldsymbol{x}=\boldsymbol{x}_i} (\Delta\boldsymbol{x}_0 + \Delta\boldsymbol{\theta}_0 \times \boldsymbol{x}_i) \\ &= -(\boldsymbol{n}_{ij})^T \Delta\boldsymbol{x}_0 - (\boldsymbol{x}_i \times \boldsymbol{n}_{ij})^T \Delta\boldsymbol{\theta}_0 \\ &= -(\boldsymbol{d}_{ij})^T \Delta\boldsymbol{q} \end{aligned} \tag{2-4}$$

where

$$\boldsymbol{d}_{ij} = \begin{bmatrix} \boldsymbol{n}_{ij} \\ \boldsymbol{x}_i \times \boldsymbol{n}_{ij} \end{bmatrix}. \tag{2-5}$$

Since apex i of the moving object lies on or outside the facet j of the fixed object, the value of eq.(2-4) must be positive or equal to zero. Thus, the following condition must be satisfied:

$$\boldsymbol{d}_{ij}^T \Delta\boldsymbol{q} \leq 0. \tag{2-6}$$

Similarly, we can derive an inequality condition for the case where the i-th apex of the fixed object contacts the j-th facet of the moving object. By replacing $\boldsymbol{x}_0$ and $\boldsymbol{\theta}_0$ by $-\boldsymbol{x}_0$ and $-\boldsymbol{\theta}_0$, the distance is given by

$$d = g_j(\boldsymbol{x}_i - \Delta\boldsymbol{x}_0 - \Delta\boldsymbol{\theta}_0 \times \boldsymbol{x}_i). \tag{2-7}$$

Let $\boldsymbol{n}_{ij}$ be the outward normal vector of the j-th facet at coordinates $\boldsymbol{x}_i$. The distance is then described as:

$$d = -(\boldsymbol{d}_{ij})^T \Delta\boldsymbol{q} \tag{2-8}$$

Since apex i lies on or outside the facet j, the value of eq.(2-8) must be positive or equal to zero. The same condition as eq.(2-6) is thus derived.

Contact conditions for other types of contact pairs can be expressed by an appropriate combination of inequalities in the form of eq.(2-6). Let us consider a special case where an apex is in contact with an edge. An arbitrary edge can be defined as the intersection of two smooth faces. When an apex i contacts a convex edge defined by the intersection of facets j and k, for example, the condition is described by

$$\boldsymbol{d}_{ij}^T \Delta\boldsymbol{q} \leq 0 \quad \text{or} \quad \boldsymbol{d}_{ik}^T \Delta\boldsymbol{q} \leq 0.$$

When an apex i contacts a concave edge defined by the intersection of facets j and k, the condition is then described by

$$\boldsymbol{d}_{ij}^T \Delta \boldsymbol{q} \leq 0 \quad \text{and} \quad \boldsymbol{d}_{ik}^T \Delta \boldsymbol{q} \leq 0.$$

We assume that the moving object is in contact with the fixed object at a finite number of contacts. The possible infinitesimal displacements of the object position and orientation must satisfy all of the conditions due to individual contact points. Expanding these conditions, a set of geometrically admissible displacements can be derived as:

$$A = \bigcup_{n=1}^{N} A_n \tag{2-9}$$

where

$$A_n = \{\Delta \boldsymbol{q} \mid (\boldsymbol{h}_{nm})^T \Delta \boldsymbol{q} \leq 0,\ \forall m \in [1, M_n]\}, \tag{2-10}$$

and

$$\boldsymbol{h}_{nm} \in \{\boldsymbol{d}_{ij}\},\ \forall n, m. \tag{2-11}$$

Set A provides a general form of inequalities representing unidirectional constraints due to mechanical contacts. This set is referred to as *Admissible Displacement Set* in this paper.

2.2.2 The Admissible Force Set

In this section, we derive the range of force and moment that satisfy static equilibrium condition, assuming that all contacts are described by a finite number of point contacts. When the i-th apex of the moving object is in contact with the j-th facet of the fixed object, a normal reaction force acting at the contact point is described by

$$\boldsymbol{R}_{ij} = -R_{ij} \boldsymbol{n}_{ij} \tag{2-12}$$

where R_{ij} denotes the magnitude of the reaction force. Similarly, we can derive a reaction force for the contact between the i-th apex of the fixed object and the j-th facet of the moving object. The result is the same as the above equation. Let $\boldsymbol{p}$ be a collective vector of force and moment acting on the object:

$$\boldsymbol{p} = \begin{bmatrix} \boldsymbol{f} \\ \boldsymbol{m} \end{bmatrix} \tag{2-13}$$

where $\boldsymbol{f}$ is a translational force and $\boldsymbol{m}$ is a moment. If all of the contact points are frictionless, the equilibrium equations are given by

$$\boldsymbol{f} + \sum_{i,j}(-R_{ij})\boldsymbol{n}_{ij} = \mathbf{o} \tag{2-14}$$

$$\boldsymbol{m} + \sum_{i,j}(-R_{ij})\boldsymbol{x}_i \times \boldsymbol{n}_{ij} = \mathbf{o} \tag{2-15}$$

where $\boldsymbol{x}_i$ denotes the coordinates of the contact point. By combining the above equations, we have

$$\boldsymbol{p} = \sum_{i,j} R_{ij}\boldsymbol{d}_{ij} \tag{2-16}$$

where vectors $\boldsymbol{d}_{ij}$ have been given by eq.(2-5). In screw theory, vector $\boldsymbol{d}_{ij}$ is called a wrench [Ohwovoriole and Roth, 81]. Note that all the coefficients R_{ij} are non-negative since the contacts are unidirectional. The range of forces that satisfy the static equilibrium condition is thus described by

$$F = \{\sum_{k=1}^{K} r_k \boldsymbol{w}_k \mid r_k \geq 0\}. \tag{2-17}$$

where

$$\boldsymbol{w}_k \in \{\boldsymbol{d}_{ij}\},\ \forall k. \tag{2-18}$$

This set is referred to as *Admissible Force Set* in this paper.

2.3 Manipulation Problems

In this section, we formulate some fundamental problems concerning the planning and synthesis for grasping, fixturing, and assembly.

(a) Form Closure Grasps by Fingers

Grasp is to constrain an object by means of fingers that provide unidirectional constraints. The condition for an object to be totally constrained, regardless of friction between the fingertips and the object, has been given by Lakshminarayana [Lakshminarayana, 78]. This condition requires the fingers to surround an object so that no geometrically admissible displacement is allowed for the object. Assuming that all the contacts are described by a finite number of point contacts, the condition for total constraint can be restated by using the admissible displacement set.

Namely, the admissible displacement set A must be a set that has no elements other than $\mathbf{o}$:

$$A = \{\mathbf{o}\} \tag{2-19}$$

If the set A involves a non-zero element, the object is not geometrically constrained in that particular direction. This total constraint is referred to as *Form Closure Grasp*. Thus, the problem of form closure grasp is basically to examine whether or not the linear simultaneous inequalities in eq.(2-10) have non-zero solutions.

(b) Accessibility and Detachability

In assembly, a workpiece is positioned at a designated location relative to a fixed object. Fundamental questions are to investigate whether the desired location is accessible for the workpiece and whether the workpiece is detachable from the fixture. Asada and By have formulated accessibility and detachability conditions by considering the local behavior of a workpiece in the vicinity of the designated location [Asada and By, 85]. Assuming that all the contacts are described by a finite number of point contacts, the conditions can be restated with regard to the admissible displacement set A. Namely, the workpiece is accessible and detachable in the vicinity of the designated location, if and only if a non-zero displacement $\Delta \boldsymbol{q}$ is involved in the set A.

$$\exists \Delta \boldsymbol{q} \neq 0 \quad \text{s.t.} \quad \Delta \boldsymbol{q} \in A \tag{2-20}$$

If there exists a geometrically admissible displacement from the designated location to a location where the workpiece is not in contact with any part of the fixture, the workpiece and the fixture are said to be *strongly accessible and detachable* [Asada and By, 85]. In this case, the workpiece can be detached from the fixture all at once. If, on the other hand, it is not strongly accessible and detachable but is merely accessible and detachable, the workpiece motion must conform to a bidirectional constraint no matter in which direction the workpiece is moved. Since bidirectional constraints may cause jamming in assembly, the strong condition is desirable. The condition for strongly accessible and detachable constraints is given by

$$\exists \Delta \boldsymbol{q} \neq \mathbf{o} \quad \text{s.t.} \quad \Delta \boldsymbol{q} \in A^{int} \tag{2-21}$$

where A^{int} denotes the interior set of A.

(c) Force Closure Grasps

In grasping an object, a robot applies unidirectional forces upon the object through its fingers. A desired condition for the robot is to guarantee that no motion occurs no matter what disturbance force and moment are imposed on the object. This condition, referred to as *Force Closure Grasp*, has been given by Ohwovoriole [Ohwovoriole and Roth, 81]. Assuming that all contacts are described by a finite number of point contacts, the condition can be restated by using the admissible force set given by eq.(2-17). If a non-zero force $\boldsymbol{p}$ is not involved in F, the force violates the force equilibrium conditions and causes some motion. Namely, the admissible force set must involve all the forces and moments in the six-dimensional vector space R^6:

$$F = R^6 \tag{2-22}$$

Thus, the problem of force closure grasp is basically to investigate whether or not the set F represented by the linear combination of vectors with non-negative coefficients covers the whole vector space.

(d) Hybrid Position/Force Control

In order to perform a task by using hybrid position/force control, we need to find the position-controlled space and the force-controlled space so that the robot motion may conform to the geometric constraints of the environment. The position-controlled space in the hybrid control is equivalent to the space of admissible infinitesimal displacements, while the force-controlled space is the space of forces that satisfy the static equilibrium condition. Namely, the former is the admissible displacement set A and the latter is the admissible force set F. Ohwovoriole and Roth have formulated the relationship between the admissible displacement set and the admissible force set when all the geometric constraints are unidirectional [Ohwovoriole and Roth, 81]. Assuming that all of the contact points are frictionless, the relationship can be restated as

$$F = \{\boldsymbol{p} \mid \boldsymbol{p}^T \Delta \boldsymbol{q} \leq 0,\ \forall \Delta \boldsymbol{q} \in A\} \tag{2-23}$$

In order to perform a task by the hybrid position/force control, the commanded displacement $\Delta \boldsymbol{q}_c$ must be involved in set A and the commanded force $\boldsymbol{p}_c$ must be involved in set F. An arbitrary pair consisting of a displacement involved in set A and a force involved in F forms a *Reciprocal* or a *Contrary* screw pair [Ohwovoriole and Roth, 81], since the work done by the force is equal to zero or negative, as shown in eq.(2-23). According to Ohwovoriole and Roth, a pair of the actual displacement and the actual force is either a reciprocal or a *Repelling* pair, since the work done by the force must be zero or positive [Ohwovoriole and Roth, 81].

It follows that the pair of the commanded displacement $\Delta \boldsymbol{q}_c$ and the commanded force $\boldsymbol{p}_c$ must be a reciprocal pair, that is, $\boldsymbol{p}_c^T \Delta \boldsymbol{q}_c = 0$ [Mason, 82]. Therefore, we have to choose a pair consisting of the commanded displacement and the commanded force from all admissible pairs so that the pair may be reciprocal.

Thus, the above problems concerning assembly, grasps, and hybrid position/force control are all described with regard to a simultaneous system of linear inequalities. For these problems given by eqs.(2-19), (2-20), (2-21), (2-22), and (2-23), we will develop a systematic computation method based on the theory of polyhedral convex cones.

2.4 Theory of Polyhedral Convex Cones

All the problems discussed in the previous section are represented generally in the same form, that is, simultaneous inequalities in terms of inner products of two vectors. Problems associated with differential motions, or instantaneous kinematics and statics, are thus reduced to the problems of solving a simultaneous system of linear inequalities. From this section, we will develop a systematic method for solving these problems by applying the theory of polyhedral convex cones attributed to Goldman and Tucker [Goldman and Tucker, 56].

2.4.1 Definitions

Let $\boldsymbol{a}_1$ through $\boldsymbol{a}_m$ be m real vectors. Let us consider a set of real vectors $\boldsymbol{x}$ given by

$$A = \{\boldsymbol{x} \mid \boldsymbol{a}_i^T \boldsymbol{x} \leq 0, \, \forall i \in [1, m]\}. \tag{2-24}$$

As shown in Figure 5, the set A represents a semi-infinite region surrounded by hyperplanes. The region is referred to as a *Polyhedral Convex Cone* and is abbreviated to PCC. Note that a vector $\boldsymbol{a}_i$ represents the normal to the i-th hyperplane shown in the figure. For the sake of simplicity, the set given by eq.(2-24) is expressed as

$$A = face\{\boldsymbol{a}_1, \boldsymbol{a}_2, \cdots, \boldsymbol{a}_m\} \tag{2-25}$$

which is referred to as the *Face Form* of the polyhedral convex cone. Each vector involved is called a face vector.

Let $\boldsymbol{u}_j$ be a vector along an edge of the polyhedral convex cone, as shown in Figure 5. An arbitrary vector in the set A is then represented by a linear combination

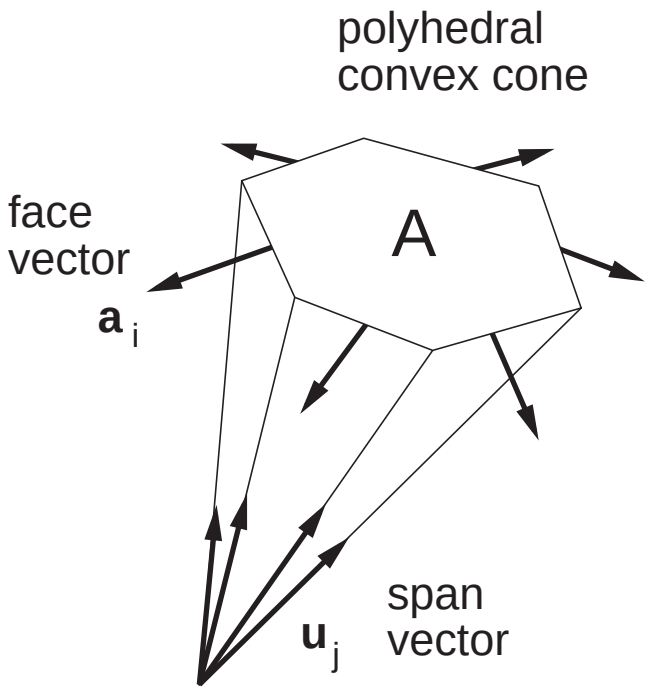

Figure 5: Polyhedral convex cone

of the vectors $\boldsymbol{u}_1$ through $\boldsymbol{u}_k$. Therefore,

$$A = \{\sum_{j=1}^{k} c_j \boldsymbol{u}_j \mid c_j \geq 0,\ \forall j \in [1,k]\}. \tag{2-26}$$

Note that the coefficients c_j are all non-negative and that in general the vectors $\boldsymbol{u}_j$ are not linearly independent. The above expression provides another form of a polyhedral convex cone. Since vectors $\boldsymbol{u}_1$ through $\boldsymbol{u}_k$ span the cone, we write the above equation simply by

$$A = span\{\boldsymbol{u}_1, \boldsymbol{u}_2, \cdots, \boldsymbol{u}_k\}. \tag{2-27}$$

This form is referred to as the *Span Form* of the polyhedral convex cone, and each vector involved is called a span vector.

Let X be an arbitrary set of real vectors $\boldsymbol{x}$. The set defined by

$$X^* = \{\boldsymbol{y} \mid \boldsymbol{x}^T \boldsymbol{y} \leq 0,\ \forall \boldsymbol{x} \in X\} \tag{2-28}$$

is called the polar of the set X. Let X and Y be two sets of real vectors. The set defined by

$$X + Y = \{\boldsymbol{x} + \boldsymbol{y} \mid \boldsymbol{x} \in X,\ \boldsymbol{y} \in Y\} \tag{2-29}$$

is called the convex sum of sets X and Y.

2.4.2 Basic Properties of Polyhedral Convex Cones

Let us consider the relationship between a polyhedral convex cone and its polar. Figure 6 illustrates a simple example of a two-dimensional polyhedral convex cone and its polar. The face form of the polyhedral convex cone A is given by $A = face\{\boldsymbol{a}_1, \boldsymbol{a}_2\}$. The cone A can be described in the span form as $A = span\{\boldsymbol{u}_1, \boldsymbol{u}_2\}$. From the figure, we can find that the vectors $\boldsymbol{a}_1$ and $\boldsymbol{a}_2$ span the polar A^*. Namely, $A^* = span\{\boldsymbol{a}_1, \boldsymbol{a}_2\}$. Thus, we can describe the polar in the face form as $A^* = face\{\boldsymbol{u}_1, \boldsymbol{u}_2\}$. According to Goldman and Tucker, the following theorem is satisfied for an arbitrary polyhedral convex cone and its polar [Goldman and Tucker, 56].

Theorem 1 *The polar of a polyhedral convex cone* $A = face\{\boldsymbol{a}_1, \boldsymbol{a}_2, \cdots, \boldsymbol{a}_m\}$ *is given by a span form:*

$$A^* = span\{\boldsymbol{a}_1, \boldsymbol{a}_2, \cdots, \boldsymbol{a}_m\}. \tag{2-30}$$

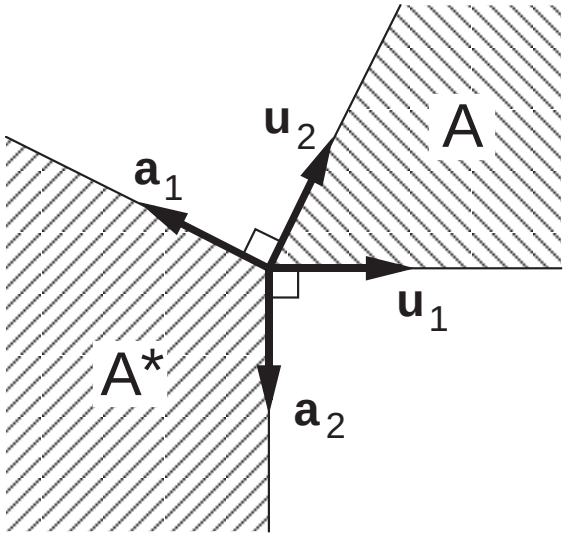

Figure 6: Polyhedral convex cone and its polar

The polar of a polyhedral convex cone in span form $A = span\{\boldsymbol{u}_1, \boldsymbol{u}_2, \cdots, \boldsymbol{u}_k\}$ *is given by a face form:*

$$A^* = face\{\boldsymbol{u}_1, \boldsymbol{u}_2, \cdots, \boldsymbol{u}_k\}. \tag{2-31}$$

From this theorem, it follows that the polar of a polyhedral convex cone is a polyhedral convex cone as well. The polar A^* is referred to as the *dual polyhedral convex cone* of A. Note that the following property is derived from the above theorem.

$$(A^*)^* = A. \tag{2-32}$$

Let us consider the conversion between face and span forms. The problem is to derive a set of span vectors from a given set of face vectors, and vise versa. The conversion from face to span form can be performed by solving linear programming (LP) problems [Goldman and Tucker, 56]. The conversion from span to face form can also be performed by solving linear programming problems and using the above theorem. As illustrated in Figure 7, we first convert a polyhedral convex cone A to its dual polyhedral convex cone, and then solve linear programming problems in order to derive vectors $\boldsymbol{a}_1$ through $\boldsymbol{a}_m$ from vectors $\boldsymbol{u}_1$ through $\boldsymbol{u}_k$. Note that we regard $\boldsymbol{a}_i$ as a span vector and $\boldsymbol{u}_j$ as a face vector in the dual polyhedral convex

cone. Thus, the conversion can be performed in both ways by simply solving linear programming problems.

In addition to the above conversions, polyhedral convex cones possess the following properties. The intersection of two polyhedral convex cones is also a polyhedral convex cone and is given by

$$\begin{aligned} & face\{\boldsymbol{a}_1, \boldsymbol{a}_2, \cdots, \boldsymbol{a}_m\} \cap face\{\boldsymbol{b}_1, \boldsymbol{b}_2, \cdots, \boldsymbol{b}_n\} \\ = \; & face\{\boldsymbol{a}_1, \boldsymbol{a}_2, \cdots, \boldsymbol{a}_m, \boldsymbol{b}_1, \boldsymbol{b}_2, \cdots, \boldsymbol{b}_n\}. \end{aligned} \tag{2-33}$$

The convex sum of two polyhedral convex cones is also a polyhedral convex cone and is given by

$$\begin{aligned} & span\{\boldsymbol{u}_1, \boldsymbol{u}_2, \cdots, \boldsymbol{u}_k\} + span\{\boldsymbol{v}_1, \boldsymbol{v}_2, \cdots, \boldsymbol{v}_l\} \\ = \; & span\{\boldsymbol{u}_1, \boldsymbol{u}_2, \cdots, \boldsymbol{u}_k, \boldsymbol{v}_1, \boldsymbol{v}_2, \cdots, \boldsymbol{v}_l\}. \end{aligned} \tag{2-34}$$

Applying the theorem to the above intersection and convex sum respectively, we can derive:

$$(A \cap B)^* = A^* + B^* \tag{2-35}$$

$$(A + B)^* = A^* \cap B^* \tag{2-36}$$

Note that the union of two polyhedral convex cones is not always a polyhedral convex cone. The polar of the union is, however, a polyhedral convex cone. The following equation is satisfied for arbitrary polyhedral convex cones, A and B:

$$(A \cup B)^* = (A + B)^* \tag{2-37}$$

The proof is shown in Appendix A. The face and the span forms have the following properties:

$$face\{\boldsymbol{a}_1, \boldsymbol{a}_2, \cdots, \boldsymbol{a}_{m-1}, \boldsymbol{a}_m\} \subset face\{\boldsymbol{a}_1, \boldsymbol{a}_2, \cdots, \boldsymbol{a}_{m-1}\} \tag{2-38}$$

$$span\{\boldsymbol{u}_1, \boldsymbol{u}_2, \cdots, \boldsymbol{u}_{k-1}, \boldsymbol{u}_k\} \supset span\{\boldsymbol{u}_1, \boldsymbol{u}_2, \cdots, \boldsymbol{u}_{k-1}\} \tag{2-39}$$

Applying the theorem to the above equations, we can derive:

$$A \subset B \iff A^* \supset B^* \tag{2-40}$$

$$A = B \iff A^* = B^* \tag{2-41}$$

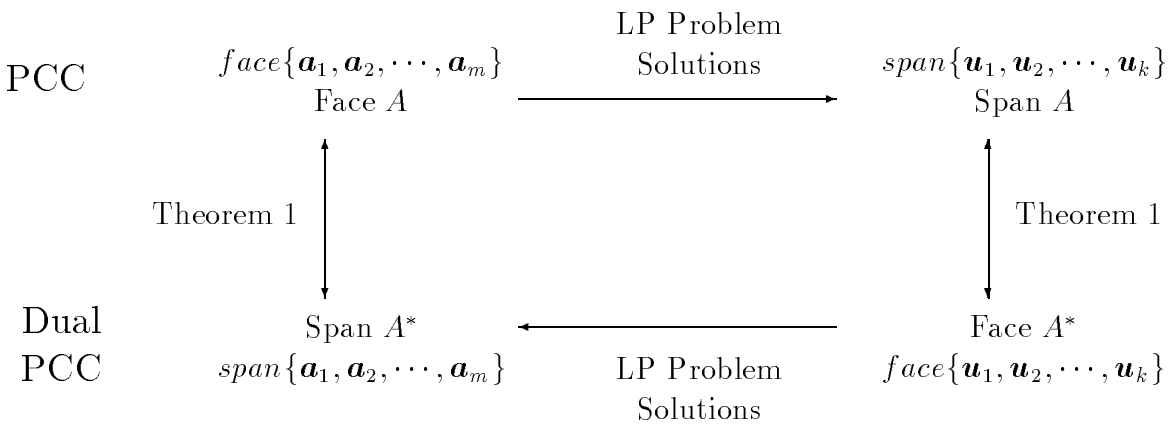

Figure 7: Relationship between face and span forms and polars

2.5 Methods for Solving the Inequality Problems

In this section, we will establish procedures for solving the inequality problems associated with assembly and grasps as described in Section 2.3 by using the theory of polyhedral convex cones. From the basic properties of PCC's, we can derive the following algorithms for the operations of PCC's.

CONVERT(A) = convert the face form of a given PCC denoted by A to the corresponding span form, and vise versa.

Solving associated linear programming problems, the two forms can be exchanged as shown in Figure 7.

DUAL(A) = compute the dual PCC of a given PCC.

Using eqs.(2-30) and (2-31), the dual PCC's can be obtained in both face and span forms.

INTERSECT(A,B) = compute the intersection of two PCC's, A and B.

If A and B are given in the span form, the algorithm CONVERT is first applied to the given PCC's in order to get face forms. For the face form PCC's, the intersection is directly obtained by eq.(2-33).

CONVEXSUM(A,B) = compute the convex sum of two PCC's, A and B.

If A and B are given in the face form, the algorithm CONVERT is first applied to the given PCC's to obtain span forms. For the span form PCC's, the convex sum is directly attained by eq.(2-34).

By using the above four algorithms, we can solve the fundamental inequality problems in a simple manner.

[1] The problem to examine whether a polyhedral convex cone A involves non-zero elements

If a polyhedral convex cone A is described in a face form, we apply algorithm CONVERT in order to describe it in the span form:

$$A = span\{\boldsymbol{u}_1, \boldsymbol{u}_2, \cdots, \boldsymbol{u}_k\}$$

An arbitrary non-zero elements $\boldsymbol{x}$ involved in A is described by a linear combination of span vectors. It implies that no non-zero elements are involved in A if $k = 0$. Thus, the polyhedral convex cone A involves non-zero elements, if and only if there exists span vectors of the polyhedral convex cone A:

$$A \neq \{\mathbf{o}\} \iff k \neq 0 \tag{2-42}$$

The above method for examining whether a polyhedral convex cone involves non-zero elements is referred to as procedure NONZERO in this paper. Procedure NONZERO(A) returns a value of TRUE if a polyhedral convex cone A has non-zero elements and a value of FALSE otherwise.

[2] The problem to examine whether a vector $\boldsymbol{r}$ is involved in a polyhedral convex cone A

If a polyhedral convex cone A is described in a span form, we apply algorithm CONVERT in order to describe it in the face form:

$$A = face\{\boldsymbol{a}_1, \boldsymbol{a}_2, \cdots, \boldsymbol{a}_m\}$$

From the definition of face form, eq.(2-24), a vector $\boldsymbol{r}$ is involved in the polyhedral convex cone A if and only if

$$\boldsymbol{a}_i^T \boldsymbol{r} \leq 0, \quad \forall i \in [1, m] \tag{2-43}$$

is satisfied.

The above method for investigating whether a vector is involved in a polyhedral convex cone is referred to as procedure ELEMENT in this paper. Procedure ELEMENT($\boldsymbol{r}$,A) returns a value of TRUE if a vector $\boldsymbol{r}$ is involved in a polyhedral convex cone A and a value of FALSE otherwise.

[3] The problem to examine whether a polyhedral convex cone A is a subset of another polyhedral convex cone B

When a polyhedral convex cone A is described in a face form, we apply algorithm CONVERT in order to describe it in the span form:

$$A = span\{\boldsymbol{u}_1, \boldsymbol{u}_2, \cdots, \boldsymbol{u}_k\}$$

The polyhedral convex cone A is a subset of another polyhedral convex cone B if and only if the following condition is satisfied:

$$\boldsymbol{u}_j \in B, \quad \forall j \in [1, m] \tag{2-44}$$

The proof of this condition is shown in Appendix B.

Using the procedure ELEMENT, we can find whether each vector $\boldsymbol{u}_j$ is involved in the polyhedral convex cone B. Thus, we can examine whether the above condition is satisfied or not. This method is referred to as procedure SUBSET in this paper. Procedure SUBSET(A,B) returns a value of TRUE if a polyhedral convex cone A is a subset of another cone B and a value of FALSE otherwise.

[4] The problem to examine whether the interior set A^{int} of a polyhedral convex cone A involves non-zero elements

Applying the algorithm CONVERT in order to obtain both face and span forms of a polyhedral convex cone A:

$$\begin{aligned} A &= face\{\boldsymbol{a}_1, \boldsymbol{a}_2, \cdots, \boldsymbol{a}_m\} \\ A &= span\{\boldsymbol{u}_1, \boldsymbol{u}_2, \cdots, \boldsymbol{u}_k\} \end{aligned}$$

The interior set A^{int} involves non-zero elements, if and only if the following condition is satisfied:

$$\forall i \in [1, m] \;\; \exists j \in [1, k] \quad \text{s.t.} \quad \boldsymbol{a}_i^T \boldsymbol{u}_j < 0. \tag{2-45}$$

The proof of this condition is shown in Appendix C.

The above method for examining whether the interior set of a polyhedral convex cone involves any elements is referred to as procedure INTERIOR in this paper. Procedure INTERIOR(A) returns a value of TRUE if the interior set A^{int} has non-zero elements and a value of FALSE otherwise.

2.6 Solving the Manipulation Problems

In this section, we apply the above methods to the manipulation problems described in Section 2.3.

(a) Form Closure Grasp

Using the notation introduced in Section 2.4, the admissible displacement set A of a grasped object is described by

$$A = \bigcup_{n=1}^{N} A_n \tag{2-46}$$

and

$$A_n = face\{\boldsymbol{h}_{n1}, \boldsymbol{h}_{n2}, \cdots, \boldsymbol{h}_{nM_n}\}. \tag{2-47}$$

Table 1: Algorithm to examine form closure grasp condition

```
for n := 1 to N do
begin
   A_n := face{h_n1, h_n2, ..., h_nM_n};
   if NONZERO(A_n) = TRUE then
      return(FALSE)
end;
return(TRUE)
```

The set A_1 through A_N are polyhedral convex cones. Thus, the admissible displacement set A is a union of polyhedral convex cones.

The condition for form closure grasps has been given eq.(2-19), which is equivalent to

$$A_n = \{\mathbf{o}\}, \quad \forall\, n \in [1, N]. \tag{2-48}$$

Using procedure NONZERO developed in the previous section, this condition is described as follows:

$$\text{NONZERO}(A_n) = \text{FALSE}, \quad \forall\, n \in [1, N] \tag{2-49}$$

The procedure to examine form closure grasps is listed in Table 1. This subroutine returns a value of TRUE if the form closure condition is met and a value of FALSE otherwise.

(b) Accessibility and Detachability

The admissible displacement set A of a workpiece at a given final configuration is the same as eqs.(2-46) and (2-47). Thus, we can examine the accessibility/detachability condition using the procedure listed in Table 1.

The condition for strongly accessible/detachable constraints has been given by eq.(2-21). Since zero is not an element of A^{int}, the problem is to examine whether A^{int} is an empty set:

$$A^{int} \neq \phi \tag{2-50}$$

By decomposing the set A to polyhedral convex cones, the above condition reduces to

$$\exists\, n \in [1, N] \ \text{ s.t. } \ A_n^{int} \neq \phi. \tag{2-51}$$

Table 2: Algorithm to examine strongly accessible/detachable condition

```
for n := 1 to N do
begin
   A_n := face{h_n1, h_n2, ..., h_nM_n};
   if INTERIOR(A_n) = TRUE then
      return(TRUE)
end;
return(FALSE)
```

Using procedure INTERIOR developed in the previous section, this condition is described by

$$\exists\, n \in [1, N] \quad \text{s.t.} \quad \text{INTERIOR}(A_n) = \text{TRUE}. \tag{2-52}$$

The procedure to examine the strongly accessible/detachable condition is listed in Table 2. This procedure returns a value of TRUE if the contact is strongly accessible and a value of FALSE otherwise.

(c) Force Closure Grasp

Using the notation introduced in section 2.4, the admissible force set F of a grasped object is described by

$$F = span\{\boldsymbol{w}_1, \boldsymbol{w}_2, \cdots, \boldsymbol{w}_K\}. \tag{2-53}$$

We find that the admissible force set F is a polyhedral convex cone. The condition for force closure grasps has been given by eq. (2-22). Applying eq.(2-41), we find that this condition is equivalent to

$$F^* = [R^6]^* = \{\mathbf{o}\}. \tag{2-54}$$

Using procedure DUAL and NONZERO developed in the previous section, this condition is described as follows:

$$\text{NONZERO}(\text{DUAL}[F]) = \text{FALSE} \tag{2-55}$$

We can examine force closure grasps with this equation.

(d) Hybrid Position/Force Control

Table 3: Procedure to compute admissible force set

$A := \{\mathbf{o}\}$;
for $n := 1$ to N
begin
  $A_n := face\{\boldsymbol{h}_{n1}, \boldsymbol{h}_{n2}, \cdots, \boldsymbol{h}_{nM_n}\}$;
  $A :=$ CONVEXSUM(A, A_n)
end;
$F :=$ DUAL(A)

Let A be the admissible displacement set, which is the position-controlled space. Comparing eqs.(2-23) and (2-28), the admissible force set F is denoted as follows:

$$F = A^*. \tag{2-56}$$

In other words, the admissible force set F is the polar of the admissible displacement set A.

The admissible displacement set A is a union of polyhedral convex cones A_1 through A_N, as mentioned in the previous section:

$$A = A_1 \cup A_2 \cup \cdots \cup A_N \tag{2-57}$$

Applying eq.(2-37) into eq.(2-56), we have

$$\begin{aligned} F &= [A_1 \cup A_2 \cup \cdots \cup A_N]^* \\ &= [A_1 + A_2 + \cdots + A_N]^*. \end{aligned} \tag{2-58}$$

We find that the admissible force set F is the dual polyhedral convex cone of the convex sum of polyhedral convex cones A_1 through A_N. Using algorithm CONVEXSUM, we can compute the convex sum. Next, using algorithm DUAL, we can compute the polar F of the convex sum. Thus, we can compute the admissible force set F using the procedure shown in Table 3. The polyhedral convex cone F computed in this procedure gives the admissible force set.

It should be noted that both the admissible displacement set and the admissible force set are linear subspaces and orthogonal complements with each other when the geometric constraints are bidirectional [Mason, 82]. On the other hand, both sets are not linear subspaces but a union of PCC and its dual PCC when the constraints are unidirectional.

2.7 Numerical Example

We demonstrate the computation procedures described in the previous section by taking a simple example shown in Figure 8. The fixture is modeled by four points P_1 through P_4. Point P_1 is in contact with surface L_1, and points P_3 and P_4 with surface L_4. Point P_2 is in contact with a convex apex defined as the intersection of surfaces L_2 and L_3. Let $\boldsymbol{x}_i$ be the coordinates of the i-th fixed point and $\boldsymbol{n}_{ij}$ be the outward normal vector of the j-th surface at the contact point.

Let us compute the admissible displacement set A. Inequality conditions for displacement $\Delta\boldsymbol{q}$ to be admissible at individual contact points are derived as:

$$\boldsymbol{d}_{11}^T \Delta\boldsymbol{q} \leq 0 \tag{2-59}$$

$$\boldsymbol{d}_{22}^T \Delta\boldsymbol{q} \leq 0 \quad \text{or} \quad \boldsymbol{d}_{23}^T \Delta\boldsymbol{q} \leq 0 \tag{2-60}$$

$$\boldsymbol{d}_{34}^T \Delta\boldsymbol{q} \leq 0 \tag{2-61}$$

$$\boldsymbol{d}_{44}^T \Delta\boldsymbol{q} \leq 0 \tag{2-62}$$

where

$$\boldsymbol{d}_{ij} = \begin{bmatrix} \boldsymbol{n}_{ij} \\ \boldsymbol{x}_i \times \boldsymbol{n}_{ij} \end{bmatrix}. \tag{2-63}$$

Computing the value of vector $\boldsymbol{d}_{ij}$, we have

$$\begin{aligned} \boldsymbol{d}_{11} &= [0,\ 1,\ 1]^T \\ \boldsymbol{d}_{22} &= [-1,\ 1,\ -2]^T \\ \boldsymbol{d}_{23} &= [-1,\ -1,\ 2]^T \\ \boldsymbol{d}_{34} &= [0,\ -1,\ 0]^T \\ \boldsymbol{d}_{44} &= [0,\ -1,\ -2]^T \end{aligned} \tag{2-64}$$

Expanding eqs.(2-59) through (2-62), the admissible displacement set A is described by

$$A = A_1 \cup A_2 \tag{2-65}$$

where

$$A_1 = face\{\boldsymbol{d}_{11}, \boldsymbol{d}_{22}, \boldsymbol{d}_{34}, \boldsymbol{d}_{44}\}, \tag{2-66}$$

$$A_2 = face\{\boldsymbol{d}_{11}, \boldsymbol{d}_{23}, \boldsymbol{d}_{34}, \boldsymbol{d}_{44}\}. \tag{2-67}$$

(a) Form Closure Grasp

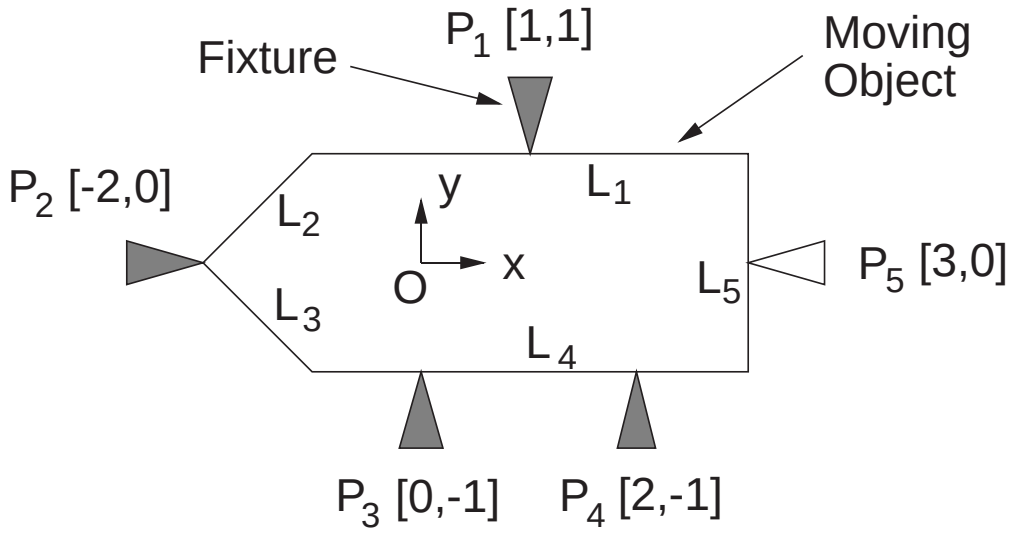

Figure 8: Simple example of planar object and fixed points

Using the procedure listed in Table 1, we find that subset A_1 involves a non-zero element, $[1,0,0]^T$. Therefore, this grasp is not form closure.

Adding another fixture P_5 as shown in the figure, the admissible displacement set A is given by

$$A = A_3 \cup A_4 \tag{2-68}$$

where

$$A_3 = face\{\boldsymbol{d}_{11}, \boldsymbol{d}_{22}, \boldsymbol{d}_{34}, \boldsymbol{d}_{44}, \boldsymbol{d}_{55}\}, \tag{2-69}$$

$$A_4 = face\{\boldsymbol{d}_{11}, \boldsymbol{d}_{23}, \boldsymbol{d}_{34}, \boldsymbol{d}_{44}, \boldsymbol{d}_{55}\}. \tag{2-70}$$

Computing vector $\boldsymbol{d}_{55}$, we have

$$\boldsymbol{d}_{55} = [1,0,0]^T. \tag{2-71}$$

Using the same procedure, we find that subsets A_3 and A_4 involve no non-zero elements. Therefore, the form closure condition is satisfied by adding the fixture P_5.

(b) Accessibility and Detachability

Since the admissible displacement set A involves non-zero elements, the accessible/detachable condition is satisfied. Using the procedure listed in Table 2, we find

that the interior sets A_1^{int} and A_2^{int} are empty sets. Therefore, this example is not strongly accessible/detachable.

Removing fixture P_1, the admissible displacement set A is given by

$$A = A_5 \cup A_6 \tag{2-72}$$

where

$$A_5 = face\{\boldsymbol{d}_{22}, \boldsymbol{d}_{34}, \boldsymbol{d}_{44}\}, \tag{2-73}$$
$$A_6 = face\{\boldsymbol{d}_{23}, \boldsymbol{d}_{34}, \boldsymbol{d}_{44}\}. \tag{2-74}$$

Using the same procedure, we find that the interior set A_5^{int} involves a non-zero element, $[2, 1, 0]^T$. Therefore, the strongly accessible/detachable condition is satisfied by removing the fixture P_1.

Let us compute the admissible force set F from the admissible displacement set $A = A_1 \cup A_2$ by using the procedure listed in Table 3. The admissible force set F is then given by

$$F = face\{[1, 0, 0]^T\}. \tag{2-75}$$

Namely,

$$F = \{[f_x, f_y, m]^T \mid f_x \leq 0\} \tag{2-76}$$

where f_x and f_y are translational forces along the x- and y-axes, respectively, and m is a moment. This equation shows that while the translational force f_x is non-positive, the force acting upon the object by a robot is balanced with reaction forces against the fixed points P_1 through P_4 and the object is not accelerated. Describing the admissible force set in the span form, we have

$$F = span\{\boldsymbol{d}_{11}, \boldsymbol{d}_{34}, \boldsymbol{d}_{44}, [-1, 0, 0]^T\} \tag{2-77}$$

Forces $\boldsymbol{d}_{11}$, $\boldsymbol{d}_{34}$, and $\boldsymbol{d}_{44}$ are balanced with reaction forces against the fixed points P_1, P_3, and P_4, respectively. Force $[-1, 0, 0]^T$ is balanced with a reaction force against point P_2. This example shows a case where a reaction force is generated between convex apices though no reaction forces act usually at the contact point between convex apices.

(c) Force Closure Grasp

Assuming that all of the contact points are frictionless, the admissible force set F is given by eq.(2-75). Examining the force closure condition eq.(2-55), we find that the polar of the admissible force set F involves a non-zero element, $[1,0,0]^T$. Therefore, this grasp is not force closure.

Let us consider friction between the moving object and the fixed points. Friction is represented by the *friction cone* [Erdmann, 86], which specifies the range of reaction forces. The axis of the cone is parallel to the normal vector of the surface, $\boldsymbol{n}_{ij}$. Sides of the cone make an angle $\tan^{-1}\mu$, where μ denotes the coefficient of friction. In the planar motion, the friction cone FC is a polyhedral convex cone given by

$$FC = span\{\boldsymbol{n}_{ij}^-, \boldsymbol{n}_{ij}^+\} \tag{2-78}$$

$$\boldsymbol{n}_{ij}^- = \boldsymbol{n}_{ij} - \mu\boldsymbol{\alpha}_{ij} \tag{2-79}$$

$$\boldsymbol{n}_{ij}^+ = \boldsymbol{n}_{ij} + \mu\boldsymbol{\alpha}_{ij} \tag{2-80}$$

where $\boldsymbol{\alpha}_{ij}$ is the tangent vector of the surface. The admissible force set is then derived by replacing span vector $\boldsymbol{d}_{ij}$ by the two vectors given by

$$\boldsymbol{d}_{ij}^- = \begin{bmatrix} \boldsymbol{n}_{ij}^- \\ \boldsymbol{x}_i \times \boldsymbol{n}_{ij}^- \end{bmatrix} \tag{2-81}$$

$$\boldsymbol{d}_{ij}^+ = \begin{bmatrix} \boldsymbol{n}_{ij}^+ \\ \boldsymbol{x}_i \times \boldsymbol{n}_{ij}^+ \end{bmatrix} \tag{2-82}$$

Removing point P_2, the admissible force set is given by

$$F = span\{\boldsymbol{d}_{11}^-, \boldsymbol{d}_{11}^+, \boldsymbol{d}_{34}^-, \boldsymbol{d}_{34}^+, \boldsymbol{d}_{44}^-, \boldsymbol{d}_{44}^+\}. \tag{2-83}$$

Examining the force closure condition eq.(2-55), we find that the polar of the admissible force set F involves no non-zero elements if coefficient μ is positive. Therefore, this grasp is a force closure grasp regardless the existence of point P_2.

2.8 Converting Forms of Polyhedral Convex Cones

As mentioned in the previous section, algorithm CONVERT is the most fundamental procedure in the analysis and planning of manipulation based on the theory of polyhedral convex cones. In this section, we develop an efficient algorithm to convert a polyhedral convex cone from face-form to span-form.

2.8.1 Solving Linear Simultaneous Inequalities

Span-form of a polyhedral convex cone can be obtained by solving linear simultaneous inequalities defined by its face vectors. In this section, we develop an efficient procedure to solve a set of linear simultaneous inequalities.

Let A be a polyhedral convex cone given by its face-form:

$$A = face\{\boldsymbol{a}_1, \boldsymbol{a}_2, \cdots, \boldsymbol{a}_m\} \tag{2-84}$$

Cone A can be divided into 2^m subsets depending upon whether inner product $\boldsymbol{a}_i^T \boldsymbol{x}$ is negative or equal to zero. Let us describe each subset as follows:

$$A[I] \stackrel{\triangle}{=} \{\boldsymbol{x} \mid \boldsymbol{a}_i^T \boldsymbol{x} < 0 \ \ \forall i \in I, \ \ \boldsymbol{a}_i^T \boldsymbol{x} = 0 \ \ \forall i \notin I\} \tag{2-85}$$

where I is a subset of indices 1 through m:

$$I \subset \{1, 2, \cdots, m\} \tag{2-86}$$

Let $O[I]$ and $L[I]$ be subsets defined as follows:

$$O[I] \stackrel{\triangle}{=} \{\boldsymbol{x} \mid \boldsymbol{a}_i^T \boldsymbol{x} < 0 \quad \forall i \in I\} \tag{2-87}$$

$$L[I] \stackrel{\triangle}{=} \{\boldsymbol{x} \mid \boldsymbol{a}_i^T \boldsymbol{x} = 0 \quad \forall i \notin I\} \tag{2-88}$$

Subset $A[I]$ is then given by an intersection of an open set $O[I]$ and a linear subspace $L[I]$:

$$A[I] = O[I] \cap L[I] \tag{2-89}$$

Note that subset $A[\phi]$ coincides a linear subspace $L[\phi]$. Let $d[I]$ be a dimension of the linear subspace $L[I]$:

$$d[I] \stackrel{\triangle}{=} dim L[I] \tag{2-90}$$

Let d be the dimension of linear subspace $A[\phi]$:

$$d = d[\phi] = dim A[\phi] \tag{2-91}$$

Let I_1 through I_k be index sets that satisfy the following conditions:

$$A[I] \neq \phi \ \text{ and } \ d[I] = d + 1 \tag{2-92}$$

Let $\boldsymbol{e}_1$ through $\boldsymbol{e}_d$ be base vectors of the linear subspace $A[\phi]$ and $\boldsymbol{f}_j$ be an arbitrary vector involved in set $A[I_j]$. According to [Goldman and Tucker, 56], the span-form of A is then described by

$$A = span\{\pm\boldsymbol{e}_1, \pm\boldsymbol{e}_2, \cdots, \pm\boldsymbol{e}_d, \boldsymbol{f}_1, \boldsymbol{f}_2, \cdots, \boldsymbol{f}_k\}. \tag{2-93}$$

We can find linearly independent vectors $\boldsymbol{e}_1$ through $\boldsymbol{e}_d$ by solving the simultaneous equations

$$\boldsymbol{a}_i^T \boldsymbol{x} = 0, \quad \forall i \in [1, m]. \tag{2-94}$$

The condition for vector $\boldsymbol{x}$ to be involved in $A[I]$ is represented by

$$\boldsymbol{a}_i^T \boldsymbol{x} < 0, \qquad \forall i \in I \tag{2-95}$$

$$\boldsymbol{a}_i^T \boldsymbol{x} = 0, \qquad \forall i \notin I \tag{2-96}$$

This condition can be reduced to a feasibility check problem in linear programming. Thus, we can examine this condition by using the first stage of the simplex method [Dantzig, 63]. The number of sets I is less than 2^m. Therefore, we can derive vectors $\boldsymbol{f}_1$ through $\boldsymbol{f}_k$ by solving at most 2^m linear programming problems.

The above procedure to convert face-form to span-form is inefficient since it requires to solve at most 2^m linear programming problems. Thus, we refine the above procedure so that it can convert face-form to span-form efficiently. In order to obtain vector $\boldsymbol{f}_j$, we first compute dimension $d[I]$, examine whether the dimension is equal to $d+1$, and then find an arbitrary vector involved in subset $A[I]$ by solving a linear programming problem. Dimension $d[I]$ can be computed by solving the following simultaneous equations:

$$\boldsymbol{a}_i^T \boldsymbol{x} = 0, \quad \forall i \notin I \tag{2-97}$$

Solving the above equations, we can obtain base vectors of linear subspace $L[I]$ as well as dimension $d[I]$. Thus, base vectors $\boldsymbol{b}_1$ through $\boldsymbol{b}_{d+1}$ can be computed when dimension $d[I]$ is equal to $d+1$. Using the following theorem, we can derive a vector involved in a subset $A[I]$ from the obtained base vectors without solving a linear programming problem.

Theorem 2 *Assume that subset $A[I]$ is not empty and that dimension $d[I]$ is equal to $d+1$. Let $\boldsymbol{b}_1$ through $\boldsymbol{b}_{d+1}$ be base vectors of a linear subspace $L[I]$. Then, there exists vector $\boldsymbol{b}_j$ which satisfies the following condition:*

$$\boldsymbol{a}_i^T \boldsymbol{b}_j < 0, \ \forall i \in I \quad or \quad \boldsymbol{a}_i^T \boldsymbol{b}_j > 0, \ \forall i \in I \tag{2-98}$$

The proof is shown in Appendix D. It implies that vector $\boldsymbol{b}_j$ is involved in subset $A[I]$ when inner products $\boldsymbol{a}_i^T \boldsymbol{b}_j$ are negative for all $i \in I$ while vector $-\boldsymbol{b}_j$ is involved in the subset when all the inner products are positive. Therefore, we can compute vectors $\boldsymbol{f}_1$ through $\boldsymbol{f}_k$ by using an algorithm to solve simultaneous equations, which is necessary to compute vectors $\boldsymbol{e}_1$ through $\boldsymbol{e}_d$ as well.

The original procedure requires to examine eq.(2-92) for all combinations of indices. In order to reduce the computation time, it is efficient to eliminate unfeasible combinations. We can reduce the number of combinations using the following theorem.

Theorem 3 *Let I and $\tilde{I}$ be subsets of indices. Assume that I is a proper subset of $\tilde{I}$ and that dimension $d[I]$ is equal to $d[\tilde{I}]$:*

$$\begin{aligned} & I \subset \tilde{I}, \\ & I \neq \tilde{I}, \\ & d[I] = d[\tilde{I}] \end{aligned} \tag{2-99}$$

Then, $A[\tilde{I}]$ is an empty set.

The proof is shown in Appendix E. Note that dimension $d[I]$ is more than or equal to $d[\tilde{I}]$ when I is a subset of $\tilde{I}$. Therefore, set $A[\tilde{I}]$ is empty or dimension $d[\tilde{I}]$ is more than $d+1$ if the following condition is satisfied.

$$\begin{aligned} & I \subset \tilde{I}, \\ & I \neq \tilde{I}, \\ & d[I] = d+1 \end{aligned} \tag{2-100}$$

It implies that set $\tilde{I}$ does not satisfy eq.(2-92). Therefore, we can eliminate all the supersets $\tilde{I}$ of an index set I if dimension $d[I]$ is equal to $d+1$.

2.8.2 Reduction of Polyhedral Convex Cones

In order to reduce the number of combinations, it is efficient to eliminate unnecessary face vectors. In this section, we develop an algorithm to simplify a polyhedral convex cone by eliminating unnecessary face vectors or span vectors.

Let us consider a simple example shown in Figure 9. In the case shown in Figure 9-(a), a polyhedral convex cone $A = span\{\boldsymbol{u}_1, \boldsymbol{u}_2, \boldsymbol{u}_3\}$ can be reduced as $A = span\{\boldsymbol{u}_1, \boldsymbol{u}_2\}$ by eliminating span vector $\boldsymbol{u}_3$. Note that span vector $\boldsymbol{u}_3$ is described by a convex sum of $\boldsymbol{u}_1$ and $\boldsymbol{u}_2$.

$$\exists c_1, c_2 \geq 0 \quad \text{s.t.} \quad \boldsymbol{u}_3 = c_1 \boldsymbol{u}_1 + c_2 \boldsymbol{u}_2$$

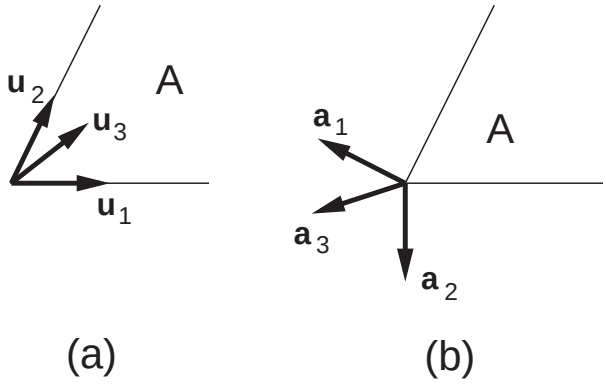

Figure 9: Simplification of polyhedral convex cones

In the case shown in Figure 9-(b), a polyhedral convex cone $A = face\{\boldsymbol{a}_1, \boldsymbol{a}_2, \boldsymbol{a}_3\}$ can be reduced as $A = face\{\boldsymbol{a}_1, \boldsymbol{a}_2\}$ by eliminating face vector $\boldsymbol{a}_3$. Note that span vector $\boldsymbol{a}_3$ is described by a convex sum of $\boldsymbol{a}_1$ and $\boldsymbol{a}_2$.

$$\exists c_1, c_2 \geq 0 \quad \text{s.t.} \quad \boldsymbol{a}_3 = c_1\boldsymbol{a}_1 + c_2\boldsymbol{a}_2$$

In general, the following theorem can be proved.

Theorem 4 *A polyhedral convex cone*

$$A = span\{\boldsymbol{u}_1, \boldsymbol{u}_2, \cdots, \boldsymbol{u}_k\} \tag{2-101}$$

can be reduced as

$$A = span\{\boldsymbol{u}_1, \cdots, \boldsymbol{u}_{j-1}, \boldsymbol{u}_{j+1}, \cdots, \boldsymbol{u}_k\} \tag{2-102}$$

if and only if the following equation is satisfied.

$$\exists c_1, \cdots, c_{j-1}, c_{j+1}, \cdots, c_k \geq 0 \quad s.t. \quad \boldsymbol{u}_j = \sum_{i=1, i\neq j}^{k} c_i\boldsymbol{u}_i. \tag{2-103}$$

A polyhedral convex cone

$$A = face\{\boldsymbol{a}_1, \boldsymbol{a}_2, \cdots, \boldsymbol{a}_m\} \tag{2-104}$$

can be reduced as

$$A = face\{\boldsymbol{a}_1, \cdots, \boldsymbol{a}_{j-1}, \boldsymbol{a}_{j+1}, \cdots, \boldsymbol{a}_m\} \tag{2-105}$$

if and only if the following equation is satisfied.

$$\exists c_1, \cdots, c_{j-1}, c_{j+1}, \cdots, c_m \geq 0 \quad s.t. \quad \boldsymbol{a}_j = \sum_{i=1, i \neq j}^{m} c_i \boldsymbol{a}_i. \tag{2-106}$$

The proof of this theorem is shown in Appendix F. The conditions given by eqs.(2-103) and (2-106) can be reduced to a feasibility check problem in linear programming, which can be examined by using the first stage of the simplex method [Dantzig, 63]. Iterating this procedure, we can obtain the simplest form of polyhedral convex cones. This procedure to derive the simplest form of polyhedral convex cones is referred to as algorithm REDUCTION in this paper. Using algorithm REDUCTION, we can eliminate unnecessary face vectors before solving simultaneous equations. Therefore, we can reduce the number of combinations using algorithm REDUCTION.

2.8.3 Finding Bidirectional Constraints

Bidirectional constraints have different properties from those of unidirectional constraints in many manipulative tasks. For example, the condition for strongly accessible/detachable constraints depends upon whether the constraints are unidirectional or bidirectional [Asada and By, 85]. In this section, we investigate the properties of bidirectional constraints and eliminate unfeasible combinations of face vectors using the properties.

Let us take the example shown in Figure 8. Removing fixture P_1 and adding fixture P_5, the admissible displacement set A is given by

$$A = face\{\boldsymbol{d}_{11}, \boldsymbol{d}_{34}, \boldsymbol{d}_{44}, \boldsymbol{d}_{55}\}.$$

The following equations are then satisfied for an arbitrary displacement $\Delta \boldsymbol{q}$ involved in A:

$$(\boldsymbol{d}_{11})^T \Delta \boldsymbol{q} = 0$$
$$(\boldsymbol{d}_{34})^T \Delta \boldsymbol{q} = 0$$
$$(\boldsymbol{d}_{44})^T \Delta \boldsymbol{q} = 0$$

These equations imply that the constraint imposed by a set of face vectors $\boldsymbol{d}_{11}$, $\boldsymbol{d}_{34}$, and $\boldsymbol{d}_{44}$ is bidirectional though individual face vectors represent unidirectional constraints as mentioned before. Note that the following equation is satisfied for these face vectors.

$$2\boldsymbol{d}_{11} + \boldsymbol{d}_{34} + \boldsymbol{d}_{44} = \boldsymbol{o}$$

In general, the following theorem can be proved.

Theorem 5 *Let A be a polyhedral convex cone given by its face-form:*

$$A = face\{\boldsymbol{a}_1, \boldsymbol{a}_2, \cdots, \boldsymbol{a}_m\} \tag{2-107}$$

The constraint imposed by a set of face vectors $\boldsymbol{a}_1$ through $\boldsymbol{a}_k$ is bidirectional, namely

$$\boldsymbol{a}_i^T \boldsymbol{r} = 0, \quad \forall \boldsymbol{r} \in A \quad \forall i \in [1, k] \tag{2-108}$$

if

$$\exists \alpha_1, \alpha_2, \cdots, \alpha_k > 0 \quad s.t. \quad \sum_{i=1}^{k} \alpha_i \boldsymbol{a}_i = \mathbf{o} \tag{2-109}$$

is satisfied.

The proof is shown in Appendix G. From this theorem, we can easily show that the inner product $\boldsymbol{a}_j \boldsymbol{r}$ is equal to zero for an arbitrary vector $\boldsymbol{r}$ involved in A, namely

$$\boldsymbol{a}_j^T \boldsymbol{r} = 0, \quad \forall \boldsymbol{r} \in A \tag{2-110}$$

if the following condition is satisfied.

$$\exists \alpha_1, \alpha_2, \cdots, \alpha_k \geq 0, \quad \exists j \in [1, k] \text{ s.t. } \alpha_j = 1, \quad \sum_{i=1}^{k} \alpha_i \boldsymbol{a}_i = \mathbf{o} \tag{2-111}$$

This condition can be reduced to a feasibility check problem in linear programming. Thus, we can examine this condition by using the first stage of the simplex method [Dantzig, 63]. Therefore, we can derive a set of face vectors which imposes bidirectional constraints. This algorithm to find a set of face vectors imposing bidirectional constraints is referred to as BIDIRECTION in this paper.

Let $\boldsymbol{a}_j$ be a face vector that satisfy eq.(2-111). Then, inner product $\boldsymbol{a}_j^T \boldsymbol{r}$ is equal to zero for an arbitrary vector $\boldsymbol{r}$ involved in cone A. It implies that subset $A[I]$ is empty set if j is involved in index set I. Let B be a set of indices that satisfy eq.(2-111), which can be derived using algorithm BIDIRECTION. Then, subset $A[I]$ is empty if index set I involves a member of set B. It implies that we can reduce the whole set of indices as follows:

$$I \subset B^c = \{1, 2, \cdots, m\} - B \tag{2-112}$$

where B^c denotes the complement of set B. Therefore, we can reduce the number of combinations of face vectors using algorithm BIDIRECTION.

2.9 Concluding Remarks

In this paper, we have presented a new approach to the kinematic and static analysis of object motion constrained by mechanical contacts. Mechanical contacts between workpieces are unidirectional constraints, which are described by a set of homogeneous linear inequalities. Thus, we developed an efficient mathematical tool based on the theory of polyhedral convex cones, which allows us to treat fundamental inequalities in a simple and systematic manner.

We first showed that the workpiece motion is described by a set of inequalities. We have also formulated the force equilibrium condition for unidirectional constraints by an inequality condition. Applying the theory of polyhedral convex cones, we developed a mathematical tool to solve the inequality conditions in a straightforward manner. We implemented computation algorithms of the polyhedral convex cones in order to treat the inequalities on a computer and we applied this method to task planning of grasping and assembly.

Appendix A Proof of eq.(2-37)

Since union $A \cup B$ is a subset of convex sum $A + B$, the polar of the convex sum is a subset of the polar of the union:

$$(A \cup B)^* \supset (A + B)^* \tag{A-1}$$

Let $\boldsymbol{z}$ be an arbitrary vector involved in $(A \cup B)^*$. From the definition of polar, we have

$$\boldsymbol{x}^T \boldsymbol{z} \leq 0, \quad \forall \boldsymbol{x} \in A, \tag{A-2}$$

$$\boldsymbol{y}^T \boldsymbol{z} \leq 0, \quad \forall \boldsymbol{y} \in B. \tag{A-3}$$

They follow that

$$(\boldsymbol{x} + \boldsymbol{y})^T \boldsymbol{z} \leq 0, \quad \forall \boldsymbol{x} \in A \quad \forall \boldsymbol{y} \in B. \tag{A-4}$$

Since $\boldsymbol{x} + \boldsymbol{y}$ is involved in convex sum $A + B$, vector $\boldsymbol{z}$ is involved in the polar of the convex sum:

$$\boldsymbol{z} \in (A + B)^* \tag{A-5}$$

Thus,

$$(A \cup B)^* \subset (A + B)^*. \tag{A-6}$$

From eqs.(A-1) and (A-6), we have

$$(A \cup B)^* = (A + B)^*. \tag{A-7}$$

Appendix B Proof of eq.(2-44)

Let A and B are polyhedral convex cones given by

$$A = span\{\boldsymbol{u}_1, \boldsymbol{u}_2, \cdots, \boldsymbol{u}_k\}, \tag{B-1}$$

$$B = face\{\boldsymbol{a}_1, \boldsymbol{a}_2, \cdots, \boldsymbol{a}_m\}. \tag{B-2}$$

An arbitrary element $\boldsymbol{x}$ involved in A can be described by

$$\boldsymbol{x} = \sum_{j=1}^{k} c_j \boldsymbol{u}_j, \quad c_j \geq 0 \tag{B-3}$$

Note that the inner product $\boldsymbol{a}_i^T \boldsymbol{u}_j$ is non-positive if all $\boldsymbol{u}_j$ is involved in B. Then, we have

$$\boldsymbol{a}_i^T \boldsymbol{x} = \sum_{j=1}^{k} c_j (\boldsymbol{a}_i^T \boldsymbol{u}_j) \leq 0, \quad \forall i \in [1, m]. \tag{B-4}$$

It implies that vector $\boldsymbol{x}$ is involved in B, namely, $A \subset B$. The sufficient condition is thus proved.
Assume that one span vector $\boldsymbol{u}_j$ is not involved in B. Note that $\boldsymbol{u}_j$ is involved in A. It implies that $A \not\subset B$. Thus, all span vectors $\boldsymbol{u}_j$ is involved in B if A is a subset of B. The necessary condition is thus proved.

Appendix C Proof of eq.(2-45)

Let A be a polyhedral convex cone given by

$$A = face\{\boldsymbol{a}_1, \boldsymbol{a}_2, \cdots, \boldsymbol{a}_m\} \tag{C-1}$$

$$= span\{\boldsymbol{u}_1, \boldsymbol{u}_2, \cdots, \boldsymbol{u}_k\}. \tag{C-2}$$

The interior set A^{int} is then described as

$$A^{int} = \{\boldsymbol{x} \mid \boldsymbol{a}_i^T \boldsymbol{x} < 0, \quad \forall i \in [1, m]\}. \tag{C-3}$$

The necessary condition is obvious since vector $\boldsymbol{u}_j$ is involved in set A^{int} given in eq.(C-3). Let us prove the sufficient condition. Since A^{int} is involved in A, an arbitrary element $\boldsymbol{x}$ involved in A^{int} can be expressed as

$$\boldsymbol{x} = \sum_{j=1}^{k} c_j \boldsymbol{u}_j, \quad c_j \geq 0. \tag{C-4}$$

Thus, any element $\boldsymbol{x}$ involved in the interior set A^{int} must satisfy the following condition:

$$\boldsymbol{a}_i^T \boldsymbol{x} = \sum_{j=1}^{k} c_j (\boldsymbol{a}_i^T \boldsymbol{u}_j) < 0, \quad \forall i \in [1, m] \tag{C-5}$$

Since coefficients c_j is non-negative, one of the inner products $\boldsymbol{a}_i^T \boldsymbol{u}_1$ through $\boldsymbol{a}_i^T \boldsymbol{u}_k$ must be negative. Namely,

$$\forall i \in [1, m] \; \exists j \in [1, k] \;\; \text{s.t.} \;\; \boldsymbol{a}_i^T \boldsymbol{u}_j < 0. \tag{C-6}$$

Appendix D Proof of theorem 2

Let $\boldsymbol{e}_1$ through $\boldsymbol{e}_d$ be base vectors of linear subspace $A[\phi]$. Since $A[\phi]$ is a proper subset of $L[\phi]$, there exists $\boldsymbol{b}_j$ not involved in $A[\phi]$. Let $\boldsymbol{x}$ be a vector involved in $A[I]$ $(\neq \phi)$. Since $\boldsymbol{b}_j$ and $\boldsymbol{e}_1$ through $\boldsymbol{e}_d$ is a set of base vectors of linear subspace $L[I]$, vector bmx can be described as

$$\boldsymbol{x} = \beta \boldsymbol{b}_j + \sum_{k=1}^{d} \beta_k \boldsymbol{e}_k. \tag{D-1}$$

The following equation is then satisfied for all indices $i \in I$:

$$\boldsymbol{a}_i^T \boldsymbol{x} = \beta \boldsymbol{a}_i^T \boldsymbol{b}_j < 0 \tag{D-2}$$

Note that β is not equal to zero since $\boldsymbol{x}$ is not involved in $A[\phi]$. The following equation is satisfied if coefficient β is positive:

$$\boldsymbol{a}_i^T \boldsymbol{b}_j < 0, \quad \forall i \in I \tag{D-3}$$

The following equation is satisfied if β is negative:

$$\boldsymbol{a}_i^T \boldsymbol{b}_j > 0, \quad \forall i \in I \tag{D-4}$$

Therefore, there exists vector $\boldsymbol{b}_j$ which satisfies eq.(2-98).

Appendix E Proof of theorem 3

Let l be an index involved in $\tilde{I} - I$. Since dimension $d[\tilde{I}]$ is equal to $d[I]$, face vector $\boldsymbol{a}_l$ can be described as a linear combination of face vectors $\boldsymbol{a}_i (i \in I)$.

$$\boldsymbol{a}_l = \sum_{i \in I} \alpha_i \boldsymbol{a}_i \tag{E-1}$$

Let $\boldsymbol{x}$ be an arbitrary vector involved in $A[\tilde{I}]$. Since I is a subset of $\tilde{I}$, the following equation is satisfied:

$$\boldsymbol{a}_i^T \boldsymbol{x} = 0, \quad \forall i \in I \tag{E-2}$$

From eqs (E-1) and (E-2), we have

$$\boldsymbol{a}_l^T \boldsymbol{x} = 0. \tag{E-3}$$

Since index l is involved in $\tilde{I}$, we have

$$\boldsymbol{a}_l^T \boldsymbol{x} < 0. \tag{E-4}$$

The above equations contradict each other. Therefore, set $A[\tilde{I}]$ is empty.

Appendix F Proof of theorem 4

Let us first consider polyhedral convex cones given by their span-forms. Let A and $\tilde{A}$ be polyhedral convex cones given by

$$\begin{aligned} A &= span\{\boldsymbol{u}_1, \boldsymbol{u}_2, \cdots, \boldsymbol{u}_k\}, & \text{(F-1)} \\ \tilde{A} &= span\{\boldsymbol{u}_1, \cdots, \boldsymbol{u}_{j-1}, \boldsymbol{u}_{j+1}, \cdots, \boldsymbol{u}_k\}. & \text{(F-2)} \end{aligned}$$

Vector $\boldsymbol{u}_j$ is involved in A when cone A coincides $\tilde{A}$. It implies that vector $\boldsymbol{u}_j$ can be described by a linear combination of span vectors of cone $\tilde{A}$. The necessary condition is thus proved.
Let $\boldsymbol{x}$ be an arbitrary vector involved in cone A. Vector $\boldsymbol{x}$ is then described as

$$\boldsymbol{x} = \sum_{i=1}^{k} b_i \boldsymbol{u}_i. \tag{F-3}$$

where all the coefficients b_i are positive or equal to zero. From eq.(2-103), we find that vector $\boldsymbol{x}$ is described as

$$\boldsymbol{x} = \sum_{i=1, i\neq j}^{k} \tilde{b}_i \boldsymbol{u}_i \tag{F-4}$$

where

$$\tilde{b}_i = b_i + b_j c_i. \tag{F-5}$$

Since all the coefficients $\tilde{b}_i$ are positive or equal to zero, vector $\boldsymbol{x}$ is involved in $\tilde{A}$. It implies that cone A is a subset of $\tilde{A}$. From the properties of polyhedral convex cones, cone $\tilde{A}$ is a subset of A. Therefore, we find that cone $\tilde{A}$ coincides A. The sufficient condition is thus proved.
Let us consider polyhedral convex cones given by their face-forms. Let A and $\tilde{A}$ be polyhedral convex cones given by

$$\begin{aligned} A &= face\{\boldsymbol{a}_1, \boldsymbol{a}_2, \cdots, \boldsymbol{a}_k\}, \\ \tilde{A} &= face\{\boldsymbol{a}_1, \cdots, \boldsymbol{a}_{j-1}, \boldsymbol{a}_{j+1}, \cdots, \boldsymbol{a}_k\}. & \text{(F-6)} \end{aligned}$$

Their dual polyhedral convex cones are then given by

$$\begin{aligned} A^* &= span\{\boldsymbol{a}_1, \boldsymbol{a}_2, \cdots, \boldsymbol{a}_k\}, \\ \tilde{A}^* &= span\{\boldsymbol{a}_1, \cdots, \boldsymbol{a}_{j-1}, \boldsymbol{a}_{j+1}, \cdots, \boldsymbol{a}_k\}. & \text{(F-7)} \end{aligned}$$

Cone A^* coincides $\tilde{A}^*$ if and only if eq.(2-106) is satisfied. It implies that original cone A coincides $\tilde{A}$ if and only if eq.(2-106) is satisfied.

Appendix G Proof of theorem 5

Let $\boldsymbol{x}$ be an arbitrary vector involved in A. The inner products $\boldsymbol{a}_1^T\boldsymbol{x}$ through $\boldsymbol{a}_k^T\boldsymbol{x}$ are then negative or equal to zero. From eq.(2-111), we have

$$\sum_{i=1}^{k} \alpha_i \boldsymbol{a}_i^T \boldsymbol{x} = 0. \tag{G-1}$$

Since coefficients α_1 through α_k are positive, all the inner products $\boldsymbol{a}_1^T\boldsymbol{x}$ through $\boldsymbol{a}_k^T\boldsymbol{x}$ are equal to zero for an arbitrary vector $\boldsymbol{x}$ involved in cone A. Therefore, eq.(2-108) is satisfied.

Chapter 3
Global Representation of Assembly Processes Using Contact State Graphs

3.1 Introduction

An arm linkage is a holonomic system, which can be formulated by a single kinematic equation. In contrast, process models of manipulative tasks such as assembly are generally non-holonomic. In assembly tasks, objects contact each other in different ways and as a result the geometric constraints vary significantly as the assembly operation proceeds. The geometric constraints are described by different equations depending on the state of contacts between the objects. Kinematic behavior of the objects strongly depends upon the geometric constraints. Thus, real control laws for manipulative tasks are varying depending on the geometric constraints. A selection matrix in hybrid control, for example, must be switched if the geometric constraints vary in the process. A particular stiffness matrix, which is valid for a certain range of tasks, will be inadequate when the task condition varies significantly. Therefore, it is required to investigate the kinematic behavior of the constrained objects so that we can develop efficient task strategies depending on the geometric constraints.

In task planning, the assembly processes of a peg-into-hole mating have been analyzed extensively and a hand for fine insertion tasks has been designed [Nevins et al., 80] [Whitney, 82] [Whitney and Rourke, 86]. The process states of an assembly operation have been introduced for the automatic synthesis of motion strategies [Lozano-Pérez et al., 84] [Donald, 88] [Desai and Volz, 89] and backprojection techniques have been developed [Erdmann, 86]. In collision avoidance, the motion of rigid objects is analyzed to obtain collision-free paths [Lozano-Pérez and Wesley, 79] [Schwartz and Sharir, 83] [Schwartz and Sharir, 89].

In order to develop efficient task strategies, the global motion of workpieces must be represented in a simple and sufficient manner. In assembly tasks, workpieces contact each other in different ways and as a result the motion of workpieces is modeled by different many equations depending on the state of contacts. The analysis of assembly processes is thus complicated, which is a bottleneck in the kinematic analysis of manipulative tasks.

In this paper, we will develop a symbolic representation of assembly processes.

The kinematic properties of objects strongly depend upon the geometric constraints, which are characterized by the states of contacts between workpieces. Thus, we will first analyze the process of an assembly operation with regard to how the workpieces contact each other, and represent assembly processes with a contact state graph. An automatic generation of the graph is required in order to develop a planning system of assembly operations. Thus, we derive an efficient algorithm for automatically generating the graph from the geometric data of workpieces.

3.2 Contact State Graphs

3.2.1 Symbolic Representation of Contact States

Assembly is a process of locating and fixing workpieces together in a desired configuration. In this assembly process, the robot mates the workpieces by moving one workpiece along the appropriate surface of the other. During the operation, the workpieces contact each other at different surfaces. As the operation proceeds, the contacting pair of surfaces may change as shown in Figure 10. At the beginning, the moving part is not in contact with the fixed part and is therefore free to move. By contacting different surfaces, the moving part is guided to the desired destination despite uncertainties such as tolerancing errors and sensing errors. During this process, the workpiece motion is constrained by the contact, and the geometric constraints vary in accordance with the change of contacting surfaces. As the constraints change, the robot needs to change its control law accordingly. If hybrid position/force control is used, for example, the selection matrix along with the constraints frame must be changed. In impedance control, stiffness and damping matrices as well as motion trajectories must be changed so as to be consistent with the geometric constraints. Therefore, the geometric constraints due to the contacts are a fundamental characteristic to investigate when control laws and task strategies are being planned.

In this paper, we use a process model of assembly based on a symbolic description of the geometric constraints [Lozano-Pérez et al., 84] [Hirai et al., 88a] [Desai and Volz, 89]. As shown in Figure 10, individual facets and apices of the workpieces are labeled facet i and apex j, respectively. The contact between facet i and apex j is denoted as facet i– apex j. The geometric constraints imposed on the workpieces are determined by listing all the contacting pairs between the two. For example, contacts shown in Figure 10-(d) are described by

$$(\text{ facet } 2 - \text{apex } 1 \quad \text{apex } 4 - \text{facet } 7 \text{ }). \tag{3-1}$$

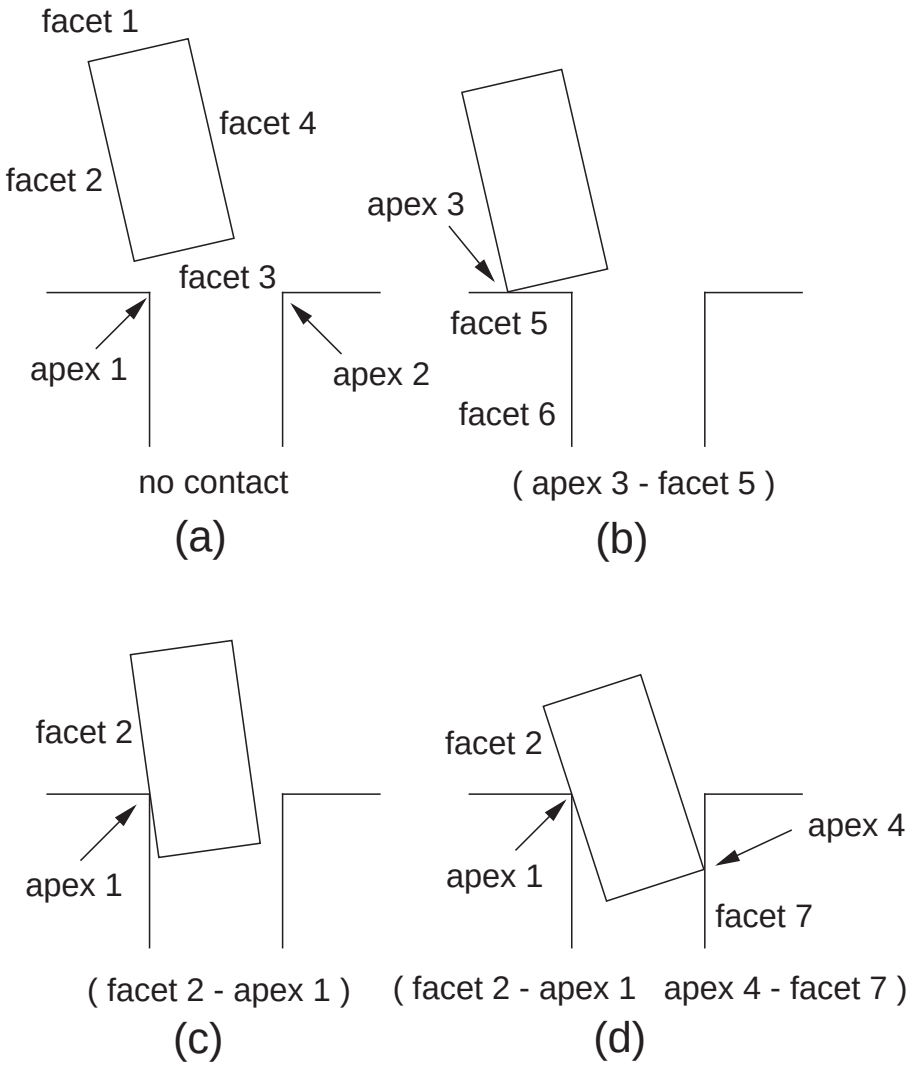

Figure 10: Contact states

The state of the assembly process described in the list of all the contacting pairs is referred to as *Contact State* [Hirai et al., 88a]. Each contact state has different constraints depending on the geometry of each contacting pair involved.

The contact state is determined by the position and orientation of one workpiece relative to the other. Without loss of generality, we assume that one workpiece is carried around by the robot and the other is fixed in space. Let us denote the position and orientation of the moving workpiece by the six-dimensional vector $\boldsymbol{q} \in V^6$ with respect to a coordinate system fixed to the other workpiece. Some configurations of the moving workpiece are prohibited because of the geometric interference between the two workpieces. The set of possible configurations is called *Admissible Configuration Space* and denoted by R [Arnold, 78] [Lozano-Pérez, 81] [Lozano-Pérez, 83]. The admissible configuration space R is divided into subsets that possess a different contact state N_i, and the set of workpiece configuration involved in the state N_i is denoted by subset $R_i \subset R$.

During assembly operations, the contact state may change from one to another. Let us model the change of contact state by a transition in a graph. As shown in Figure 11, we represent each contact state by a node of the graph and the possible transition between two contact states is denoted by the arc connecting the corresponding nodes. This graph is referred to as *Contact State Graph* in this paper. Investigating all admissible contact states and all possible transitions among the contact states, we can generate a contact state graph that provides a symbolic representation of assembly.

3.2.2 Mathematical Description of Contact States

Each contact pair determines a geometric constraint imposed on the workpieces. Let us formulate a geometric constraint provided by each contact pair. We assume that the moving and the fixed objects are rigid and that each object consists of a finite set of smooth faces. As shown in Figure 12, coordinate system $C - \xi\eta\zeta$ is fixed to the moving object while $O - xyz$ is fixed to the fixed object. Note that individual edges and apices can be described by an intersection of faces. Thus, some contact pairs can be decomposed into basic contact pairs. For example, when apex j of the moving object is in contact with an edge of the fixed object defined by the intersection of two faces, k and l, the contact pair between the apex and the edge can be expressed by two contact pairs, apex j – facet k and apex j – facet l. A contact pair between planar facets can be expressed by a set of apex – facet and facet – apex contact pairs. Contact pairs between non-planar facets can not be expressed by these two contact pairs. Excluding this particular case, in this paper we deal with the case where each contact pair can be expressed by a set of the following

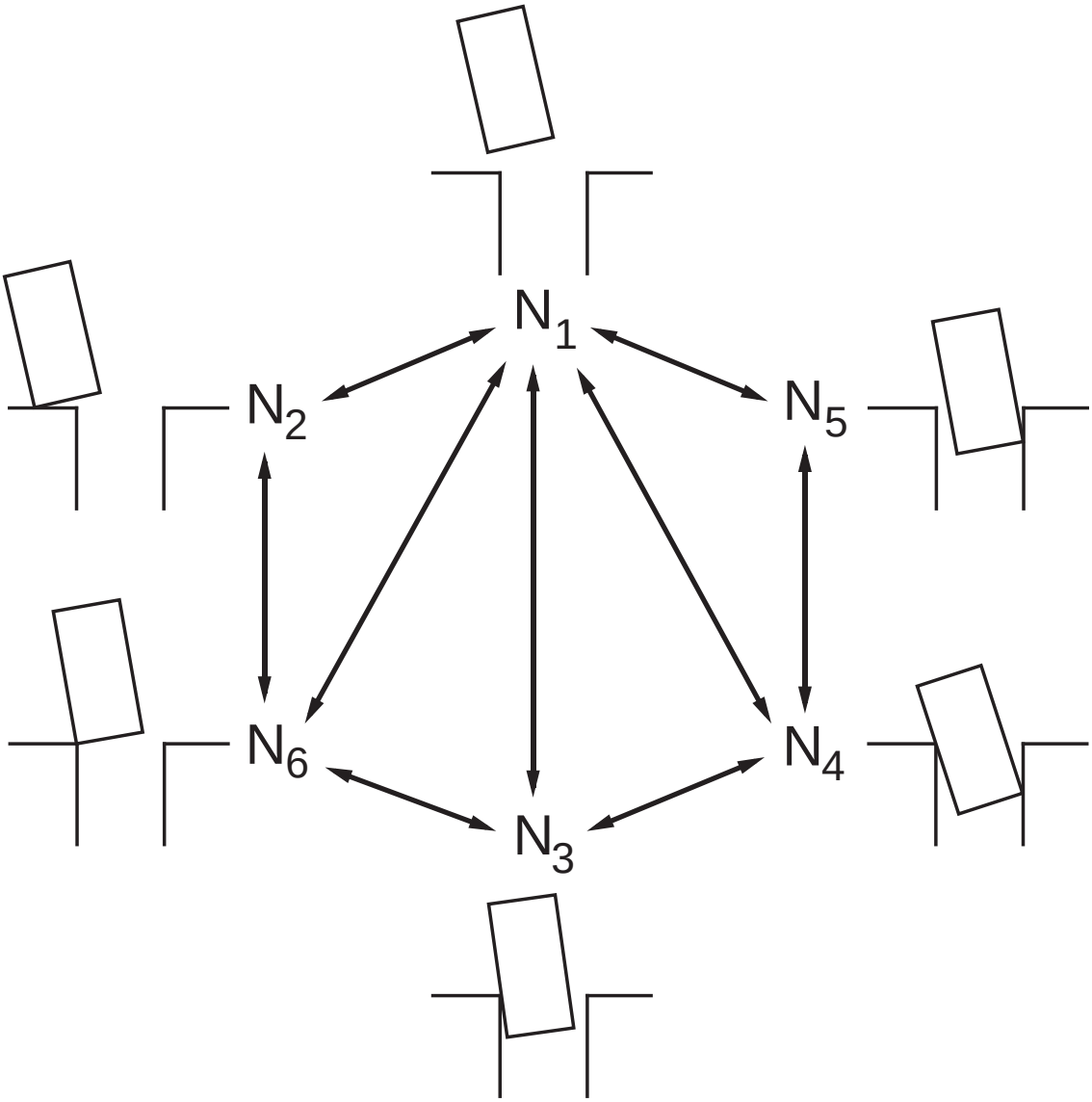

Figure 11: Graph representation of contact state transitions

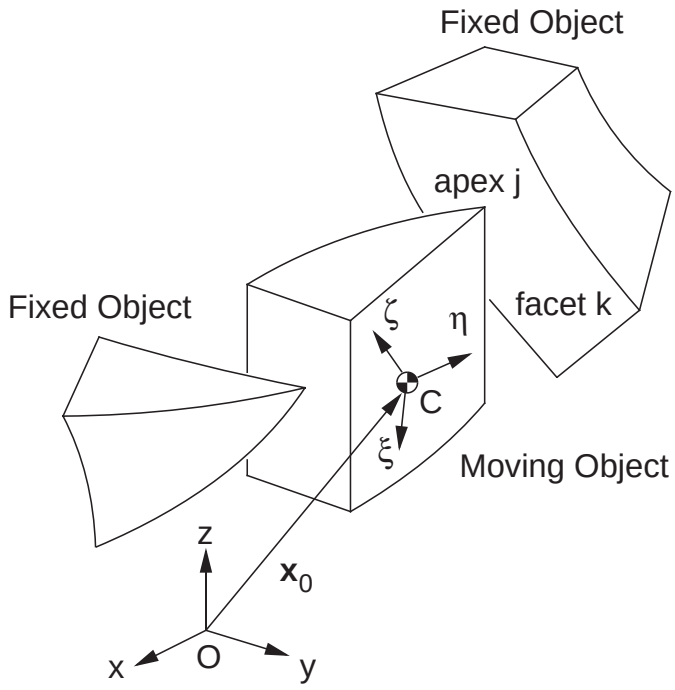

Figure 12: Geometric modeling of assembly process

pairs; apex – facet pairs and facet – apex pairs.

Let us first consider the case where an apex of the moving object is in contact with a facet of the fixed object. Let $h_k(\boldsymbol{x})$ be the distance between the coordinates $\boldsymbol{x} = [x, y, z]^T$ and the k-th smooth face of the fixed object. Let $\boldsymbol{x}_0 = [x_0, y_0, z_0]^T$ and $\boldsymbol{\theta}_0 = [\theta_0, \phi_0, \psi_0]^T$ be the position and the orientation of the moving object, respectively. The coordinate transformation from $\boldsymbol{\xi} = [\xi, \eta, \zeta]^T$ to $\boldsymbol{x}$ is then given by

$$\boldsymbol{x} = A(\boldsymbol{\theta}_0)\boldsymbol{\xi} + \boldsymbol{x}_0 \tag{3-2}$$

where $A(\boldsymbol{\theta}_0)$ is a rotation matrix. Let $\boldsymbol{\xi}_j$ be the coordinates of apex j on the moving object. Then, the condition for apex j of the moving object to be in contact with facet k of the fixed object is given by

$$h_k[A(\boldsymbol{\theta}_0)\boldsymbol{\xi}_j + \boldsymbol{x}_0] = 0. \tag{3-3}$$

Similarly, let us consider the case where an apex of the fixed object is in contact with a smooth facet of the moving object. Let $h_k(\boldsymbol{\xi})$ be the distance between the

coordinates $\boldsymbol{\xi}$ and the k-th smooth face of the moving object and $\boldsymbol{x}_j$ be the coordinates of apex j on the fixed object. The coordinate transformation from $\boldsymbol{x}$ to $\boldsymbol{\xi}$ is given by

$$\boldsymbol{\xi} = A^T(\boldsymbol{\theta}_0)(\boldsymbol{x} - \boldsymbol{x}_0) \tag{3-4}$$

since $A(\boldsymbol{\theta}_0)$ is a orthogonal matrix. The condition for apex j of the fixed object to be in contact with facet k of the moving object is then given by

$$h_k[A^T(\boldsymbol{\theta}_0)(\boldsymbol{x}_j - \boldsymbol{x}_0)] = 0. \tag{3-5}$$

Both eqs.(3-3) and (3-5) are implicit functions of the position and orientation of the moving object; $\boldsymbol{q} = [x_0, y_0, z_0, \theta_0, \phi_0, \psi_0]^T$. Thus, in general, the contact condition of an individual contact pair is given by

$$H_{jk}(\boldsymbol{q}) = 0 \tag{3-6}$$

where j and k denote an apex and a facet, respectively. Function $H_{jk}(\boldsymbol{q})$ can be regarded as the distance between an apex and a facet. This condition is referred to as a *Contact Equation*. An arbitrary configuration involved in R_i must satisfy all the contact equations that are defined by individual contact pairs.

The region R_i is determined primarily by the contact equations. A set of these equations, however, provides merely necessary condition for a configuration $\boldsymbol{q}$ to be involved in the region R_i. Let l and m be a pair of an apex and a facet which is not involved in the contact state. Function $H_{lm}(\boldsymbol{q})$ must be positive for all configurations involved in R_i since apex l is not in contact with facet m. Configuration $\boldsymbol{q}$ involved in region R_i must be admissible. Therefore, region R_i is described as follows:

$$\begin{aligned} R_i = \{\, \boldsymbol{q} \mid\ & H_{jk}(\boldsymbol{q}) = 0,\ \forall j,k, \\ & H_{lm}(\boldsymbol{q}) > 0,\ \forall l,m, \\ & \boldsymbol{q} \in R\} \end{aligned} \tag{3-7}$$

where j and k be contacting pairs while l and m be non-contacting pairs. Namely, region R_i is described by the contact equations associated with the contact pairs involved in the contact state and the inequality conditions associated with the pairs not involved in the state. Note that contact state N_i is admissible if and only if region R_i given in eq.(3-7) is not empty. It is thus necessary to compute region R_i in order to find possible contact states.

3.2.3 Mathematical Description of Contact State Transitions

An arbitrary transition of the contact state can be divided into some minimal transitions. Consider a transition from N_3 to N_5 shown in Figure 11. Let $\boldsymbol{q}_3$ and $\boldsymbol{q}_5$ be arbitrary configurations involved in contact states N_3 and N_5, respectively. In order to move the object from configuration $\boldsymbol{q}_3$ to $\boldsymbol{q}_5$, it is inevitable to transit state N_1 or N_4, as shown in the figure. It implies that a direct transition from state N_3 to N_5 is not possible. The transition from N_3 to N_5 can be divided into a series of direct state transitions. For example, it can be divided into two direct state transitions $N_3 \rightarrow N_4$ and $N_4 \rightarrow N_5$. Direct state transitions are the minimal transitions of a contact state and an arbitrary possible transition can be represented by a series of the minimal transitions. Thus, we represent a direct transition between two contact states by an arc connecting the corresponding nodes. An assembly process is then described by a path of a contact state graph.

An arbitrary motion of the moving object can be represented by a trajectory in the configuration space. Let us formulate a direct state transition using the configuration trajectory. An arbitrary trajectory can be described by a function with one parameter t as follows:

$$\boldsymbol{q} = \boldsymbol{q}(t) \qquad t \in [0,1] \tag{3-8}$$

The state transition from N_i to N_j is then represented by a trajectory connecting configurations involved in regions R_i and R_j. Direct transition from state N_i to N_j is admissible if we can move the object without transiting other contact states but N_i or N_j. Namely, direct state transition $N_i \rightarrow N_j$ is possible when an arbitrary configuration along the trajectory is involved in either R_i or R_j. Therefore, direct state transition $N_i \rightarrow N_j$ is possible if and only if the following condition is satisfied.

$$\begin{aligned} \exists \boldsymbol{q}(t) \quad t \in [0,1] \quad \text{s.t.} \quad & \boldsymbol{q}(0) \in R_i, \\ & \boldsymbol{q}(1) \in R_j, \\ & \boldsymbol{q}(t) \in R_i \cup R_j, \quad \forall t \in (0,1) \end{aligned} \tag{3-9}$$

Let us derive some properties of direct state transitions based on their definition given in the above equation. First, we derive a necessary condition for possible direct transitions.

Theorem 6 *The following condition is satisfied if direct state transition $N_i \rightarrow N_j$ is possible:*

$$N_i \subset N_j \quad \textit{or} \quad N_i \supset N_j \tag{3-10}$$

where $N_i \subset N_j$ denotes that all contact pairs in state N_i are involved in state N_j.

The proof of this theorem is shown in Appendix A. As defined before, regions R_i and R_j are sets of configurations involved in states N_i and N_j, respectively. Assuming that all contact pairs in state N_j is involved in N_i, we derive the following relation between regions R_i and R_j.

Theorem 7 *Let N_i and N_j be contact states that satisfy*

$$N_i \supset N_j. \tag{3-11}$$

The following equation is then satisfied.

$$\boldsymbol{q} \notin \partial R_i, \quad \forall \boldsymbol{q} \in R_j \tag{3-12}$$

where ∂R_i is a boundary set of region R_i.

The proof of this theorem is shown in Appendix B. The necessary and sufficient condition for possible direct transitions can be derived using theorem 7.

Theorem 8 *Let N_i and N_j be contact states that satisfy*

$$N_i \supset N_j. \tag{3-13}$$

Direct state transition $N_i \rightarrow N_j$ is possible if and only if the following condition is satisfied:

$$\exists \boldsymbol{q} \in R_i \quad s.t. \quad \boldsymbol{q} \in \partial R_j \tag{3-14}$$

The proof of this theorem is shown in Appendix C.

3.3 Automatic Generation of Contact State Graphs

3.3.1 The Monte Carlo Method

We have to examine whether region R_i is empty in order to find all possible contact states. In this section, we develop an efficient method based on the Monte Carlo method in order to obtain the regions R_i.

The regions R_i have been defined to be individual regions partitioned in the configuration space with respect to contact states. The boundary of each region R_i

is determined primarily by the contact equations associated with the contact pairs, as described in Section 3.2.2. These equations, however, provide merely necessary conditions for a configuration $\boldsymbol{q}$ to be involved in region R_i. One must include conditions of inequality in addition to the contact equations given by eqs.(3-3) and (3-5). As a result, it is very difficult and inefficient to attain an analytic, closed form solution to the problem of finding the boundary of region R_i.

State N_i is possible if and only if there exists a configuration involved in the region R_i. Thus, it is not necessary to obtain a closed form solution in order to examine whether state N_i is possible. We will use a set of sample points involved in each R_i in the derivation of possible measurement sets, which will be developed later. Thus, our goal here is to obtain an approximate set of sample points that cover the region R_i rather than the derivation of analytic solutions. To this end, we apply the Monte Carlo method to the generation of sample points.

Using the standard Monte Carlo method, we first generate an arbitrary point in the configuration space randomly, examine which region the configuration is involved in, and then store the point in the corresponding region R_i. The problem with this method is the following: the entire configuration space consists of three parts: 1) the region where the moving object is not in contact with any fixture, *free space*, 2) the region where the moving object interferes with the fixed objects, *non-admissible space*, and 3) the *contact space* in which the two objects are in contact at some points. The contact space is the boundary of the admissible space, and therefore the dimension of this space is substantially smaller than the other two. In consequence, it is rare that a randomly generated point impinges on the boundary surface, that is the contact space. It is therefore inefficient to use the standard Monte Carlo method to investigate the regions R_i that are mostly involved in the contact space.

In order to cope with this difficulty, we modify the method so that the test points may be involved in the contact space. An arbitrary configuration involved in the contact space satisfies at least one contact equation. Thus, we select several contact equations a priori and move the randomly generated points towards the contact space in which the selected equations are satisfied. Let $H_1(\boldsymbol{q})$ through $H_j(\boldsymbol{q})$ be a set of selected equations. We can find a configuration that satisfies the equations by minimizing the following function.

$$E(\boldsymbol{q}) = \sum_{i=1}^{j} \; [\; H_i(\boldsymbol{q}) \;]^2 \tag{3-15}$$

By applying a minimization algorithm of a nonlinear function [Avriel, 76], we can find the minimum value of function $E(\boldsymbol{q})$. The configuration $\boldsymbol{q}$ satisfies the original

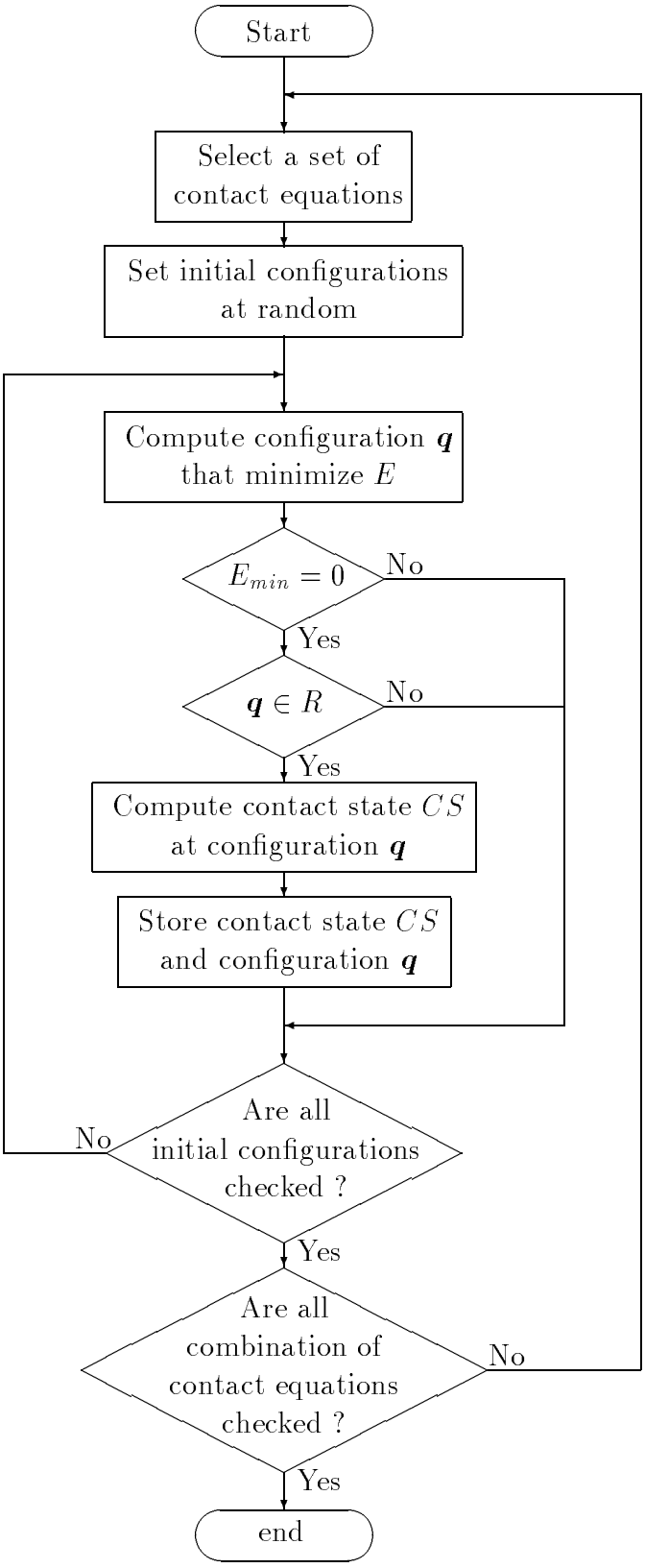

Figure 13: Algorithm to obtain sample configurations

contact equations if and only if the minimum value E_{min} is equal to zero:

$$E_{min} = 0 \quad \Longleftrightarrow \quad \exists \boldsymbol{q} \ \text{ s.t. } \ H_i(\boldsymbol{q}) = 0, \ \ \forall i \in [1, j] \tag{3-16}$$

Thus, we can find a solution vector of contact equations through a minimization process of $E(\boldsymbol{q})$. This minimization process is done for many initial configurations generated at random in order to attain sufficient sample points. Note that we have no solution that satisfies more than six independent contact equations, since six-dimensional vector $\boldsymbol{q}$ is a unknown parameter. Therefore, the number of contact equations given a priori should be less than or equal to six.

The obtained sample points are examined in which region they are involved and are stored in the corresponding region R_i. Since the points are moved towards the contact space, it is common that the points are involved in the contact space. It is therefore efficient to use the modified Monte Carlo method illustrated in Figure 13.

We can reduce the combination of contact equations selected a priori in the following way. Assume that two contact pairs $e_1^m - e_1^f$ and $e_2^m - e_2^f$ are involved in contact state N_i, where e_1^m and e_2^m be apices or facets of the moving object and e_1^f and e_2^f be those of the fixed object. The distance between e_1^m and e_2^m is equal to the distance between e_1^f and e_2^f since elements e_1^m and e_2^m are in contact with e_1^f and e_2^f, respectively. Thus, the following condition is satisfied:

$$\begin{aligned} &\exists \boldsymbol{x}_1 \in e_1^m, \ \boldsymbol{x}_2 \in e_2^m \\ &\quad \boldsymbol{y}_1 \in e_1^f, \ \boldsymbol{y}_2 \in e_2^f \qquad \text{s.t.} \quad \| \boldsymbol{x}_1 - \boldsymbol{x}_2 \| = \| \boldsymbol{y}_1 - \boldsymbol{y}_2 \| \end{aligned} \tag{3-17}$$

It implies that

$$dist(e_1^m, e_2^m) \cap dist(e_1^f, e_2^f) \neq \phi \tag{3-18}$$

where

$$dist(e_i, e_j) \stackrel{\triangle}{=} \{ \ \| \boldsymbol{x}_i - \boldsymbol{x}_j \| \ | \ \boldsymbol{x}_i \in e_i, \ \boldsymbol{x}_j \in e_j \}. \tag{3-19}$$

From this discussion, we can derive the necessary condition for a contact state N_i to be admissible. Let $e_1^m - e_1^f$ and $e_2^m - e_2^f$ be arbitrary contact pairs involved in state N_i. Contact state N_i is not admissible if the following equation is satisfied:

$$dist(e_1^m, e_2^m) \cap dist(e_1^f, e_2^f) = \phi \tag{3-20}$$

Note that we can compute the distance $dist(e_i, e_j)$ a priori for the moving and the fixed objects. Therefore, we can reduce the combination of contact equations by eliminating contact pairs that satisfy eq.(3-20).

3.3.2 Finding Admissible State Transitions

In this section, we develop a method to find possible direct transitions among the contact states using the theory of polyhedral convex cones.

From theorem 6, we find that neither $N_i \rightarrow N_j$ nor $N_j \rightarrow N_i$ is admissible if eq.(3-10) is not satisfied. Note that transition $N_j \rightarrow N_i$ is possible if and only if transition $N_i \rightarrow N_j$ is possible. Thus, we can find all possible direct transitions by examining all transitions connecting two contact states N_i and N_j which satisfy $N_i \supset N_j$. In the following analysis, we assume that two contact states N_i and N_j satisfy a condition that all contact pairs in N_j is involved in N_j.

Let N_i and N_j be sets of contact pairs given by

$$N_i = (P_1, \cdots, P_s, P_{s+1}, \cdots, P_m), \tag{3-21}$$

$$N_j = (P_{s+1}, \cdots, P_m) \tag{3-22}$$

where P_1 through P_m represent contact pairs between the moving and the fixed objects. All contact pairs in N_j is involved in N_i, that is, a condition $N_i \supset N_j$ is satisfied. Let $\boldsymbol{q}$ be an arbitrary configuration involved in region R_i. A set of admissible displacement at configuration $\boldsymbol{q}$ is described by a union of polyhedral convex cones as mentioned before. First, let us consider the case that the admissible displacement set at configuration $\boldsymbol{q}$ is given by a polyhedral convex cone

$$A(\boldsymbol{q}) = face\{\boldsymbol{a}_1, \boldsymbol{a}_2, \cdots, \boldsymbol{a}_m\} \tag{3-23}$$

where $\boldsymbol{a}_r$ be a face vector associated with a contact pair P_r. From theorem 8, we find that direct transition $N_i \rightarrow N_j$ is possible if there exists an admissible displacement $\Delta\boldsymbol{q}$ that satisfies the following condition:

$$\boldsymbol{a}_r^T \Delta\boldsymbol{q} < 0, \qquad \forall r \in [1, s] \tag{3-24}$$

$$\boldsymbol{a}_r^T \Delta\boldsymbol{q} = 0, \qquad \forall r \in [s+1, m] \tag{3-25}$$

since contact state N_j consists of contact pairs P_{s+1} through P_m. Inner products $\boldsymbol{a}_1^T \Delta\boldsymbol{q}$ through $\boldsymbol{a}_s^T \Delta\boldsymbol{q}$ must be positive since contact pairs P_1 through P_s are not involved in state N_j. Note that an arbitrary displacement satisfying the above conditions is involved in a subset $A[I]$ defined in the previous chapter. It implies that direct state transitions can be formulated based on the theory of polyhedral convex cones. Let us derive a condition for direct state transitions to be admissible based on the cone theory. We can compute the span-form of the cone given by eq.(3-23) using algorithm CONVERT developed in the previous chapter.

$$A(\boldsymbol{q}) = span\{\boldsymbol{u}_1, \boldsymbol{u}_2, \cdots, \boldsymbol{u}_k\} \tag{3-26}$$

An arbitrary admissible displacement $\boldsymbol{q}$ is then described by a convex sum of span vectors.

$$\Delta \boldsymbol{q} = \sum_{l=1}^{k} c_l \boldsymbol{u}_l, \qquad c_l \geq 0, \quad l \in [1,k] \tag{3-27}$$

Substituting this equation into eqs.(3-24) and (3-25), we find that direct transition $N_i \rightarrow N_j$ is possible if the following condition is satisfied:

$$\forall r \in [1,s], \qquad \exists l \in [1,k], \qquad \boldsymbol{a}_r^T \boldsymbol{u}_l < 0, \tag{3-28}$$

$$\forall r \in [s+1,m], \quad \forall l \in [1,k], \qquad \boldsymbol{a}_r^T \boldsymbol{u}_l = 0. \tag{3-29}$$

In the case that the admissible displacement set is given by a union of polyhedral convex cones, this condition must be checked for individual cones. A direct transition is possible if an admissible displacement involved in one of the cones satisfies the above condition. Therefore, we can investigate whether direct transition $N_i \rightarrow N_j$ is possible by examining eqs.(3-28) and (3-29).

3.4 Implementation

We demonstrate the computation procedures of contact state graphs for planar assembly. Let us assume that all the surfaces of the moving and the fixed objects are plains. Let $\boldsymbol{x}_0 = [x_0, y_0]^T$ and θ_0 be the position and the orientation of the moving object, respectively. The computation process consists of two stages; [1] The Monte Carlo Method and [2] Finding Admissible State Transitions. Details of the two stages are described below.

[1] The Monte Carlo Method

Let $\boldsymbol{x}_k^1$ and $\boldsymbol{x}_k^2$ be the end points of the k-th facet, and $\boldsymbol{n}_k = [n_x^k, n_y^k]^T$ be the unit normal vector of the facet. Then, the distance between the coordinate $\boldsymbol{x} = [x,y]^T$ and the k-th facet is given by

$$h_k(\boldsymbol{x}) = \begin{cases} \| \boldsymbol{x} - \boldsymbol{x}_k^1 \| & \text{if } (\boldsymbol{x}_k^2 - \boldsymbol{x}_k^1)^T(\boldsymbol{x} - \boldsymbol{x}_k^1) < 0 \\ \| \boldsymbol{x} - \boldsymbol{x}_k^2 \| & \text{if } (\boldsymbol{x}_k^1 - \boldsymbol{x}_k^2)^T(\boldsymbol{x} - \boldsymbol{x}_k^2) < 0 \\ | \boldsymbol{n}_k^T(\boldsymbol{x} - \boldsymbol{x}_k^1) | & \text{otherwise} \end{cases} \tag{3-30}$$

The coordinate transformation from $\boldsymbol{\xi} = [\xi, \eta]^T$ to $\boldsymbol{x}$ is given by

$$\begin{bmatrix} x \\ y \end{bmatrix} = \begin{bmatrix} c_0 & -s_0 \\ s_0 & c_0 \end{bmatrix} \begin{bmatrix} \xi \\ \eta \end{bmatrix} + \begin{bmatrix} x_0 \\ y_0 \end{bmatrix} \tag{3-31}$$

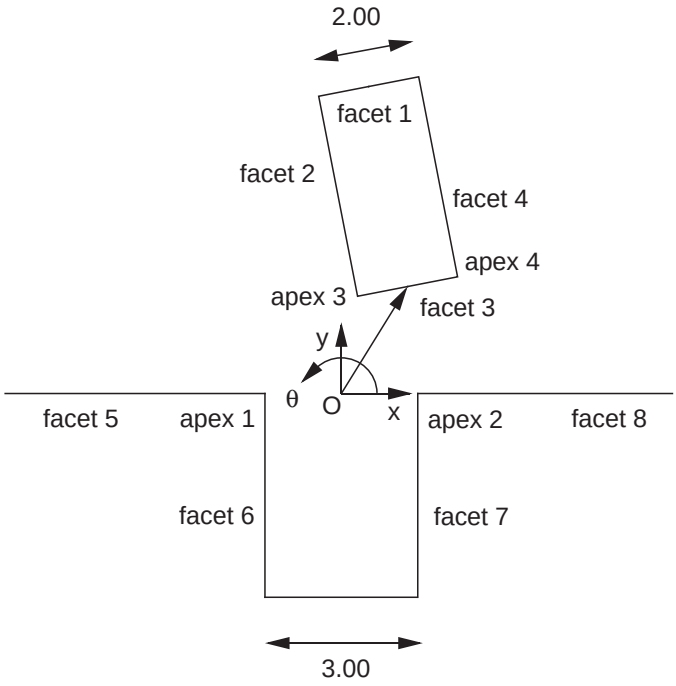

Figure 14: Simple example of planar objects

where $c_0 = \cos\theta_0$ and $s_0 = \sin\theta_0$. The contact equation given by eq.(3-6) is thus expressed by an implicit function of four variables, x_0, y_0, c_0, and s_0, with one constraint, $c_0^2 + s_0^2 = 1$. Let us express the contact conditions as

$$H_{jk}(x_0, y_0, c_0, s_0) = 0. \tag{3-32}$$

The function $E(\boldsymbol{q})$ given by eq.(3-15) is then described as

$$E(x_0, y_0, c_0, s_0) = \sum_{j,k} H_{jk}(x_0, y_0, c_0, s_0) + \rho(c_0^2 + s_0^2 - 1) \tag{3-33}$$

where ρ is an appropriate constant. A nonlinear function $E(\boldsymbol{q})$ can be minimized applying the quasi-Newton method [Avriel, 76]. Using the procedure shown in Figure 13, we can find sample configurations, x_0, y_0, and $\theta_0 = \tan^{-1}(s_0/c_0)$, involved in region R_i. Note that contact state N_i is admissible if and only if there exists a configuration involved in R_i. Therefore, we can find all admissible contact states by examining whether sets of sample configurations are empty.

[2] Finding Admissible State Transitions

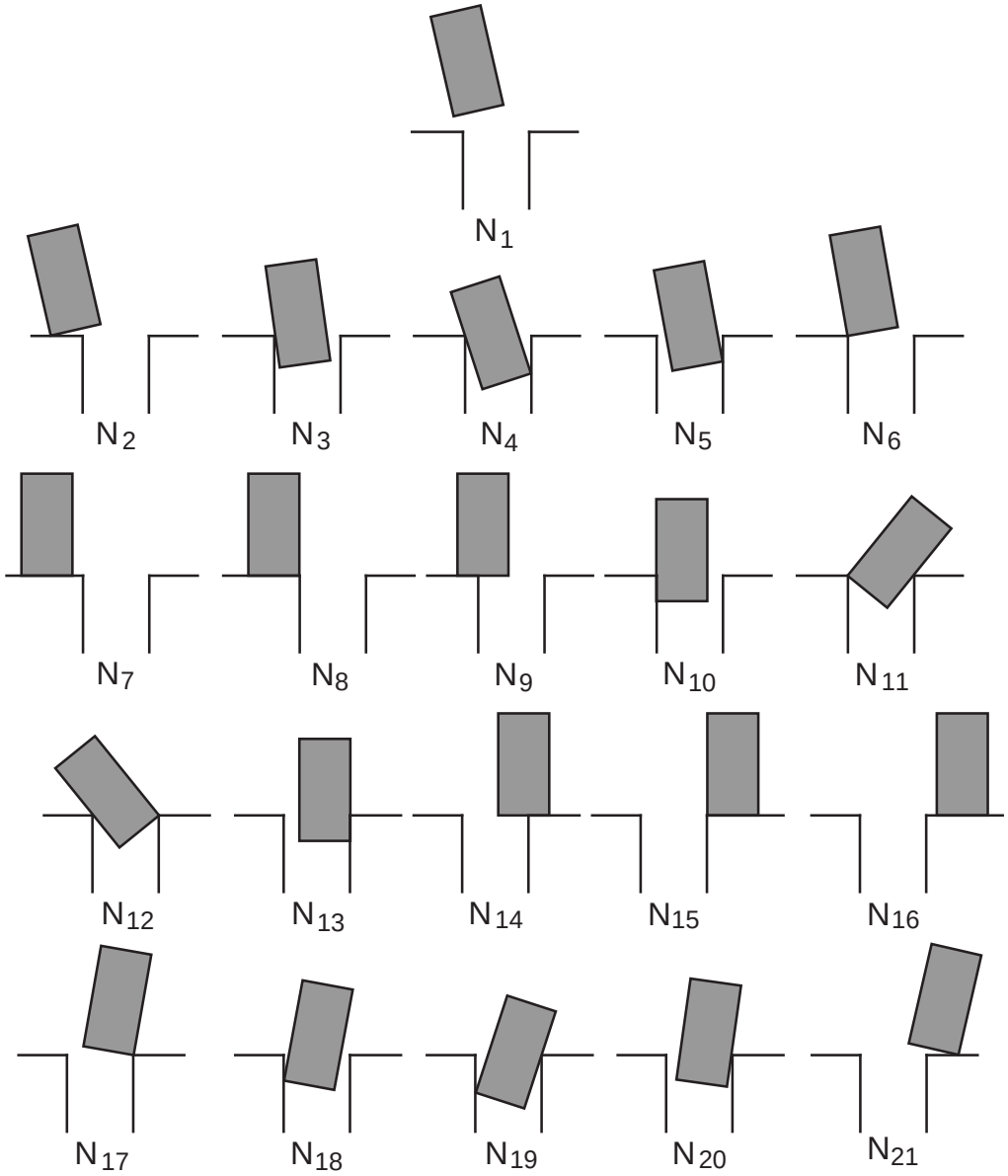

Figure 15: Obtained contact states

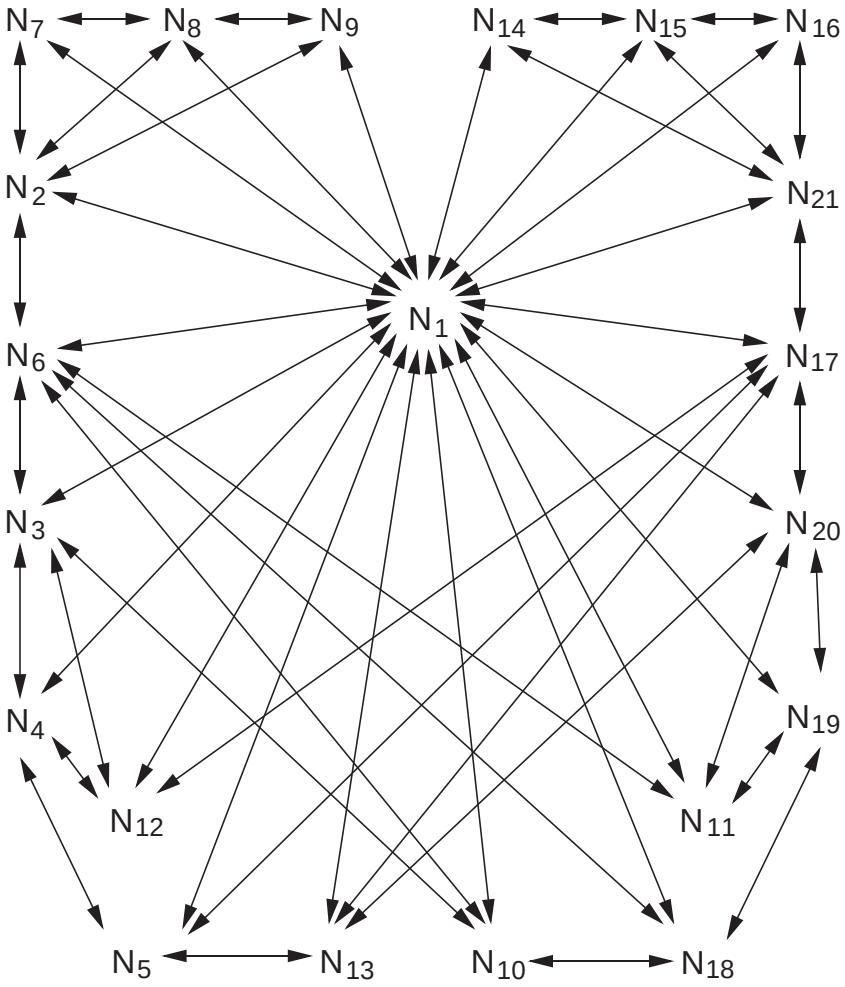

Figure 16: Generated contact state graph

Table 4: Initial contact equations selected a priori

no contact	N_1
(apex 3 - facet 5)	N_2
(facet 2 - apex 1)	N_3
(apex 4 - facet 7 facet 2 - apex 1)	N_4
(apex 4 - facet 7)	N_5
(apex 3 - facet 5 apex 4 - facet 5)	N_7
(apex 3 - facet 8 apex 4 - facet 8)	N_{16}
(apex 3 - facet 6)	N_{18}
(apex 3 - facet 6 facet 4 - apex 2)	N_{19}
(facet 4 - apex 2)	N_{20}
(apex 4 - facet 8)	N_{21}

Let us first derive vector $\boldsymbol{d}_{jk}$ given in eq.(2-5) for planar assembly. Vector $\boldsymbol{d}_{jk}$, corresponding to a contact pair apex j – facet k, is given by

$$\boldsymbol{d}_{jk} = \begin{bmatrix} n_x^k \\ n_y^k \\ (c_0\xi_j - s_0\eta_j)n_y^k - (s_0\xi_j + c_0\eta_j)n_x^k \end{bmatrix} \tag{3-34}$$

where $\boldsymbol{n}_k = [n_x^k, n_y^k]^T$ be the inward normal vector of the k-th facet. Vector $\boldsymbol{d}_{jk}$, corresponding to a contact pair facet j – apex k, is derived as

$$\boldsymbol{d}_{jk} = \begin{bmatrix} c_0 n_x^k - s_0 n_y^k \\ s_0 n_x^k + c_0 n_y^k \\ (c_0[x_j - x_0] + s_0[y_j - y_0])n_y^k + (s_0[x_j - x_0] - c_0[y_j - y_0])n_x^k \end{bmatrix} \tag{3-35}$$

where $\boldsymbol{n}_k = [n_x^k, n_y^k]^T$ be the outward normal vector of the k-th facet.

Note that vector $\boldsymbol{d}_{jk}$ depends on the position $[x_0, y_0]$ and the orientation θ_0 of the moving object. The admissible displacement set at a configuration is described by these vectors using eqs.(2-9) and (2-10). Examining whether eqs.(3-28) and (3-29) are satisfied, we can find all admissible direct transitions of the contact state.

We have implemented the procedure to generate contact state graphs for planar assembly on a SUN 3/260 workstation in C language. Let us demonstrate the generation of a contact state graph for simple objects shown in Figure 14. Table 4 shows sets of contact pairs associated with initial contact equations selected a

priori. Eleven sets of contact equations have chosen to modify initial configurations. Using the modified Monte Carlo method, we can find twenty-one contact states illustrated in Figure 15 in addition to the original eleven contact states. Namely, ten new contact states were found using the modified Monte Carlo method. No sample configurations can be obtained for a set of initial contact equations given by

$$(\text{apex } 3 - \text{facet } 5 \quad \text{apex } 4 - \text{facet } 8). \tag{3-36}$$

Thus, we find that this contact state is not admissible. Note that eq.(3-20) is satisfied for the two contact pairs given in the above list. The admissible direct transitions among the contact states are shown in Figure 16.

3.5 Concluding Remarks

In this paper, we have developed a new method for representing assembly processes with respect to mechanical contacts. Kinematic properties of workpieces strongly depend on the state of contacts between workpieces. Thus, we developed contact state graphs to describe the assembly processes in an understandable manner.

First, contact states between workpieces were defined by regarding how workpieces contact each other. The process of workpiece assembly was then modeled as a set of transitions of contact states and represented by a state graph. Contact states were formulated using distance functions between the workpieces. Contact state transitions were analyzed to derive conditions to be admissible. An efficient method to generate a contact state graph from the geometric data of workpieces has been developed by using the Monte Carlo method.

Appendix A Proof of theorem 6

Assume that eq.(3-10) is not satisfied. Then, there exists a contact pair apex k – facet l which is involved in N_i but is not involved in N_j. There also exists another contact pair apex m – facet n which is not involved in N_i but is involved in N_j. Let $\boldsymbol{q}(t)$ be a trajectory connecting regions R_i and R_j. We assume that configurations $\boldsymbol{q}(0)$ and $\boldsymbol{q}(1)$ are involved in R_i and R_j, respectively. Since a contact pair apex k – facet l is involved in N_i while apex m – facet n is not involved in N_i, we have

$$H_{kl}[\boldsymbol{q}(0)] = 0, \tag{A-1}$$

$$H_{mn}[\boldsymbol{q}(0)] > 0. \tag{A-2}$$

Since a contact pair apex k – facet l is not involved in N_j while apex m – facet n is involved in N_j, we have

$$H_{kl}[\boldsymbol{q}(0)] > 0, \tag{A-3}$$

$$H_{mn}[\boldsymbol{q}(0)] = 0. \tag{A-4}$$

From these equations, we find that there exists t_1, t_2, and ϵ that satisfy the following equations:

$$H_{kl}[\boldsymbol{q}(t)] \quad \begin{cases} = 0 & t \in [0, t_1] \\ > 0 & t \in (t_1, t_1 + \epsilon) \end{cases} \tag{A-5}$$

$$H_{mn}[\boldsymbol{q}(t)] \quad \begin{cases} > 0 & t \in [0, t_2) \\ = 0 & t = t_2 \end{cases} \tag{A-6}$$

since distance functions $H_{kl}(\boldsymbol{q})$ and $H_{mn}(\boldsymbol{q})$ are continuous. When t_1 is greater than t_2, the following equation is satisfied at $t = t_2$:

$$H_{kl}[\boldsymbol{q}(t)] = 0 \tag{A-7}$$

$$H_{mn}[\boldsymbol{q}(t)] = 0 \tag{A-8}$$

It implies that there exists another contact state along the trajectory, which involves both apex k – facet l and apex m – facet n. When t_1 is less than or equal to t_2, the following condition is satisfied at $t = t_1 + \epsilon/2$:

$$H_{kl}[\boldsymbol{q}(t)] > 0 \tag{A-9}$$

$$H_{mn}[\boldsymbol{q}(t)] > 0 \tag{A-10}$$

It implies that there exists another contact state along the trajectory, which involves neither apex k – facet l nor apex m – facet n. In both cases, we find that there exists another contact state along an arbitrary trajectory connecting two states N_i and N_j. Therefore, direct transition from N_i to N_j is not admissible.

Appendix B Proof of theorem 7

Assume that eq.(3-12) is not satisfied. Then, there exists a configuration $\boldsymbol{q}_1 \in R_j$ that is involved in ∂R_i. Let $\boldsymbol{q}_0$ be an arbitrary configuration involved in R_i. Since $\boldsymbol{q}_1$ is involved in ∂R_i, there exists a trajectory $\boldsymbol{q}(t)$ that satisfies

$$\begin{aligned} &\boldsymbol{q}(0) = \boldsymbol{q}_0, \\ &\boldsymbol{q}(1) = \boldsymbol{q}_1, \\ &\boldsymbol{q}(t) \in R_i, \quad \forall t \in (0,1) \end{aligned} \tag{B-1}$$

Namely,

$$\begin{aligned} &\boldsymbol{q}(t) \in R_i, \quad \forall t \in [0,1) \\ &\boldsymbol{q}(1) \in R_j. \end{aligned} \tag{B-2}$$

Let apex k – facet l be a contact pair that is involved in N_i but is not involved in N_j. Then, the following condition is satisfied:

$$\begin{aligned} &H_{kl}[\boldsymbol{q}(t)] = 0, \quad \forall t \in [0,1) \\ &H_{kl}[\boldsymbol{q}(1)] > 0 \end{aligned} \tag{B-3}$$

From these equations, we find that function $H_{kl}[\boldsymbol{q}(t)]$ is not continuous at $t = 1$. It contradicts to the continuity of distance function $H_{kl}(\boldsymbol{q})$. Therefore, eq.(3-12) is satisfied.

Appendix C Proof of theorem 8

Assume that eq.(3-14) is satisfied. Then, there exists a configuration $\boldsymbol{q}_0 \in R_i$ involved in the boundary set ∂R_j. Let $\boldsymbol{q}_1$ be an arbitrary configuration involved in R_j. Since $\boldsymbol{q}_0$ is involved in ∂R_j, there exists a trajectory $\boldsymbol{q}(t)$ that satisfies

$$\begin{aligned} &\boldsymbol{q}(0) = \boldsymbol{q}_0, \\ &\boldsymbol{q}(1) = \boldsymbol{q}_1, \\ &\boldsymbol{q}(t) \in R_j, \quad \forall t \in (0,1) \end{aligned} \tag{C-1}$$

It implies that the contact state can transit directly from N_i to N_j by moving the object along the trajectory $\boldsymbol{q}(t)$. The sufficient condition is thus proved.

Assume that eq.(3-14) is not satisfied. Then, all configurations in region R_i are not involved in the boundary set ∂R_j. Let $\boldsymbol{q}(t)$ be an arbitrary trajectory that

satisfies

$$\begin{aligned} &\boldsymbol{q}(0) \in R_i, \\ &\boldsymbol{q}(1) \in R_j, \\ &\boldsymbol{q}(t) \in R_i \cup R_j, \quad \forall t \in (0,1) \end{aligned} \tag{C-2}$$

Let t_c be a point where the contact state transits from N_i to N_j. Assume that there exists t_c that satisfies the following condition:

$$\begin{aligned} &\boldsymbol{q}(t) \in R_i, \quad \forall t \in [0, t_c) \\ &\boldsymbol{q}(t) \in R_j, \quad t = t_c \end{aligned} \tag{C-3}$$

From theorem 7, all configurations in region R_j are not involved in the boundary set ∂R_i, since all contact pairs of N_j is involved in N_i. Thus, we find that the above equation contradicts to theorem 7. Assume that there exist t_c and ϵ that satisfy the following condition:

$$\begin{aligned} &\boldsymbol{q}(t) \in R_i, \quad \forall t \in [0, t_c] \\ &\boldsymbol{q}(t) \in R_j, \quad \forall t \in (t_c, t_c + \epsilon) \end{aligned} \tag{C-4}$$

Then, we find that configuration $\boldsymbol{q}(t_c)$ is involved in ∂R_j as well as R_i. It contradicts to the assumption that all configurations in region R_i are not involved in the boundary set ∂R_j. Therefore, there does not exist a trajectory that satisfy eq.(C-3). Namely, direct state transition from N_i to N_j is not admissible. The necessary condition is thus proved.

Chapter 4
A Model-Based Approach to the Recognition of Assembly Process States Using the Theory of Polyhedral Convex Cones

4.1 Introduction

Force feedback control is a key to advanced manipulation, where robots interact with the environment, adapt themselves to unpredicatable change, and perform dextrous operations. In past decades, a number of theories and techniques have been developed, including bi-lateral servo [Inoue, 71], generalized spring and damper [Whitney, 77], hybrid position/force control [Mason, 82] [Raibert and Craig, 81], impedance control [Hogan, 85] and so on [Whitney, 87]. These provide efficient means to construct force feedback control systems, where force information is needed to modify the robot motion in accordance with predetermined control laws and control schemes.

The majority of manipulative tasks, however, are still out of the range of today's robotics technologies. These are often so complex and intricate that efficient strategies cannot be generated by single control laws and schemes. Real control laws are varying depending on the state of the process. A selection matrix in hybrid control, for example, must be switched if the geometric constraints vary in the process. A particular stiffness matrix, which is valid for a certain range of tasks, will be inadequate when the task condition varies significantly. The direct feedback of force signals is thus limited in validity, unless the control law is modified in accordance with the change in the process state. A higher level control that allows the robot to recognize the process state and modify the task strategy depending on the process state is therefore necessary to extend the task range and deal with varying task conditions, which are often uncertain. While the direct feedback is primarily a signal-level feedback, the higher level feedback is a symbol-level feedback, where the original sensory information is mapped into a process state described at a signed-level [Rasmussen, 83]. Note that the latter requires the interpretation of sensory information to recognize the process state [Lozano-Pérez et al., 84] [Donald, 88] [Desai and Volz, 89].

In this paper, we develop a technique for mapping sensory information into the process state described at a symbol-level. Specifically, we deal with assembly tasks, in which workpieces contact each other in different ways and as a result the geometric constraints vary significantly as the assembly operation proceeds. We will first analyze the process of the assembly operation with regard to how the workpieces contact each other, and represent the process with a graph. The main issue to be tackled is to recognize the current contact state of workpieces by using sensory information. We will develop a systematic method for mapping the sensory information into individual contact states so that the robot can recognize which situation the assembly processes are currently involved in. Based on a geometric model of workpieces, we will generate a set of discriminant functions that classify a measured signal pattern into the individual contact states. Using this technique, it is expected that the robot can fully utilize the sensory information in order to perform a higher-level control including the switching of control strategies and schemes.

4.2 Symbolic Representation of Assembly Processes

Assembly is a process of locating and fixing workpieces together in a desired configuration. In this assembly process, the robot mates the workpieces by moving one workpiece along the appropriate surface of the other. During the operation, the workpieces contact each other at different surfaces. As the operation proceeds, the contacting pair of surfaces may change as shown in Figure 10. During this process, the workpiece motion is constrained by the contact, and the geometric constraints vary in accordance with the change of contacting surfaces. As the constraints change, the robot needs to change its control law accordingly. Therefore, the geometric constraints due to the contacts are a fundamental characteristic to investigate when control laws and task strategies are being planned.

In this paper, we use a process model of assembly based on a symbolic description of the geometric constraints [Lozano-Pérez et al., 84] [Hirai et al., 88a] [Desai and Volz, 89]. As shown in Figure 10, individual facets and apices of the workpieces are labeled facet i and apex j, respectively. The contact between facet i and apex j is denoted as facet i– apex j. The geometric constraints imposed on the workpieces are determined by listing all the contacting pairs between the two. For example, contacts shown in Figure 10-(d) are described by

$$(\text{ facet } 2 - \text{apex } 1 \quad \text{apex } 4 - \text{facet } 7 \text{ }). \tag{4-1}$$

The state of the assembly process described in the list of all the contacting pairs is referred to as *Contact State* [Hirai et al., 88a]. Each contact state has different constraints depending on the geometry of each contacting pair involved.

The contact state is determined by the position and orientation of one workpiece relative to the other. Without loss of generality, we assume that one workpiece is carried around by the robot and the other is fixed in space. Let us denote the position and orientation of the moving workpiece by the six-dimensional vector $\boldsymbol{q} \in V^6$ with respect to a coordinate system fixed to the other workpiece. Some configurations of the moving workpiece are prohibited because of the geometric interference between the two workpieces. The set of possible configurations is called *Admissible Configuration Space* and denoted by R [Lozano-Pérez, 81]. The admissible configuration space R is divided into subsets that possess a different contact state N_i, and the set of workpiece configuration involved in the state N_i is denoted by subset $R_i \subset R$.

During assembly operations, the contact state may change from one to another. Let us model the change of contact state by a transition in a graph. We represent each contact state by a node of the graph and the possible transition between two contact states is denoted by the arc connecting the corresponding nodes. This graph is referred to as *Contact State Graph*, which provides a symbolic representation of assembly processes.

4.3 Kinematic and Static Modeling Using Polyhedral Convex Cones

In this section, we formulate kinematic and static relationships of constrained workpieces at a given configuration and derive some fundamental properties to be used for the recognition of contact states. Hirai and Asada have established an efficient mathematical tool based on the theory of *Polyhedral Convex Cones* [Goldman and Tucker, 56] in order to deal with unidirectional constraints due to mechanical contacts [Hirai et al., 88b]. This tool provides an efficient formalization for treating unidirectional constraints that we need to deal with in assembly. In the following analysis, we will investigate two quantities at each contact state:

- geometrically admissible displacement $\Delta\boldsymbol{q} \in V^6$
- statically admissible force and mement $\boldsymbol{p} \in V^6$

The former is the infinitesimal translational and rotational displacement of a constrained workpiece that does not violate the geometric constraints at a given contact

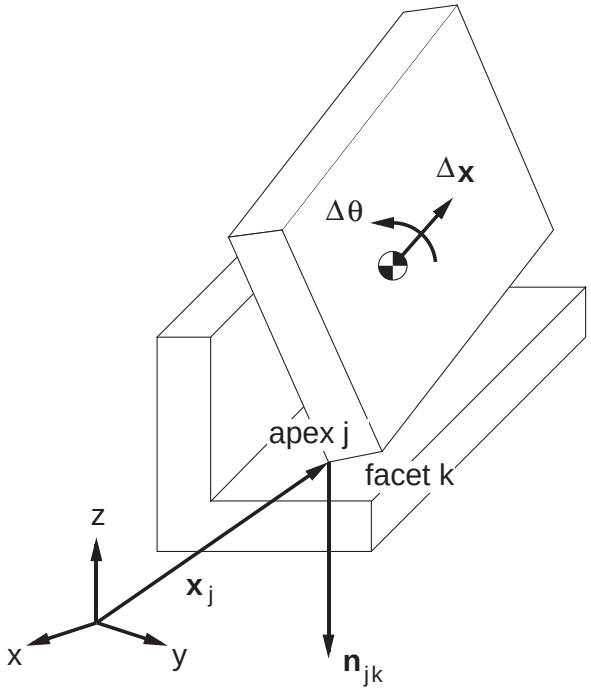

Figure 17: Geometric constraints

state. The latter is the force and moment acting on the workpiece that satisfy the static equilibrium condition.

Each contact state is described by a list of contact pairs, as mentioned before. Each contacting pair provides a geometric constraint that the workpiece motion must satisfy. Let $\Delta \boldsymbol{q}$ be an infinitesimal displacement of the moving object. In the case where apex j is in contact with facet k at a configuration $\boldsymbol{q}$, we can derive the condition for the admissible displacement given by

$$\boldsymbol{d}_{jk}^T \Delta \boldsymbol{q} \leq 0 \tag{4-2}$$

$$\boldsymbol{d}_{jk} \triangleq \begin{bmatrix} \boldsymbol{n}_{jk} \\ \boldsymbol{x}_j \times \boldsymbol{n}_{jk} \end{bmatrix} \tag{4-3}$$

where $\boldsymbol{d}_{jk}$ is a six-dimensional vector, $\boldsymbol{n}_{jk}$ is the inward unit vector of facet k at the contacting point with apex j, and $\boldsymbol{x}_j$ is the position vector of the contact point, as shown in Figure 17. Note that the inequality results from the unidirectional constraints.

The possible displacement must satisfy the above conditions for every contacting pair. Thus, a set of geometrically admissible displacements at a configuration $\boldsymbol{q}$ is represented by the solution set of the linear simultaneous inequalities. The set of admissible displacements A is given by eqs.(2-9) and (2-10) as follows:

$$A = \bigcup_{n=1}^{N} A_n \tag{4-4}$$

and

$$A_n = \{\Delta \boldsymbol{q} \mid \boldsymbol{h}_{nm}^T \Delta \boldsymbol{q} \leq 0 \ \ \forall m \in [1, M_n]\}$$

where $\boldsymbol{h}_{nm}$ is a six-dimensional vector:

$$\boldsymbol{h}_{nm} \in \{\boldsymbol{d}_{jk}\}$$

As mentioned in the previous chapter, set A_n is expressed by the *face form* of a polyhedral convex cone (PCC) [Goldman and Tucker, 56] and is described by

$$A_n = face\{\boldsymbol{h}_{nm} \mid m \in [1, M_n]\} \tag{4-5}$$

where each vector involved is referred to as a *face vector*. Therefore, the admissible displacement set is described by a union of PCC's.

We can apply the theory of polyhedral convex cones to the static analysis, too. The range of admissible static forces is derived from the theory in a straightforward manner. We assume that the workpiece motion is quasi-static and that friction is negligible. Let $\boldsymbol{p} \in V^6$ be the force and moment acting on the workpiece, these being the resultant force and moment of gravity and the one exerted by the robot. The range of admissible forces that do not cause movements, that is, statically balanced forces is given by eq. (2-17):

$$F = \{\boldsymbol{p} \mid \boldsymbol{p}^T \Delta \boldsymbol{q} \leq 0, \quad \forall \Delta \boldsymbol{q} \in A\}$$

In deriving this set of admissible forces, the following theory of polyhedral convex cones is useful. Let X be a set of real vectors $\boldsymbol{x}$. Then the set defined by eq.(2-28) is called the polar of the set X [Goldman and Tucker, 56]:

$$X^* \triangleq \{\boldsymbol{y} \mid \boldsymbol{x}^T \boldsymbol{y} \leq 0, \quad \forall \boldsymbol{x} \in X\}$$

Comparing eqs.(2-17) and (2-28), we can conclude that the range of admissible force and moment denoted by set F is given by the polar of the admissible displacement set A.

$$F = A^*$$

The admissible force set given by the above equation can be computed by applying a procedure developed by Hirai and Asada and is given by

$$F = \{\sum_{l=1}^{L} R_l \boldsymbol{w}_l \mid R_l \geq 0 \ \ \forall l \in [1, L]\}$$

where $\boldsymbol{w}_l$ is a six-dimensional vector. The above equation gives the *span form* of a PCC and is expressed by

$$F = span\{\boldsymbol{w}_l \mid l \in [1, L]\} \tag{4-6}$$

where each vector involved is referred to as a *span vector*.

4.4 Contact State Classifiers

4.4.1 Discriminant Rules

It is a fundamental requirement for robots to recognize the process states in order to modify the control law and the motion strategy. To recognize contact states, it is necessary to derive the mapping from the sensory information to the graph nodes. Let us describe the mapping by using IF–THEN rules, which define the relationships between sensor signals and the individual nodes.

Let us consider contact state N_2 shown in 10. Let f_x and f_y be reaction forces acting along x and y axes, respectively. At the state N_2, the reaction forces must be involved in the following set:

$$S_2 = \{[f_x, f_y]^T \mid f_x = 0, f_y \geq 0\} \tag{4-7}$$

We may conclude that the current state is N_2 if the measured reaction forces are involved in set S_2. Thus, discriminant rules can be generally described in the following form:

$$\text{IF } \boldsymbol{s}_m \in S_i \text{ THEN } N_i \tag{4-8}$$

where $\boldsymbol{s}_m$ is a vector consisting of measured sensor data and S_i is a set of possible signal vectors measured at contact state N_i. Set S_i is referred to as *Measurement Set* at N_i in this paper. The above rule expresses the mapping from the signal level information to the symbolic or signed level information. Once we know the range of possible signals at individual process states, we will be able to determine the current contact state from the measured signals by applying the above rules.

In the following sections, we will investigate measured force and moment. This sensory information strongly depends on the geometric characteristics of workpieces. Thus, the range of possible forces can be computed from the geometric model of the workpieces. In the next section, we will develop a systematic method for computing sets of possible signals at each contact state. Each set computed in this manner provides a set of linear discriminant functions. Therefore, we will be able to obtain the discriminant functions on a computer from the geometric model of the workpieces.

4.4.2 Measurement Sets at Individual Contact States

In this section, the classifiers of contact states are obtained on the basis of the kinematic and static formulation using PCC's. Our objective is to discriminate contact states by monitoring the force and moment acting on the workpiece.

First, let $\boldsymbol{s}_m$ be a six-dimensional vector consisting of the measured force and moment $\boldsymbol{p}_m$. The measured force must be within the admissible force set F. Therefore, the set of possible measurements at a configuration $\boldsymbol{q}$ is given by

$$S(\boldsymbol{q}) \triangleq \{\boldsymbol{s}_m \mid \boldsymbol{s}_m \in F\}. \tag{4-9}$$

Note that set F derived in the previous section is dependent on the configuration $\boldsymbol{q}$. To discriminate the contact states, we need to know the range of measured vectors $\boldsymbol{s}_m$ that can be obtained for an arbitrary configuration involved in each contact state. As defined before, the set of configurations that belong to contact state N_i is denoted by R_i. Then, the overall range of possible measurements at state N_i is given by

$$S_i = \bigcup_{\boldsymbol{q} \in R_i} S(\boldsymbol{q}). \tag{4-10}$$

The admissible force set depends on the configuration $\boldsymbol{q}$ since the static relationship mentioned in the previous section is derived from the differential motion at one specific configuration. On the other hand, region R_i represents the gross motion of the workpieces in the configuration space. In order to obtain measured set S_i using eq.(4-10), we first compute the admissible force set F at all configurations involved in the region R_i, derive sets of measured signals $S(\boldsymbol{q})$, and compute the union of all the sets of measured signals, $S(\boldsymbol{q})$. Since it is inefficient to compute the sets $S(\boldsymbol{q})$ at all configurations involved in region R_i, we evaluate the set at a finite number of representative points involved in the region. Let $\boldsymbol{q}_1^i$ through $\boldsymbol{q}_K^i$ be a finite number of sample configurations involved in region R_i. We approximate a union of sets over

region R_i by a union of sets at a finite number of sample points. Then, possible measurement set S_i given in eq.(4-10) is approximated by

$$S_i = \bigcup_{k=1}^{K} S(\boldsymbol{q}_k^i) \tag{4-11}$$

where $S(\boldsymbol{q}_k^i)$ are polyhedral convex cones. Therefore, measurement set S_i is expressed by a union of a finite number of polyhedral convex cones. Note that the face form of PCC's directly yields a set of linear discriminant functions commonly used in pattern recognition [Duda and Hart, 73]. Thus, measurement set S_i given in eq.(4-11) can be regarded as a set of discriminant functions.

Let $\boldsymbol{s}_m$ be a six-dimensional vector consisting of the measured displacement $\Delta\boldsymbol{q}_m$. The measured displacement must be within the admissible displacement set A. Therefore, the set of possible measurements at a configuration $\boldsymbol{q}$ is given by

$$S(\boldsymbol{q}) \stackrel{\triangle}{=} \{\boldsymbol{s}_m \mid \boldsymbol{s}_m \in A\}. \tag{4-12}$$

Note that set A derived in the previous section is also dependent on the configuration $\boldsymbol{q}$. Possible measurement set S_i is then given by eq.(4-10). The admissible displacement set A is described by a union of polyhedral convex cones. Thus, set S_i is approximated by eq.(4-11) where sets $S(\boldsymbol{q}_k^i)$ are unions of polyhedral convex cones. Therefore, measurement set S_i is represented by a union of finite number of polyhedral convex cones. In the following analysis, we assume that the individual possible measurement sets are given by unions of PCC's.

4.5 Minimum Groups of Contact State Classifiers

4.5.1 Classifying Two Polyhedral Convex Cones

In this section, we will derive a minimum group of discriminant functions using some reduction rules of polyhedral convex cones. We first derive a minimum group of face vectors to differentiate two polyhedral convex cones. Let us consider a case in which we differentiate two states, N_i and N_j. Let us assume that the possible measurement set S_i is merely a polyhedral convex cone given by

$$S_i = face\{\boldsymbol{a}_1^i, \boldsymbol{a}_2^i, \cdots, \boldsymbol{a}_h^i\} \tag{4-13}$$

where the face vectors are $\boldsymbol{a}_j^i \in V^6$. The group of discriminant functions associated with the face vectors are redundant if they include functions that are unnecessary

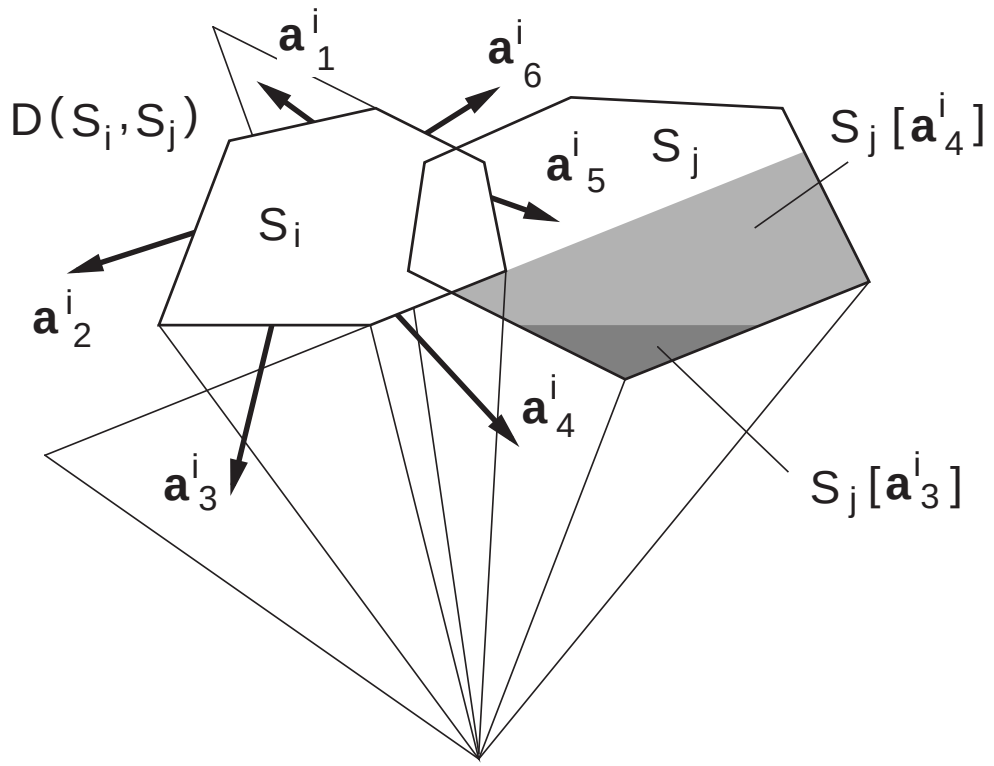

Figure 18: Compact discriminant functions

to evaluate for differentiating the two states. As shown in Figure 18, consider the polyhedral convex cones, S_i and S_j, that correspond to contact states N_i and N_j, respectively. Obviously, the discriminant functions associated with the face vectors $\boldsymbol{a}_1^i$, $\boldsymbol{a}_2^i$, and $\boldsymbol{a}_3^i$ are irrelevant to the differentiation of N_i from N_j. Only $\boldsymbol{a}_4^i$, $\boldsymbol{a}_5^i$, and $\boldsymbol{a}_6^i$ are sufficient to discriminate whether the current contact state is N_i or not. Namely, the minimum set of discriminant functions at this time is given by $face\{\boldsymbol{a}_4^i, \boldsymbol{a}_5^i, \boldsymbol{a}_6^i\}$.

Let $S_j[\boldsymbol{a}_k^i]$ be a subset of signals involved in S_j that are differentiated by face vector $\boldsymbol{a}_k^i$. Namely,

$$S_j[\boldsymbol{a}_k^i] = \{\boldsymbol{s}_m \mid \boldsymbol{s}_m \in S_j, \ \ (\boldsymbol{a}_k^i)^T \boldsymbol{s}_m > 0\}. \tag{4-14}$$

In the above example, the subset $S_j[\boldsymbol{a}_3^i]$ is involved in subset $S_j[\boldsymbol{a}_4^i]$, as shown in the figure. It implies that any signals differentiated by the discriminant function associated with face vector $\boldsymbol{a}_3^i$ can be discriminated by another function associated

with $\boldsymbol{a}_4^i$. Thus, we can find that face vector $\boldsymbol{a}_k^i$ is irrelevant in discriminating S_i from S_j if the following condition is satisfied:

$$\exists l \neq k \quad \text{s.t} \quad S_j[\boldsymbol{a}_k^i] \subset S_j[\boldsymbol{a}_l^i]. \tag{4-15}$$

The minimum group of discriminant functions is given by the face vectors which satisfy the above condition. In general, the minimum group of discriminant functions can be formulated by using the polar and the convex sum of polyhedral convex cones. It can be proved that the non-redundant group of discriminant functions to differentiate state N_i from N_j is given by

$$D(S_i, S_j) \triangleq face\{\boldsymbol{a}_k^i \mid \boldsymbol{a}_k^i \notin S_i[k]^* + S_j^*\} \tag{4-16}$$

where * represents the polar of a set and $+$ represents the convex sum of sets. Set $S_i[k]$ is a set of face vectors consisting of S_i except $\boldsymbol{a}_k^i$:

$$S_i[k] = face\{\boldsymbol{a}_1^i, \cdots, \boldsymbol{a}_{k-1}^i, \boldsymbol{a}_{k+1}^i, \cdots, \boldsymbol{a}_h^i\} \tag{4-17}$$

The proof of eq.(4-16) is shown in Appendix A.

Note that the polar of a polyhedral convex cone and the convex sum of two polyhedral convex cones are also convex cones. The compact set of discriminant function $D(S_i, S_j)$ consists of the face vectors that are not involved in the polyhedral convex cone $S_i[k]^* + S_j^*$.

4.5.2 Classifying Two Contact States

As mentioned before, individual possible measurement sets are described by unions of polyhedral convex cones. In this section, we derive the minimum set of discriminant functions to differentiate two contact states based on the above result.

Let S_i and S_j be possible measurement sets given by

$$S_i = \bigcup_{k=1}^{K} S_i^k, \tag{4-18}$$

$$S_j = \bigcup_{l=1}^{L} S_j^l \tag{4-19}$$

where sets S_i^k and S_j^l are polyhedral convex cones.

Note that we can differentiate a polyhedral convex cone S_i^k from another cone S_j^l using a minimum set of discriminant functions $D(S_i^k, S_j^l)$ derived in the previous section. Since the measurement set S_j is a union of polyhedral convex cones, S_j^1 through

S_j^L, we need to examine all the sets of discriminant functions; $D(S_i^k, S_j^l), \quad \forall l \in [1, L]$. Namely, we have to differentiate S_i^k from all of the cones S_j^1 through S_j^L in order to conclude that the signal $\boldsymbol{s}_m$ is involved in S_i^k:

$$\boldsymbol{s}_m \in D(S_i^k, S_j^l), \quad \forall l \in [1, L] \tag{4-20}$$

Therefore, the minimum set of discriminant functions to differentiate S_i^k from S_j is given by

$$\boldsymbol{s}_m \in \bigcap_{l=1}^{L} D(S_i^k, S_j^l). \tag{4-21}$$

Note that possible measurement set S_i is also a union of polyhedral convex cones S_i^1 through S_i^K. Thus, sensor signal $\boldsymbol{s}_m$ is involved in set S_i if and only if the following is satisfied:

$$\exists k \in [1, K] \text{ s.t. } \boldsymbol{s}_m \in S_i^k \tag{4-22}$$

Therefore, the minimum set of discriminant functions to differentiate S_i from S_j is given by

$$\boldsymbol{s}_m \in DS(S_i, S_j) \tag{4-23}$$

where

$$DS(S_i, S_j) \triangleq \bigcup_{k=1}^{K} \bigcap_{l=1}^{L} D(S_i^k, S_j^l). \tag{4-24}$$

Recall that the intersection of polyhedral convex cones is a convex cone as well. The compact set of discriminant function $DS(S_i, S_j)$ is described by a union of polyhedral convex cones, each of which consists of face vectors that provide linear discriminant functions directly.

4.5.3 Classifying Multiple Contact States

In this section, we derive a compact set of discriminant functions to differentiate one state among multiple states using a contact state graph representing the assembly process at a symbolic level.

Let us consider four possible measurement sets, S_i, S_j, S_k, and S_l in signal space, as shown in Figure 19. Suppose that the contact state has been N_i and that direct transitions from N_i to N_l are not possible. Then, we can determine the contact state

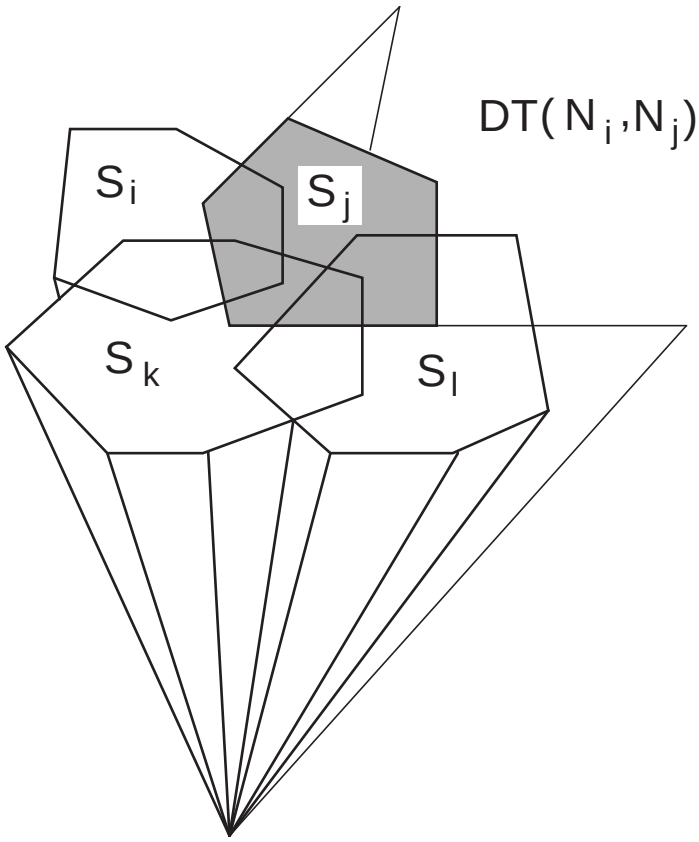

Figure 19: Discriminant functions to recognize state transitions

by examining whether the measured signal $\boldsymbol{s}_m$ is involved in S_i, S_j, and S_k. We do not have to check whether vector $\boldsymbol{s}_m$ is involved in S_l since a direct transition from N_i to N_l is not allowed. In order to conclude that the contact state has been changed from N_i to N_j, we have to differentiate N_j from both N_i and N_k. Thus, we can detect a transition from N_i to N_j by use of the two groups of functions; $DS(S_j, S_i)$ and $DS(S_j, S_k)$. Therefore, the minimum group of the discriminant functions is given by an intersection, $DS(S_j, S_i) \cap DS(S_j, S_k)$.

We can derive the minimum set of discriminant functions by using a set of nodes to which direct transitions are allowed. Let $T(N_i)$ be a set of nodes to which the contact state can transit from node N_i:

$$T_i = \{k \mid \text{direct transition from } N_i \text{ to } N_k \text{ is allowed}\} \tag{4-25}$$

The compact set of discriminant functions given by

$$DT(N_i, N_j) = \bigcap_{\substack{k \in T_i \\ k \neq j}} DS(S_j, S_k) \tag{4-26}$$

detects a transition from N_i to N_j, whereas possible states to which direct transitions from N_i are allowed are T_i. If a measured signal $\boldsymbol{s}_m$ is involved in $DT(N_i, N_j)$, we can conclude that the contact state has been changed to N_j among the possible states T_i. Since the intersection of polyhedral convex cones is also a polyhedral convex cone, the minimums set of discriminant functions $DT(N_i, N_j)$ is given by a union of polyhedral convex cones which are described in the face form. Therefore, we can derive the classifiers to sort out measured signals $\boldsymbol{s}_m$ and determine possible contact states occurring in the process.

4.6 Computation of Measurement Sets

4.6.1 Interpolation of Polyhedral Convex Cones

In order to obtain measurement set S_i corresponding to node N_i using eq.(4-11), we have to compute a union of polyhedral convex cones over a continuous region R_i. The set of configurations R_i is described by a finite number of sample configurations as mentioned in the previous section. In this section, we develop a technique to approximate a union of polyhedral convex cones from a finite number of sample configurations.

Let $P(\boldsymbol{q})$ be a polyhedral convex cone at configuration $\boldsymbol{q} \in R_i$ given by its span form.

$$P(\boldsymbol{q}) = span\{\boldsymbol{u}_1(\boldsymbol{q}), \boldsymbol{u}_2(\boldsymbol{q}), \cdots, \boldsymbol{u}_k(\boldsymbol{q})\} \tag{4-27}$$

Let $\boldsymbol{q}_1$ and $\boldsymbol{q}_2$ are two configurations in R_i neighboring each other. Let $T \subset R_i$ be a line segment between $\boldsymbol{q}_1$ and $\boldsymbol{q}_2$, as shown in Figure 20. An arbitrary configuration $\boldsymbol{q}$ involved in T is then given by

$$\boldsymbol{q} = t_1 \boldsymbol{q}_1 + t_2 \boldsymbol{q}_2 \tag{4-28}$$

where

$$t_1 + t_2 = 1, \quad t_1, t_2 \geq 0. \tag{4-29}$$

Every span vector $\boldsymbol{u}_j(\boldsymbol{q})$ is differentiable with respect to configuration $\boldsymbol{q}$ in region T since all configurations $\boldsymbol{q}$ in T are involved in region R_i, where the contact state is the same. Span vector at configuration $\boldsymbol{q}$ is then described by

$$\boldsymbol{u}_j(\boldsymbol{q}) = t_1\boldsymbol{u}_j(\boldsymbol{q}_1) + t_2\boldsymbol{u}_j(\boldsymbol{q}_2) \tag{4-30}$$

The proof is shown in Appendix B. Let $\boldsymbol{x}$ be an arbitrary vector involved in a polyhedral convex cone $P(\boldsymbol{q})$. Vector $\boldsymbol{x}$ is expressed by

$$\boldsymbol{x} = \sum_{j=1}^{k} c_j\boldsymbol{u}_j(\boldsymbol{q}) \tag{4-31}$$

where all coefficients c_j are non-negative. Substituting eq.(4-30) into eq.(4-31), we have

$$\boldsymbol{x} = \sum_{j=1}^{k}(t_1c_j)\boldsymbol{u}_j(\boldsymbol{q}_1) + \sum_{j=1}^{k}(t_2c_j)\boldsymbol{u}_j(\boldsymbol{q}_2). \tag{4-32}$$

Thus, the vector $\boldsymbol{x}$ is involved in a convex sum of two polyhedral convex cones $P(\boldsymbol{q}_1)$ and $P(\boldsymbol{q}_2)$ since coefficients t_1c_j and t_2c_j are all non-negative. Therefore, the union of polyhedral convex cones $P(\boldsymbol{q})$ over region T is described by the convex sum given by

$$\bigcup_{\boldsymbol{q}\,\in\,T} P(\boldsymbol{q}) = P(\boldsymbol{q}_1) + P(\boldsymbol{q}_2). \tag{4-33}$$

In general, the following theorem can be proved in the same way.

Theorem 9 *Let $\boldsymbol{q}_1$ through $\boldsymbol{q}_m$ be configurations neighboring each other and $P(\boldsymbol{q})$ be a polyhedral convex cone whose span vectors are differential with respect to configuration $\boldsymbol{q}$. Let T be a small region defined by*

$$T \triangleq \{\sum_{i=1}^{m} c_i\boldsymbol{q}_i \mid \sum_{i=1}^{m} c_i = 1,\ c_i \geq 0\ \ \forall i \in [1,m]\}. \tag{4-34}$$

The union of polyhedral convex cones $P(\boldsymbol{q})$ over T is then given by the convex sum of $P(\boldsymbol{q}_1)$ through $P(\boldsymbol{q}_m)$:

$$\bigcup_{\boldsymbol{q}\,\in\,T} P(\boldsymbol{q}) = P(\boldsymbol{q}_1) + P(\boldsymbol{q}_2) + \cdots + P(\boldsymbol{q}_m) \tag{4-35}$$

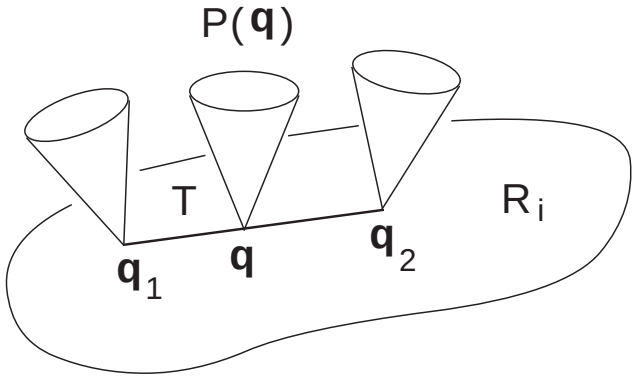

Figure 20: Interpolation of polyhedral convex cones

From this theorem, we find that we can interpolate the union of polyhedral convex cones by convex sums.

Let T be an arbitrary region connected in the configuration space. Let us divide the region T into a finite number of small regions. From the above theorem, the union of polyhedral convex cones over each small region can be approximated by its convex sum. The union over T is then given by the union of the obtained convex sums. Let $\boldsymbol{q}_1$ through $\boldsymbol{q}_m$ be sample configurations involved in T. The union of polyhedral convex cones over T is then approximated by

$$\bigcup_{\boldsymbol{q} \in T} P(\boldsymbol{q}) \quad \simeq \bigcup_{\boldsymbol{q}_j \approx \boldsymbol{q}_k} [P(\boldsymbol{q}_j) + P(\boldsymbol{q}_k)] \tag{4-36}$$

where $\boldsymbol{q}_j \approx \boldsymbol{q}_k$ represents that the distance between $\boldsymbol{q}_j$ and $\boldsymbol{q}_k$ is smaller than a small positive value ϵ. Note that a convex sum of polyhedral convex cones is also a polyhedral convex cone. We find that the union of polyhedral convex cones can be approximated by a finite number of polyhedral convex cones.

Using eq.(4-36), the measurement set S_i in eq.(4-10) is approximated by

$$S_i = \bigcup_{\boldsymbol{q}_j \approx \boldsymbol{q}_k} [S(\boldsymbol{q}_j) + S(\boldsymbol{q}_k)]. \tag{4-37}$$

Recall that the convex sum of polyhedral convex cones is also a polyhedral convex cone. Therefore, the measurement set is described by a union of finite number of polyhedral convex cones:

$$S_i = \bigcup_{l=1}^{L} S_i^l \tag{4-38}$$

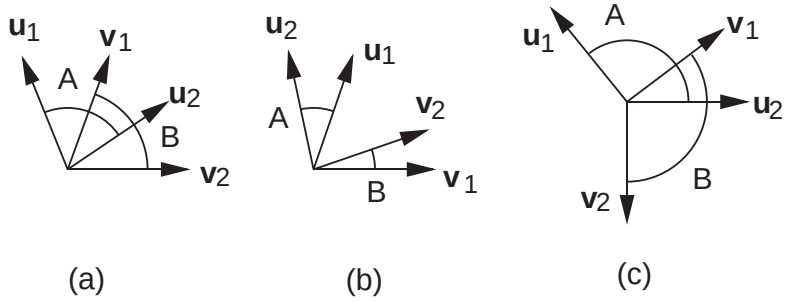

Figure 21: Simplification of union of polyhedral convex cones

where sets S_i^1 through S_i^L are polyhedral convex cones.

4.6.2 Simplification of Measurement Sets

Measurement set S_i obtained by eq.(4-37) is described by a union of many polyhedral convex cones. In order to derive the minimum group of state classifiers using the method developed in the previous section, we have to reduce the number of polyhedral convex cones involved in each individual measurement set. Figure 21 illustrates the conditions for two polyhedral convex cones to be reduced to one polyhedral convex cone. Let A and B be two polyhedral convex cones in the span form; $A = span\{\boldsymbol{u}_1, \boldsymbol{u}_2\}$ and $B = span\{\boldsymbol{v}_1, \boldsymbol{v}_2\}$. Figure 21-(a) shows a case where the union of two polyhedral convex cones is equal to the convex sum of the cones. Since the convex sum of polyhedral convex cones is also a polyhedral convex cone [Hirai et al., 88b], we can reduce the two polyhedral convex cones into one. In this case, the sum of two span vectors $\boldsymbol{u}_i$ and $\boldsymbol{v}_j$ is involved in either A or B. On the other hand, Figure 21-(b) and (c) show the cases where the union of polyhedral convex cones is not equal to the convex sum of the cones. The two polyhedral convex cones cannot be reduced to one cone. Note that the sum of span vectors $\boldsymbol{u}_1$ and $\boldsymbol{v}_2$ is involved in neither A nor B. In general, the following theorem can be proved.

Theorem 10 *Let A and B are polyhedral convex cones given by their span forms:*

$$A = span\{\boldsymbol{u}_1, \boldsymbol{u}_2, \cdots, \boldsymbol{u}_k\} \quad (4\text{-}39)$$

$$B = span\{\boldsymbol{v}_1, \boldsymbol{v}_2, \cdots, \boldsymbol{v}_l\} \quad (4\text{-}40)$$

The union of two polyhedral convex cones, A and B, is equal to the convex sum of the two if and only if

$$\boldsymbol{u}_i + \boldsymbol{v}_j \in A \cup B, \quad \forall i \in [1,k], \ \ \forall j \in [1,l] \quad (4\text{-}41)$$

is satisfied.

The proof is shown in Appendix C. Using this theorem, we can check whether the union of two polyhedral convex cones A and B is provided by their convex sum. When the union is equal to the convex sum, two polyhedral convex cones A and B can be reduced to one polyhedral convex cone, $A + B$. In this way, we can obtain the simplest form of measurement set.

4.7 Implementation

The theory of polyhedral convex cones is useful not only for formulating discriminant functions but for the computation and derivation of the functions. In the previous sections, many steps of computations were needed to derive the compact discriminant functions. Polars and convex sums of PCC's, for example, must be computed to obtain $D(S_i, S_j)$ in eq.(4-16). Intersections of PCC's must be computed to obtain $DT(N_i, N_j)$ in eq.(4-26). Convex sums of PCC's must be computed to interpolate PCC's in the computation of measurement sets S_i. The authors have developed efficient algorithms for the computations of PCC's and implemented the algorithms on a SUN 3/260 workstation in C language [Hirai et al., 88b]. The following constitute some of the package programs.

- CONVERT = Convert the form of a given PCC: face form to span form and vise versa
- DUAL = Obtain the polar of a given PCC.
- INTERSECT = Compute the intersection of two PCC.
- CONVEXSUM = Compute the convex sum of two PCC.
- ELEMENT = Examine whether a given vector is involved in a PCC.
- SUBSET = Investigate whether a given PCC is a subset of another PCC.
- REDUCE = Eliminate unnecessary face or span vectors to get a minimum set of face or span vectors

Using this package program, we can derive the minimum set of discriminant functions from geometric models of workpieces on the computer. Namely, the programs for processing sensory information to recognize the contact states are generated on a computer with minimum human intervention.

We demonstrate the computation procedures of state classifiers by taking a simple example shown in Figure 14. Let us assume that all the surfaces of the moving

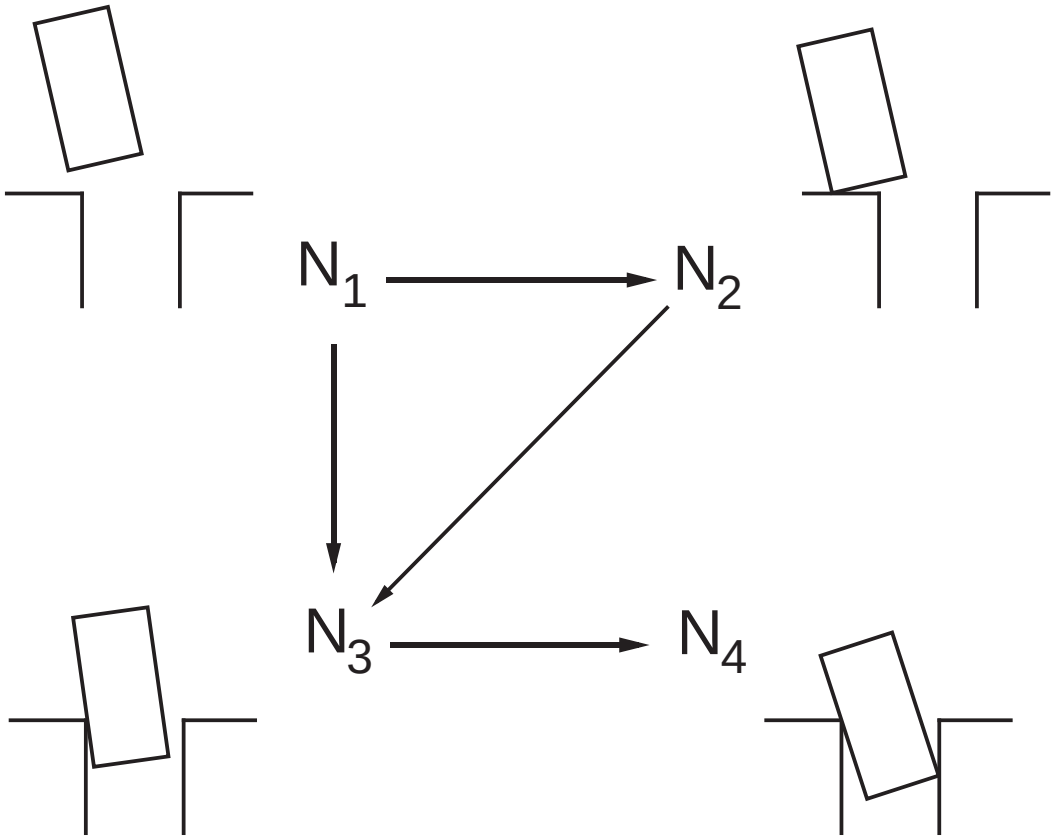

Figure 22: Simple example of assembly process

and the fixed objects are plains, as shown in the figure. Let $\boldsymbol{x}_0 = [x_0, y_0]^T$ and θ_0 be the position and the orientation of the moving object, respectively. The computation process consists of three stages; [1] Computation of Sample Configurations, [2] Interpolation of Measurement Sets and [3] Reduction of State Classifiers. Details of the three stages are described below.

[1] Computation of Sample Configurations

First, we need to compute a set of sample configurations involved in state N_i using the modified Monte Carlo method developed in the previous chapter. For the sake of simplicity, we deal with four nodes N_1 through N_4 among the whole contact states as shown in the Figure 10. Table 5 shows sets of obtained sample configurations $\boldsymbol{q} = [x_0, y_0, \theta_0]$ involved in contact state N_1 through N_4.

Table 5: Example of obtained sample configurations

```
no contact                          ( apex 3 - facet 5 )
 -9.87516 -0.00196039 -1.26804       -1.83164 .998921 1.52434
 11.114 -3.45393 .897865             -2.77709 .633807 .686465
 7.35285 -6.07908 -.459526           -2.89437 0.0569517 0.0569825
 6.97559 -9.79556 -.332086           -3.32054 .996523 1.48738
 8.3037 1.9007 .238096               -1.88392 .557976 .591945
 6.46616 -13.3399 -.138779           -3.59624 .600891 .644615
 -11.7016 -4.09544 -.343418          -2.44534 .204418 .205869
 2.05756 4.18133 1.15522             -1.85565 .986096 1.40384
 -10.1043 -9.48982 -.752848          -1.77021 .997336 1.49779
 12.7228 -6.28155 .909368            -1.98365 .225795 .227759

( facet 2 - apex 1 )                ( facet 2 - apex 1  apex 4 - facet 7 )
 -.126021 .244488 .94804             .707289 -1.22989 .655554
 -.365466 -3.88133 0.0344948         .832624 -.747578 .840117
 -.278171 .620316 1.22258            .658549 -1.51076 .570833
 -.777667 .695846 .843813            .673465 -1.41493 .597872
 -.115079 -1.29941 .262679           .536717 -3.58277 .271824
 -.510564 .180663 .287996            .833291 -.745488 .841012
 .885466 .944987 1.54763             .743821 -1.06474 .713343
 .321822 -2.08112 .349131            .666844 -1.45617 .586007
 -.475391 .32081 .676007             .720476 -1.1669 .676891
 -.868446 .775385 .896344            .536676 -3.58491 .271671
```

Table 6: Measurement sets obtained by interpolation technique

```
no contact
[ 0.000000  0.000000  1.000000 ]
[ 0.000000  1.000000  0.000000 ]
[ 1.000000  0.000000  0.000000 ]
[ -0.000000  -0.000000  -1.000000 ]
[ -0.000000  -1.000000  -0.000000 ]
[ -1.000000  -0.000000  -0.000000 ]
```

```
( apex 3 - facet 5 )
[ 1.000000  0.000000  0.000000 ]
[ -1.000000  -0.000000  -0.000000 ]
[ -0.000000  -0.046440  -1.000000 ]
[ 0.000000  0.998377  1.000000 ]
```

```
( facet 2 - apex 1 )
[ -0.303960  1.000000  -0.068729 ]
[ 1.000000  0.592024  0.260282 ]
[ 1.000000  -0.610791  -0.248616 ]
[ 1.000000  -0.804673  -0.443150 ]
[ -0.142827  0.102581  -1.000000 ]
```

```
( facet 2 - apex 1  apex 4 - facet 7 )
[ -1.000000  -0.138369  -0.377961 ]
[ -1.000000  -0.287817  -0.417221 ]
[ -0.895973  -1.000000  -0.600460 ]
[ -1.000000  -0.755479  -0.550071 ]
[ -1.000000  0.674780  -0.195623 ]
[ -1.000000  0.036819  -0.337039 ]
[ -1.000000  -0.012028  -0.348241 ]
[ -0.663462  1.000000  -0.092698 ]
[ -0.319406  -1.000000  -0.428551 ]
[ 0.000000  1.000000  0.000000 ]
[ -1.000000  -0.400926  -0.448018 ]
[ 0.019246  1.000000  0.071721 ]
```

[2] Interpolation of Measurement Sets

The admissible force set is computed from the admissible displacement set by using algorithm DUAL and CONVEXSUM. Thus, a set of measured vectors can be computed at one configuration.

From the sample configurations obtained in the previous stage, we can compute the measurement set S_i. Sets of measured vectors are first computed at individual sample configurations by using eq.(4-9). Applying the interpolation technique of PCC's to the sets of measurements, set S_i is computed by the use of eq.(4-37). Set S_i, which consists of many PCC's, is then reduced to a simple form by using the method developed in Section 4.6.2. Measurement set S_i is described by a union of the face form PCC's. Table 6 shows face vectors of set S_i computed from the sample configurations listed in Table 5. We find that possible signal set S_2 corresponding to state $N_2 =$ (apex 3 – facet 5) consists of four face vectors, as shown in the table.

Table 7: Result of computing discriminant functions

```
1 -> 1                                  3 -> 3
[ -1.000000  -0.000000  -0.000000 ]     [ 1.000000  0.592024  0.260282 ]
[ -0.000000  -1.000000  -0.000000 ]     [ 1.000000  -0.610791  -0.248616 ]

1 -> 2                                  3 -> 4
[ -1.000000  -0.000000  -0.000000 ]     [ -1.000000  -0.138369  -0.377961 ]
                                        [ -1.000000  -0.287817  -0.417221 ]
1 -> 3                                  [ -0.895973  -1.000000  -0.600460 ]
[ 1.000000  -0.804673  -0.443150 ]      [ -1.000000  -0.755479  -0.550071 ]
                                        [ -1.000000  0.674780  -0.195623 ]
 2 -> 2                                 [ -1.000000  0.036819  -0.337039 ]
[ -1.000000  -0.000000  -0.000000 ]     [ -1.000000  -0.012028  -0.348241 ]
                                        [ -0.663462  1.000000  -0.092698 ]
 2 -> 3                                 [ -0.319406  -1.000000  -0.428551 ]
[ 1.000000  -0.804673  -0.443150 ]      [ -1.000000  -0.400926  -0.448018 ]
                                        [ 0.019246  1.000000  0.071721 ]
```

[3] Reduction of State Classifiers

From measurement sets S_i computed in the previous stage, the minimum set of contact classifiers is obtained by using eqs.(4-16), (4-24), and (4-26). For the sake of simplicity, we deal with four nodes among the whole contact states and seven arcs among the whole transitions, as shown in the Figure 22. Table 7 shows the discriminant functions computed for the assembly process shown in the figure. We find that two linear discriminant functions are needed at most in this example to recognize the current contact state except a transition $N_3 \rightarrow N_4$.

4.8 Concluding Remarks

A new method for processing force and displacement information to discriminate the state of an assembly process has been developed. Contact state classifiers are automatically derived from the geometric model of assembly parts using the theory of polyhedral convex cones. First, the process of workpiece assembly was modeled as a set of transitions of contact states and represented by a state graph. Kinematic and static properties were analyzed and formulated by applying the theory of polyhedral convex cones. The ranges of possible force and displacement signals that can be

measured at each contact state have been derived and represented by a union of polyhedral convex cones. The face vectors of the polyhedral convex cones directly provide the discriminant functions to determine contact states from sensor signals. An efficient method to compute the range of sensor signals has been developed based on the theory of polyhedral convex cones.

The method based on the theory of polyhedral convex cones is thus a systematic approach to generating state classifiers for the monitoring of assembly processes. This is a bridge between sensor signals and symbolic-level state recognition.

Appendix A Proof of eq.(4-16)

Let $\boldsymbol{a}_k$ be a vector that is not involved in $D(S_i, S_j)$:

$$\boldsymbol{a}_k^i \in S_i[k]^* + S_j^* \tag{A-1}$$

From the above equation, we have

$$span\{\boldsymbol{a}_k^i\} \subset S_i[k]^* + S_j^*. \tag{A-2}$$

Based on the theory of polyhedral convex cones, we have

$$face\{\boldsymbol{a}_k^i\} \supset S_i[k] \cap S_j. \tag{A-3}$$

Let $\boldsymbol{s}_m$ be an arbitrary signal vector that satisfies

$$\boldsymbol{s}_m \in S_j,\ \boldsymbol{a}_k^T \boldsymbol{s}_m > 0. \tag{A-4}$$

Note that $\boldsymbol{s}_m$ is not involved in $face\{\boldsymbol{a}_k^i\}$. From eq.(A-3), we have

$$\boldsymbol{s}_m \notin S_i[k] \cap S_j. \tag{A-5}$$

Since $\boldsymbol{s}_m$ is involved in S_j,

$$\boldsymbol{s}_m \notin S_i[k]. \tag{A-6}$$

Namely,

$$\exists l \neq k \text{ s.t. } \boldsymbol{a}_l^i \boldsymbol{s}_m > 0. \tag{A-7}$$

This equation directly yields eq.(4-15). Thus, an arbitrary face vector that is not involved in $D(S_i, S_j)$ is redundant for the discrimination.
Let $\boldsymbol{a}_k$ be a vector involved in $D(S_i, S_j)$. In the same way as before, we have

$$face\{\boldsymbol{a}_k^i\} \not\supset S_i[k] \cap S_j. \tag{A-8}$$

From this equation,

$$\exists \boldsymbol{s}_m \text{ s.t. } (\boldsymbol{a}_k^i)^T \boldsymbol{s}_m > 0,\ \boldsymbol{s}_m \in S_i[k],\ \boldsymbol{s}_m \in S_j. \tag{A-9}$$

This equation directly yields the following:

$$S_j[\boldsymbol{a}_k^i] \not\subset S_j[\boldsymbol{a}_l^i] \quad \forall l \neq k \tag{A-10}$$

Thus, an arbitrary face vector involved in $D(S_i, S_j)$ is necessary for the discrimination. Therefore, it is proved that the minimum set of face vectors is given by eq.(4-16).

Appendix B Proof of eq.(4-30)

Since $t_1 + t_2 = 1$, we have

$$\begin{aligned} \boldsymbol{u}_j(\boldsymbol{q}) &= \boldsymbol{u}_j(t_1\boldsymbol{q}_1 + t_2\boldsymbol{q}_2) \\ &= \boldsymbol{u}_j[\boldsymbol{q}_1 + t_2(\boldsymbol{q}_2 - \boldsymbol{q}_1)]. \end{aligned} \tag{B-1}$$

Since $\boldsymbol{q}_1$ and $\boldsymbol{q}_2$ are neighboring each other

$$\boldsymbol{u}_j(\boldsymbol{q}) = \boldsymbol{u}_j(\boldsymbol{q}_1) + t_2\frac{\partial \boldsymbol{u}_j}{\partial \boldsymbol{q}}(\boldsymbol{q}_1)[\boldsymbol{q}_2 - \boldsymbol{q}_1]. \tag{B-2}$$

Substituting $t_2 = 1$ into the above equation

$$\frac{\partial \boldsymbol{u}_j}{\partial \boldsymbol{q}}(\boldsymbol{q}_1)(\boldsymbol{q}_2 - \boldsymbol{q}_1) = \boldsymbol{u}_j(\boldsymbol{q}_2) - \boldsymbol{u}_j(\boldsymbol{q}_1). \tag{B-3}$$

Substituting eq.(B-3) into eq.(B-2), we have

$$\begin{aligned} \boldsymbol{u}_j(\boldsymbol{q}) &= \boldsymbol{u}_j(\boldsymbol{q}_1) + t_2[\boldsymbol{u}_j(\boldsymbol{q}_2) - \boldsymbol{u}_j(\boldsymbol{q}_1)] \\ &= t_1\boldsymbol{u}_j(\boldsymbol{q}_1) + t_2\boldsymbol{u}_j(\boldsymbol{q}_2). \end{aligned} \tag{B-4}$$

Appendix C Proof of theorem 10

The sum of two span vectors $\boldsymbol{u}_i$ and $\boldsymbol{v}_j$ is involved in union $A \cup B$ when the union is equal to the convex sum $A + B$. The necessary condition is thus proved.
Let us assume that union $A \cup B$ is not equal to convex sum $A + B$. Then, there exist $\boldsymbol{x} \in A$ and $\boldsymbol{y} \in B$ that satisfy $\boldsymbol{x} + \boldsymbol{y} \notin A \cup B$. Let $\boldsymbol{z}(t)$ be a line between $\boldsymbol{x}$ and $\boldsymbol{y}$:

$$\boldsymbol{z}(t) = (1 - t)\boldsymbol{x} + t\boldsymbol{y} \tag{C-1}$$

From the assumption, we have

$$\boldsymbol{z}(0) \in A, \quad \boldsymbol{z}(1/2), \boldsymbol{z}(1) \notin A, \tag{C-2}$$

$$\boldsymbol{z}(0), \boldsymbol{z}(1/2) \notin B, \quad \boldsymbol{z}(1) \in B. \tag{C-3}$$

Thus, there exist t_a and t_b that satisfy

$$\boldsymbol{z}(t) \in A \ \ \forall t \in [0, t_a], \quad \boldsymbol{z}(t) \notin A \ \ \forall t \in (t_a, 1], \tag{C-4}$$

$$\boldsymbol{z}(t) \notin B \ \ \forall t \in [0, t_b), \quad \boldsymbol{z}(t) \in B \ \ \forall t \in [t_b, 1]. \tag{C-5}$$

Note that

$$t_a < 1/2 < t_b. \tag{C-6}$$

From eq.(C-4), we find that there exists a face vector $\boldsymbol{a}_r$ of polyhedral convex cone A that satisfies

$$\boldsymbol{a}_r^T \boldsymbol{z}(t_a) = 0, \quad \boldsymbol{a}_r^T \boldsymbol{z}(t) > 0 \ \ \forall t \in (t_a, 1]. \tag{C-7}$$

Similarly, we find that there exists a face vector $\boldsymbol{b}_s$ of polyhedral convex cone B that satisfies

$$\boldsymbol{b}_s^T \boldsymbol{z}(t_b) = 0, \quad \boldsymbol{b}_s^T \boldsymbol{z}(t) > 0 \ \ \forall t \in [0, t_b). \tag{C-8}$$

Let I be a set of span vectors of A perpendicular to $\boldsymbol{a}_r$:

$$\boldsymbol{a}_r^T \boldsymbol{u}_p = 0 \quad \forall p \in I \tag{C-9}$$

Since vector $\boldsymbol{z}(t_a)$ is perpendicular to $\boldsymbol{a}_r$, this vector can be expressed as

$$\boldsymbol{z}(t_a) = \sum_{p \in I} c_p \boldsymbol{u}_p, \quad c_p \geq 0. \tag{C-10}$$

Since $t_a < t_b$, we have

$$\boldsymbol{b}_s \boldsymbol{z}(t_a) = \sum_{p \in I} c_p (\boldsymbol{b}_s^T \boldsymbol{u}_p) > 0. \tag{C-11}$$

Since all the coefficients c_p are non-negative, there exists $i \in I$ that satisfies

$$\boldsymbol{b}_s^T \boldsymbol{u}_i > 0. \tag{C-12}$$

From eq.(C-9), we directly have

$$\boldsymbol{a}_r^T \boldsymbol{u}_i = 0. \tag{C-13}$$

Similarly, we find that there exists $\boldsymbol{v}_j$ that satisfies

$$\boldsymbol{a}_r^T \boldsymbol{v}_j > 0, \tag{C-14}$$

$$\boldsymbol{b}_s^T \boldsymbol{v}_j = 0. \tag{C-15}$$

From eqs.(C-12) through (C-15), we have

$$\boldsymbol{a}_r^T (\boldsymbol{u}_i + \boldsymbol{v}_j) > 0, \tag{C-16}$$

$$\boldsymbol{b}_s^T (\boldsymbol{u}_i + \boldsymbol{v}_j) > 0. \tag{C-17}$$

These equations imply that the sum of two span vectors $\boldsymbol{u}_i$ and $\boldsymbol{v}_j$ is not involved in either A or B. Therefore, the sufficient condition is proved.

Chapter 5
Concluding Remarks

A new methodology for analyzing and planning of manipulation using the theory of polyhedral convex cones has been developed. This paper can be summerized as follows.

First, a new approach to the kinematic and static analysis of manipulation is presented. Mechanical contacts between workpieces unidirectional constraints, which are described by a set of linear inequalities. We developed an efficient mathematical tool based on the theory of polyhedral convex cones, which allows us to treat fundamental inequalities in a simple and systematic manner.

Second, we have developed a method for representing assembly processes with respect to mechanical contacts. Gross motion of workpieces is analyzed by regarding how workpieces contact each other and is represented by a contact state graph. An algorithm for generating the graph from the geometric model of workpieces was developed.

Third, a new method for processing force and displacement information to discriminate the state of an assembly process has been developed. Contact state classifiers are automatically derived from the geometric model of workpieces using the theory of polyhedral convex cones. This is a bridge between sensor signals and symbolic-level state recognition.

It is required to understand the mechanism of manipulation to construct a higher-level control system, which extends the task range and deals with varying task conditions. This research provides a fundamental methodology for analysis and planning of manipulative tasks based on the theory of polyhedral convex cones.

Acknowledgements

A large number of people contributed to this research. I will recall the major contribution here.

I would like to thank Prof. Hidekatsu Tokumaru for his wise advice on the research. The Laboratory of Applied Systems Analysis provided me an excellent environment that enabled me to finish this project.

Prof. Haruhiko Asada was the guiding force of this research. He frequently advised me on the direction of the research. He provided me a chance to stay in Boston so that I could complete this research. He also advised me on many other aspects of academic life.

I would like to thank all members of the laboratory, especially Hiroshi Douzono for his teaching me about computers and programming. I would also thank BooHo Yang for his help during my stay in Boston.

Finally, I would like to thank my family for the emotional support.

References

[Akella and Cutkosky, 89] Akella, P. and Cutkosky, M., *Manipulation with Soft Fingers: Modeling Contacts and Dynamics*, IEEE Int. Conf. Robotics and Automation, pp.764–769, 1989

[Arnold, 78] Arnold, V. I., *Mathematical Methods of Classical Mechanics*, Springer-Verlag, 1978

[Asada and By, 85] Asada, H. and By, A.B., *Kinematic Analysis of Workpart Fixturing for Flexible Assembly with Automatically Reconfigurable Fixtures*, IEEE Trans. J. Robotics and Automation, RA-1-2, pp.86–94, 1985

[Asada and Izumi, 87] Asada, H. and Izumi, H., *Direct Teaching and Automatic Program Generation for the Hybrid Control of Robot Manipulators*, IEEE Int. Conf. Robotics and Automation, pp.1401–1406, 1987

[Asada and Hirai, 89] Asada, H. and Hirai, S., *Towards a Symbolic-Level Force Feedback : Recognition of Assembly Process States*, Proc. 5-th Int. Symp. of Robotics Research, Tokyo, pp.290–295, 1989

[Asada and Slotine, 86] Asada, H. and Slotine, J. E., *Robot Analysis and Control*, Wiley Interscience, 1986

[Avriel, 76] Avriel, M., *Nonlinear Programming: Analysis and Methods*, Prentice-Hall, 1976

[Brooks, 82] Brooks, R. A., *Symbolic Error Analysis and Robot Planning*, Int. J. Robotics Res., Vol.1, No.4, pp.29–68, 1982

[Brost, 88] Brost, R. B., *Automatic Grasp Planning in the Presence of Uncertainty*, Int. J. Robotics Res., Vol.7, No.1, pp.3–17, 1988

[Buckley, 87] Buckley, S. J., *Planning and Teaching Compliant Motion Strategies*, AI-TR-936, MIT. AI. Lab, 1987

[Cole et al., 88] Cole, A., Hauser, J, and Sastry, S., *Kinematics and Control of Multifingered Hands with Rolling Contact*, IEEE Int. Conf. Robotics and Automation, pp.228–233, 1988

[Dantzig, 63] Dantzig, G. B., *Linear Programming and Extensions*, Princeton University Press, 1963

[Desai and Volz, 89] Desai, R. S. and Volz, R. A., *Identification and Verification of Termination Conditions in Fine Motion in Presence of Sensor Errors and Geometric Uncertainties* IEEE Int. Conf. Robotics and Automation, pp.800–807, 1989

[Donald, 88] Donald, B. R., *Planning Multi-Step Error Detection and Recovery Strategies*, IEEE Int. Conf. Robotics and Automation, pp.892–897, 1988

[Duda and Hart, 73] Duda, R. O. and Hart, P. E., *Pattern Classification and Scene Analysis*, John Wiley, 1973

[Dufay and Latombe, 84] Dufay, B. and Latombe, J., *An Approach to Automatic Robot Programming Based on Inductive Learning*, Int. J. Robotics Res., Vol.3, No.4, pp.3–22, 1984

[Erdmann, 86] Erdmann, M., *Using Backprojections for Fine Motion Planning with Uncertainty*, Int. J. Robotics Res., Vol.5, No.1, pp.19–45, 1986

[Erdmann and Mason, 86] Erdmann, M. and Mason, T. M., *An Exploration of Sensorless Manipulation*, IEEE Int. Conf. Robotics and Automation, pp.1569–1574, 1986

[Goldman and Tucker, 56] Goldman, A. J. and Tucker, A. W., *Polyhedral Convex Cones*, Kuhn, H. W. and Tucker, A. W. eds., *Linear Inequalities and Related Systems*, Annals of Math. Studies, Vol.38, Princeton, pp.19–39, 1956

[Hirai et al., 88a] Hirai, S., Asada, H., and Tokumaru, H., *Kinematic Analysis of Contact State Transitions in Assembly Operations and Automatic Generation of Transition Network*, Trans. Society of Instrument and Control Engineers, Vol.24, No.4, pp.84–91, 1988

[Hirai et al., 88b] Hirai, S., Asada, H., and Tokumaru, H., *Kinematics of Manipulation Using the Theory of Polyhedral Convex Cones and Its Applications to Grasping and Assembly Operations*, IEEE Int. Workshop on Intelligent Robots and Systems, pp.451–456, 1988

[Hirai and Asada, 90] Hirai, S. and Asada, H., *A Model-Based Approach to the Recognition of Assembly Process States Using the Theory of Polyhedral Convex Cones*, Proc. 3rd Japan-U.S.A. Symp. on Flexible Automation, pp.809–816, 1990

[Hogan, 85] Hogan, N., *Impedance Control: An Approach to Manipulation*, ASME J. of Dynamic Systems, Measurement and Control, Vol.107–1, pp.1–22, 1985

[Inoue, 71] Inoue, H., *A Computer-Controlled Bilateral Manipulator*, Bulletin of JSME, Vol.14, pp.69–76, 1971

[Juan and Paul, 86] Juan, J. and Paul, R. P., *Automatic Programming of Fine-motion for Assembly*, IEEE Int. Conf. Robotics and Automation, pp.1582–1587, 1986

[Kamel and Kaufmann, 88] Kamel, M. S. and Kaufmann, P. M., *Representing Uncertainty in Robot Task Planning*, IEEE Int. Conf. Robotics and Automation, pp.1728–1734, 1988

[Kerr and Roth, 86] Kerr, J. and Roth, B., *Analysis of Multifingered Hands*, Int. J. Robotics Res., Vol.4, No.4, pp.3–17, 1986

[Lakshminarayana, 78] Lakshminarayana, K., *Mechanics of Form Closure*, ASME report No.78–DET–32, 1978

[Lozano-Pérez, 81] Lozano-Pérez, T., *Automatic Planning of Manipulator Transfer Movement*, IEEE Trans. SMC, Vol.11–10, pp.681–698, 1981

[Lozano-Pérez, 83] Lozano-Pérez, T., *Spatial Planning: A Configuration Space Approach*, IEEE Trans. Comput., Vol.C-32, No.2, pp.108–120, 1983

[Lozano-Pérez et al., 84] Lozano-Pérez, T., Mason, M. T., and Taylor, R. H., *Automatic Synthesis of Fine Motion Strategies for Robots*, Int. J. Robotics Res., Vol. 3, No. 1, pp.3–24, 1984.

[Lozano-Pérez and Wesley, 79] Lozano-Pérez, T. and Wesley, M., *An Algorithm for Planning Collision-Free Paths among Polyhedral Obstacles*, Commun. ACM, Vol.22, No.10, pp.560–570, 1979

[Mason, 81] Mason, M. T., *Compliance and Force Control for Computer Controlled Manipulators*, IEEE Trans. SMC, SMC–11, No.6, pp.418–432, 1981

[Mason, 82] Mason, M. T., *Compliant Motion*, Brady, M. et al. eds., *Robot Motion*, Cambridge, MIT press, pp.305–322, 1982

[Mason, 85] Mason, M. T., *The Mechanics of Manipulation*, IEEE Int. Conf. Robotics and Automation, pp.544–548, 1985

[Mason, 86] Mason, M. T., *Mechanics and Planning of Manipulator Pushing Operations*, Int. J. Robotics Res., Vol.5, No.3, pp.53–71, 1986

[Nevins et al., 80] Nevins, J. L. et al., *Exploratory Research in Industrial Assembly Part Mating*, R-1276, Draper Lab., 1980

[Nguyen, 86] Nguyen, V, *Constructing Force-Closure Grasps*, IEEE Int. Conf. Robotics and Automation, pp.1368–1373, 1986

[Nguyen, 87] Nguyen, V, *Constructing Force-Closure Grasps in 3D*, IEEE Int. Conf. Robotics and Automation, pp.240–245, 1987

[Ohwovoriole and Roth, 81] Ohwovoriole, M. S. and Roth, B., *An Extension of Screw Theory*, ASME J. Mechanical Design, Vol.103, Oct., pp.725–735, 1981

[Raibert and Craig, 81] Raibert, M. H. and Craig, J. J., *Hybrid Position/Force Control of Manipulators*, ASME J. of Dynamic Systems, Measurement and Control, Vol.102, pp.126–133, 1981

[Rajan et al., 87] Rajan, V. T., Burridge, R., and Schwartz, J. T., *Dynamics of a Rigid Body in Frictional Contact with Rigid Walls: Motion in Two Dimensions*, IEEE Int. Conf. Robotics and Automation, pp.671–677, 1987

[Rasmussen, 83] Rasmussen, J., *Skills, Rules, and Knowledges; Signals, Signs, and Symbols, and Other Distinctions in Human Performance Models*, IEEE Trans. on Systems, Man, and Cybernetics, Vol.SMC-13, No.3, pp.257–266, 1983

[Salisbury, 80] Salisbury, J. K., *Active Stiffness Control of a Manipulator in Cartesian Coordinates*, Proc. 19th IEEE Conf. on Decision and Control, 1980

[Salisbury and Craig, 82] Salisbury, J. K. and Craig, J. J., *Articulated Hands: Force Control and Kinematic Issues*, Int. J. Robotics Res., Vol.1, No.1, pp.4–17, 1982

[Schwartz and Sharir, 83] Schwartz, J. T. and Sharir, M., *On the Piano Movers' Problem 1: The Case of a Two-Dimensional Rigid Polygonal Body Moving Admist Polygonal Barriers*, Commun. on Pure and Applied Math., Vol.36, pp.345–398, 1983

[Schwartz and Sharir, 89] Schwartz, J. T. and Sharir, M., *A survey of Motion Planning and Related Geometric Algorithms*, Kapur, D and Mundy, J. L. eds., *Geometric Reasoning*, Cambridge, MIT press, pp.157–169, 1989

[Suehiro and Takase, 89] Suehiro, T. and Takase, K., *Representation and Control of Motion in Contact and Its Application to Assembly Tasks*, Proc. 5-th Int. Symp. of Robotics Research, Tokyo, pp.351–358, 1989

[Trinkle et al., 87] Trinkle, J. C., Abel, J. M., and Paul, R. P., *Enveloping, Frictionless, Planar Grasping*, IEEE Int. Conf. Robotics and Automation, pp.246-251, 1987

[Yamada et al., 87] Yamada, S., Abe, N. and Tsuji, S., *Construction of a Consulting System from Structural Description of a Mechanical Object*, IEEE Int. Conf. Robotics and Automation, pp.1413–1418, 1987

[Whitney, 77] Whitney, D. E., *Force Feedback Control of Manipulator Fine Motions*, ASME J. of Dynamic Systems, Measurement and Control, Vol.98, pp.91–97, 1977

[Whitney, 82] Whitney, D. E., *Quasi-Static Assembly of Compliantly Supported Rigid Parts*, ASME J. of Dynamic Systems, Measurement and Control, Vol.104, pp.65–77, 1982

[Whitney and Rourke, 86] Whitney, D. E. and Rourke, J. M., *Mechanical Behavior and Design Equations for Elastomer Shear Pad Remote Center Compliances*, ASME J. of Dynamic Systems, Measurement and Control, Vol.108, pp.223–232, 1986

[Whitney, 87] Whitney, D. E., *Historical Perspective and State of the Art in Robot Force Control*, Int. J. Robotics Res., Vol.6, No.1, pp.3-14, 1987

[Will and Grossman, 75] Will, P. M. and Grossman, D. D., *An Experimental System for Computer Controlled Mechanical Assembly*, IEEE Trans. Comput., Vol.C-24, No.9, pp.879–888, 1975

[Xiao and Volz, 89] Xiao, J. and Volz, R. A., *On Replanning for Assembly Tasks Using Robots in the Presence of Uncertainties*, IEEE Int. Conf. Robotics and Automation, pp.638–645, 1989